STATUS OF THESIS

Title of thesis: A STUDY OF THE OPTIMIZED WELDING PARAMETERS ON THE TENSILE STRENGTH, MICROSTRUCTURE AND CORROSION RESISTANCE DURING RESISTANCE SPOT WELDING OF TITANIUM ALLOY TI-6AL-4V

I ICHWAN FATMAHARDI

hereby allow my thesis to be placed at the Information Resource Center (IRC) of Universiti Teknologi PETRONAS (UTP) with the following conditions:

1. The thesis becomes the property of UTP

2. The IRC of UTP may make copies of the thesis for academic purposes only.

3. This thesis is classified as

☐ Confidential

☑ Non-confidential

If this thesis is confidential, please state the reason:

____

____

____

The contents of the thesis will remain confidential for ___________ years.

Remarks on disclosure:

____

____

____

Signature of Author

Permanent address: Universiti Teknologi Petronas (UTP), Bandar Seri Iskandar, 31750 Tronoh, Perak, Malaysia

Date : January 14th, 2022

Endorsed by

Signature of Supervisor

Name of Supervisor
Dr. Mazli Mustapha

Date : January 14th, 2022

UNIVERSITI TEKNOLOGI PETRONAS

A STUDY OF THE OPTIMIZED WELDING PARAMETERS ON THE TENSILE STRENGTH, MICROSTRUCTURE AND CORROSION RESISTANCE DURING RESISTANCE SPOT WELDING OF TITANIUM ALLOY TI-6AL-4V

by

ICHWAN FATMAHARDI

The undersigned certify that they have read and recommend to the Postgraduate Studies Programme for acceptance this thesis for the fulfillment of the requirements for the degree stated.

Dr. Mazli Mustapha
Senior Lecturer
Mechanical Engineering Department
Universiti Teknologi PETRONAS

Signature: ______________________

Main Supervisor: Dr. Mazli Mustapha

Ts. DR AZLAN AHMAD
Lecturer
Universiti Teknologi PETRONAS
Bandar Seri Iskandar, 31750 Tronoh
Perak Darul Ridzuan, Malaysia

Signature: ______________________

Co-Supervisor: Ts Dr. Azlan Ahmad

Signature: ______________________

Head of Department: Assoc. Professor Dr. Masdi Muhammad

Date: 18/1/2022

A STUDY OF THE OPTIMIZED WELDING PARAMETERS ON THE TENSILE STRENGTH, MICROSTRUCTURE AND CORROSION RESISTANCE DURING RESISTANCE SPOT WELDING OF TITANIUM ALLOY TI-6AL-4V

by

ICHWAN FATMAHARDI

A Thesis

Submitted to the Postgraduate Studies Programme

as a Requirement for the Degree of

MASTER OF SCIENCE

MECHANICAL ENGINEERING

UNIVERSITI TEKNOLOGI PETRONAS

BANDAR SERI ISKANDAR,

PERAK

JANUARY 2022

DECLARATION OF THESIS

Title of thesis	A STUDY OF THE OPTIMIZED WELDING PARAMETERS ON THE TENSILE STRENGTH, MICROSTRUCTURE AND CORROSION RESISTANCE DURING RESISTANCE SPOT WELDING OF TITANIUM ALLOY TI-6AL-4V

I ICHWAN FATMAHARDI

hereby declare that the thesis is based on my original work except for quotations and citations which have been duly acknowledged. I also declare that it has not been previously or concurrently submitted for any other degree at UTP or other institutions.

Witnessed by

Dr. Mazli Mustapha
Senior Lecturer
Mechanical Engineering Department
Universiti Teknologi PETRONAS

Signature of Author

Signature of Supervisor

Permanent address: Universiti Teknologi Petronas (UTP), Bandar Seri Iskandar, 31750 Tronoh, Perak, Malaysia

Name of Supervisor
Dr. Mazli Mustapha

Date : January 14th, 2022

Date : January 14th, 2022

DEDICATION

“This work I dedicate to my beloved family, my wife, sons, and parents, who always on my side during this whole time, it was never easy at all, but we did it”

ACKNOWLEDGEMENTS

All praise belongs to Allah azza wa jalla, who with all the blessings of all goodness becomes perfect. With all of his might, grace, love, and affection, I was guided to finish this work properly. May shalawat and salam always be poured out to the prophet Muhammad shalallahu alaihi wa sallam.

With all due respect to my supervisor Dr. Mazli Mustapha, I would like to express honorable gratitude for these times, untired, guide me for the right path of research. He is very gentle, wise, and professional to encourage me for managing the step by step of works properly. Under his guidance, I could find the best way to uncover the problems and discover appropriate solutions for a better research outcome.

I also deliver great gratitude and an endless compliment to Dr. Turnad Lenggo Ginta as my former supervisor. Who was kindly, offered me this opportunity and also guided me to encounter all the challenges patiently. This expression is also delivered to Ts Dr. Azlan Ahmad as well as my co-supervisor, his support, guidance, and professional advice always keep my work right on track.

In addition, I would like to thank the authority of Universiti Teknologi PETRONAS (UTP) for providing a good environment and facilities to conduct the research. All the lecturers and students also gave significant contributions to me during this time. I also thank technologists, particularly in the mechanical engineering department and centralized analytical laboratory (CAL) for their skillful assistance and cooperation to help me finish my work.

The utmost appreciation goes to all my closest brothers, sisters, and friends for their continuous moral, support, knowledge sharing, inspiration, and encouragement during my study at UTP.

ABSTRACT

Resistance spot welding (RSW) process with titanium alloy Ti-6Al-4V are selected for producing products in various industries for decades, commonly automotive and aerospace industries. They provide effective and efficient industrial processes and also good quality products. Some problems that were commonly occurred during the the RSW process with titanium alloy Ti-6Al-4V such as a low strength weld nugget, some pores were observed in the fusion zone, no study yet about generating the mathematical models and also no study yet about investigating the effect of the heat input into the corrosion resistance. In order to solve the problems, the objectives of this research are made: to determine the optimum RSW parameters, to investigate the influence of RSW parameters into weld nugget physical and mechanical properties, generating the mathematical models, and investigating the influence of RSW parameters into corrosion rate and pitting susceptibility. In this study, the Taguchi method is adopted to define the optimum level of parameters with tensile-shear strength as the response. Under the Analysis of Variance (ANOVA) from the Taguchi table, 9 kA of welding current, 32 cycles of welding time, and 5 kN of welding force were selected to be the optimum level of parameters on the response of 44.98 kN maximum load. The mathematical models were also formed by the regression analysis of the tensile-shear strength data. The β phase transformation into the acicular α' phase in the β transus temperature was mostly identified in the fusion zone. Creating a highly-stressed hexagonal-closed packed (HCP) structure to form a martensite microstructure in there. This causes a higher hardness value in the fusion zone than in the base metal and heat-affected zone (HAZ). After the potentiodynamic polarization test, the result identified that the higher heat input with higher welding current proved to decrease the corrosion rate in the fusion zone and more susceptible to pitting. The coarser microstructure caused by the higher heat input is reducing the fusion zone capability to create a dense passive anti-corrosion film.

ABSTRAK

Proses kimpalan titik rintangan (KTR) dengan aloi titanium Ti-6Al-4V dipilih untuk menghasilkan produk dalam pelbagai industri selama beberapa dekad, biasanya industri automotif dan aeroangkasa. Mereka menyediakan proses perindustrian yang berkesan dan cekap dan juga produk berkualiti. Beberapa masalah yang biasa berlaku semasa proses KTR dengan aloi titanium Ti-6Al-4V seperti nugget kimpalan berkekuatan rendah, beberapa liang diperhatikan dalam zon gabungan, belum ada kajian mengenai penjanaan model matematik dan juga belum ada kajian tentang menyiasat kesan input haba ke dalam rintangan kakisan. Bagi menyelesaikan masalah, objektif kajian ini dibuat iaitu: untuk menentukan parameter KTR optimum, untuk menyiasat pengaruh parameter KTR ke dalam sifat fizikal dan mekanikal nugget kimpal, menjana model matematik, dan menyiasat pengaruh parameter KTR ke dalam kakisan. kadar dan kerentanan pitting. Dalam kajian ini, kaedah Taguchi diguna pakai untuk menentukan tahap optimum parameter dengan kekuatan ricih tegangan sebagai tindak balas. Di bawah Analisis Varians (ANOVA) daripada jadual Taguchi, 9 kA arus kimpalan, 32 kitaran masa kimpalan, dan 5 kN daya kimpalan dipilih untuk menjadi tahap parameter optimum pada tindak balas beban maksimum 44.98 kN. Model matematik juga dibentuk melalui analisis regresi data kekuatan ricih tegangan. Transformasi fasa β kepada fasa α' acicular dalam suhu transus β kebanyakannya dikenal pasti dalam zon gabungan. Mencipta struktur pembungkusan tertutup heksagon (HCP) bertekanan tinggi untuk membentuk struktur mikro martensit di dalamnya. Ini menyebabkan nilai kekerasan yang lebih tinggi dalam zon pelakuran berbanding logam asas dan zon terjejas haba (HAZ). Selepas ujian polarisasi potensiodinamik, keputusan mengenal pasti bahawa input haba yang lebih tinggi dengan arus kimpalan yang lebih tinggi terbukti dapat mengurangkan kadar kakisan dalam zon gabungan dan lebih mudah terdedah kepada pitting. Struktur mikro yang lebih kasar disebabkan oleh input haba yang lebih tinggi mengurangkan keupayaan zon gabungan untuk mencipta filem anti-karat pasif yang padat.

TABLE OF CONTENT

LIST OF FIGURES

LIST OF TABLES

CHAPTER 1

INTRODUCTION

1.1 Chapter Overview

This chapter is purposed to explain the background of the study, problem statement, objectives of the research, scope of research, and the organization of the thesis. Background of study to investigate the influence of RSW parameters into weld nugget physical, mechanical properties, and corrosion resistance uncover some subjects. This leads to the problem statement establishment where research objectives are obtained based on the research gap that is discovered in the literature review. To encounter the present study is kept on the research path and does not deviate from the objectives, the scope of research is defined. The thesis outline and general overview are derived from the organization description at the end of this chapter.

1.2 Background of Study

In the modern industrial sectors, the effective and efficient welding method such as RSW is commonly utilized, used in many production processes, and offered a large space for improvement. The welding process is relatively simple, and the joint is generated by a heat input combined with an electrode force given to materials at a certain time. The material resistivity is also proved to be vital in localizing the heating area in the contact zone between the welding electrode and the material, which is then this welding method's name taken from [1]. One of the best materials that have been used for so many years for industrial applications and welded using RSW is titanium alloy, especially Ti-6Al-4V, for example in the automotive industry [2]. Titanium alloy grade 5 or Ti-6Al-4V has a tensile strength of 130 Ksi or 895 MPa with a yield strength of 120 Ksi or 828 MPa, making it one of the strongest alloys [4]. Titanium has low density around 4.5 g/cm^3, leading to deform easily during RSW with a high force, but in another way, it has a high melting point around 1660 °C (3020 °F) [5]. To define the best quality of Ti-6Al-4V weld nugget strength, a precise investigation of the weld nugget's physical and mechanical properties plays an essential role. Welding current, welding time, and force as the primary RSW parameters are proved to be the most significant affected parameters to develop the weld nugget properties, including mechanical and physical properties. For example in 1 mm of titanium alloy Ti-6Al-4V, when the welding current raised from 7 kA to 9 kA, the maximum tensile load was achived up to 14.3 kN, while the welding time and force have less significant effect [6].

In the corrosion issues, because of the prevailing temperature conditions during weld metal solidification, weld fusion zones usually have coarse columnar grains. As a result, weld mechanical characteristics and resistance to hot cracking are frequently compromised. The fusion zone of titanium alloy fusion welds is characterized by coarse, columnar formed β grains. Thus, a large β grain size is blamed for poor mechanical properties and corrosion resistance in the weld fusion zone [12]. But in this previous research, the welding method is different, still, there has not been studied yet the RSW parameters influence weld nugget corrosion rate and pitting susceptibility. For the whole gaps of the previous studies, it needs vital research work to overcome these issues and close the outcome gaps.

1.3 Problem Statements

The heat input and welding force as two main RSW parameters are still important subjects to discuss regarding the properties transformations in the weld nugget as mentioned in the previous background of the study. The heat input influence which is affected by the amount of welding current, material resistivity, and welding time, gives the main transformation variable to the localized welding area more than the force. Unfortunately, some frailty and defects were still identified in the weld nugget such as low strength cold weld with PIF mode and pore created [6]. These phenomenons were particularly observed when the low heat input was applied. Otherwise, when the higher heat input was applied in a short welding time, the subsequent expulsion was observed in the weld nugget. This expulsion would rather reduce the weld nugget strength than increase it, regarding material degradation in the fusion zone [6].

The mathematical models are required to do a mass rapid work planning in the industries today to increase the productivity. These mathematical models are calculating the weld nugget properties such as the maximum load of tensile-shear testing and weld diameter, with RSW parameters as their variables. But, there is not well reported yet about finding the mathematical models for RSW of Ti-6Al-4V.

It is similar to corrosion resistance transformation matter. Although Ti-6Al-4V is known for its very small corrosion rate which indicates its high corrosion resistance capability but to investigate the corrosion resistance changing in the fusion zone is also an important subject. This is because the metal corrosion resistance capability is commonly much affected by the microstructure transformation. But again, there is not explored yet about analyzing the effect of RSW parameter to the corrosion resistance and pitting susceptibility.

1.4 Objectives of the Research

Considering the restriction subjects discussed in the previous sections, and to discover the better outcomes, some objectives of this research are:

1. To determine the optimum RSW parameters which can create a high maximum load in tensile-shear testing in the titanium alloy Ti-6Al-4V weld nugget

2. To investigate the influence of RSW current, time, and force for titanium alloy TI-6Al-4V weld nugget physical & mechanical properties

3. Establishing a mathematical model for weld nugget maximum load and diameter through regression model with the welding parameters as the variables

4. To study the effect of welding parameters variation with the transformation of corrosion resistance and pitting susceptibility

1.5 Scope of Research

This research was conducted to acquire the better quality of weld nugget in titanium alloy Ti-6Al-4V with the RSW process. To encounter that matter, the scope of this research was developed structurally. In this research, the RSW parameters were varied to meet the optimum level of weld nugget quality. This research comprised of five phases: phase I is the material and equipment preparation, from cutting the material, preparing the RSW machine and dressing the RSW electrode, phase II RSW experiments with Taguchi method design, phase III is measuring the weld diameter and indentation depth, microstructure analysis using a scanning electron microscope (SEM), and Energy Dispersive X-Ray (EDX) analysis to capture the weld composition, tensile-shear testing with maximum load as the response of Taguchi method, calculating the analysis of variance (ANOVA) to define the optimum parameters, and also regression analysis to determine the mathematical model, phase IV is investigating the corrosion rate and pitting susceptibility with RSW parameters as the variables, the last phase is comprehensive data analysis and concluding.

The Taguchi method which is adopted in this research will be arranged with RSW parameters as its variables, which much influence the RSW heat input such as welding current, time, and force. The response of the ANOVA and regression model will be obtained from the tensile-shear testing from the whole sample. The microstructure and microhardness analysis will reveal the connectivity between the variation of parameters with the weld nugget properties. The microstructure and micro-hardness test were only tested for the optimum level sample, that was got from the ANOVA of the Taguchi method. To figure out the relationship between weld nugget properties transformation and corrosion resistance, the electrochemical experiment was conducted to identify the changing of corrosion rate and pitting susceptibility.

The medium tension-testing machine which has 50 kN of maximum capacity was utilized to do the tensile-shear testing for the whole samples. The ANOVA and regression analysis was conducted using Minitab software to improve the result's accuracy. To obtain the microstructure, hardness, and corrosion testing, each sample was cut using electrical discharge machining (EDM) with wire cutting, to get the weld nugget cross-sectional area. This was done to avoid any microstructural changes in the weld nugget if the heat cutting was applied. The microstructure analysis was conducted by etching the sample's cross-sectional area, then the microstructure figure was captured using SEM. The EDX was also utilized to analyze the transition of material compositions in the base metal, HAZ, and the fusion zone. This also provides an obvious transition phenomenon and its correlation with the localized heating process during welding. The micro-hardness value was acquired using a Vickers microhardness testing machine along with the base metal, HAZ, and fusion zone. In the corrosion testing, the potentiodynamic polarization process was utilized with 1 M NaCl as the medium. This process was conducted only for the sample with optimum welding current and force results from previous phase III ANOVA, while the welding time is varied. The corrosion rate for each sample was calculated using ASTM standard formula. The pitting figures were captured from the sample's cross-sectional area using an optical microscope.

1.6 Organization of The Thesis

This thesis consists of five chapters: introduction, literature review, methodology, results and discussion, and conclusions.

A summary of the background of the study is provided in chapter 1. It mentions a brief introduction and explanation about the issues of RSW on Ti-6Al-4V. Some subjects which arise from the research related to it are formulated into some problem statements. The problem statements and objectives of this study are linked with each other. The scope of study and organization of the thesis are also presented in this chapter.

Chapter 2 explains the literature review for a comprehensive background that triggers the research efforts. A basic explanation about RSW theoretical background, Ti-6Al-4V base metal properties, and some advantages on its applications. The discussion also contains some of the previous study discoveries and reported conclusions. The discussion leads to the reveal some important matters such as the mechanical and physical properties issues which are closely related to the variation of the RSW parameters. And also an extensive explanation regarding the corrosion rate and pitting susceptibility investigation particularly in the weld nugget area.

In chapter 3, the scope of work start from the material preparations are defined. The detail about sample geometry and standard operating procedures of RSW usage are also described clearly. The methodology section depicts the obvious step-by-step of how the research was conducted. The standards used for tensile-shear testing, sample etching, SEM analysis, micro-hardness analysis, potentiodynamic polarization, and optical microscopy are adopted from the internationally recognized standard.

In chapter 4, the outcomes of the research are presented and discussed. The Taguchi method ANOVA and regression analysis results are provided comprehensively, particularly for optimum level parameters. The physical properties, mechanical properties, and potentiodynamic polarization or corrosion analysis results are also shown. The data are illustrated in the obvious figures, tables, and graphs. The detail of analysis is carried out in the discussion section, where the hypothesis, assumption, and reasonable explanation are explicitly elaborated, related to the data presented, and are also synchronized with the other literature.

Chapter 5 summarizes the results and discussion that can be drawn from the current study. Specify recommendation is also given for related future work, for the better possible outcomes.

CHAPTER 2

LITERATURE REVIEW

2.1 Chapter Overview

The chapter consists of all background literature regarding the topic of the research and also the outline of previous studies. The principal of the RSW method and Ti-6Al-4V properties including their advantages and utilizations are reviewed comprehensively. Some of the studies which have been organized to investigate the influence of RSW parameters on Ti-6Al-4V properties and corrosion behavior are also put in a broad discussion in this chapter. This chapter presents sufficient information to reveal the gaps in the current research work. This also gives some benefits for defining the following experiment to fill the gaps and for future analysis to get accurate results.

2.2 Introduction

Welding is the process of joining two or more metals by melting some of the metal. In the industrial world, welding is needed, especially to make metal-based products such as in the automotive, aviation, household appliances, etc. Welding is also very important in the construction industries, especially steel construction which requires high joint strength and has good quality. The development of the welding process is growing significantly, especially to obtain better results. In the industrial world which is increasingly being demanded to be more effective and efficient, studies on welding process improvement are increasingly being carried out. The following are some classifications of welding processes that are commonly used [13]:

1. Arc welding : Bare Metal Arc Welding (BMAW), Carbon Arc Welding (CAW), Flux Cored Arc Welding (FCAW), Gas Metal Arc Welding (GMAW), Gas Tungsten Arc Welding (GTAW), Plasma Arc Welding (PAW), Svc/hielded Metal Arc Welding (SMAW), Submerged Arc Welding (SAW), Magnetically Impelled Arc Butt Welding (MIAB) and Atomic Hydrogen Welding (AHW)

2. Oxyfuel welding : Air Acetylene Welding (AAW), Oxyacetylene Welding (OAW), Oxygen/Propane Welding, Oxyhydrogen Welding (OHW), Pressure Gas Welding (PGW)

3. Resistance welding : Resistance Spot Welding (RSW), Resistance Seam Welding (RSEW), Projection Welding (PW), Flash Welding (FW), Upset Welding (UW)

4. Solid-state welding : Coextrusion Welding (CEW), Cold Pressure Welding (CW), Diffusion Welding (DFW), Explosion Welding (EXW), Electromagnetic Pulse Welding, Forge Welding (FOW), Friction Welding (FRW), Friction Stir Welding (FSW), Friction Stir Spot Welding (FSSW), Hot Pressure Welding (HPW), Hot Isostatic Pressure Welding (HIPW), Roll Welding (ROW), Ultrasonic Welding (USW)

5. Other types : Electron Beam Welding (EBW), Electroslag Welding (ESW), Flow Welding, Induction Welding (IW), Laser Beam Welding (LBW), Laser-hybrid Welding, Percussion Welding (PEW), Thermite Welding (TW), Electrogas Welding, Stud Arc Welding

The Resistance Spot Welding (RSW) is quite different from other types of welding. When the other welding methods are occurring some sparks and arcs along the welding process and conducted for some of a long time, and joining the metals by melting the whole edge of the purposed metal sheet edge, The RSW only occurred on one purposed spot on the sheet for a certain time to create welded joint. The primary parameters such as welding current, welding time, and welding force which contribute highly in generating the weld in the specimen are reckoned and attributed as the most important process parameters, and essentially close with affecting the weld quality. Figure 2.1 shows the RSW process diagram to develop the weld nugget and the correlation between the welding time and the temperature during welding. The transformation of the solid phase to the liquid phase defined around 1625-1750^{o}C. Particularly for titanium titanium alloy Ti-6Al-4V, the phase diagram with the cooling medium of water and air is shown in Figure 2.2 [14].

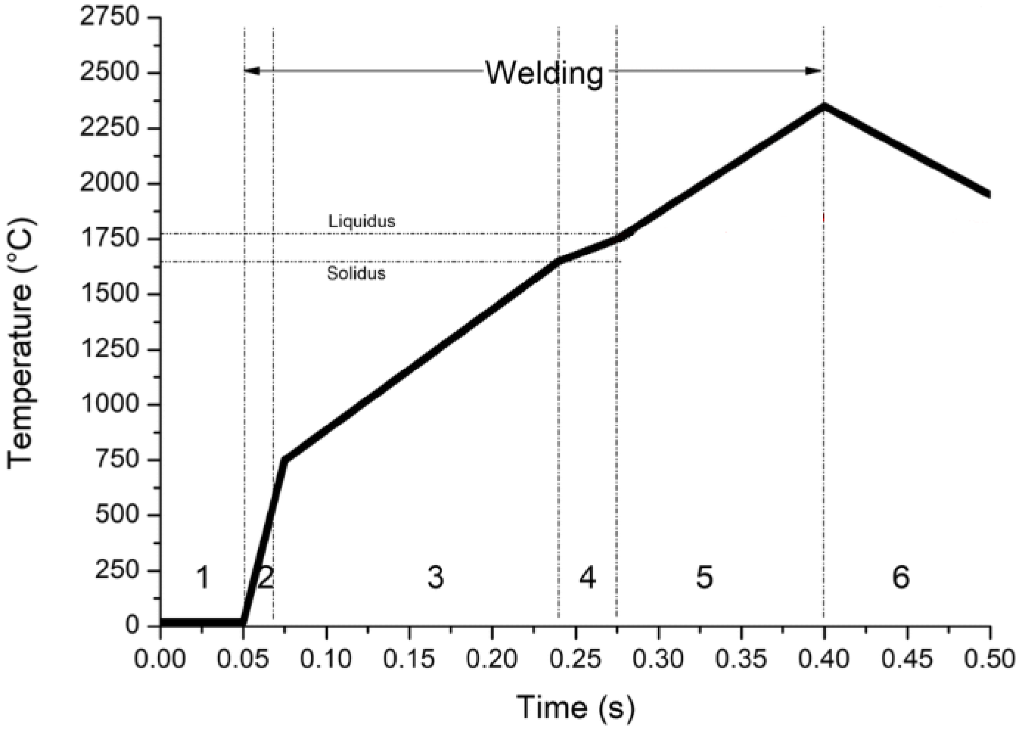

Figure 2.1 : RSW process diagram [15]

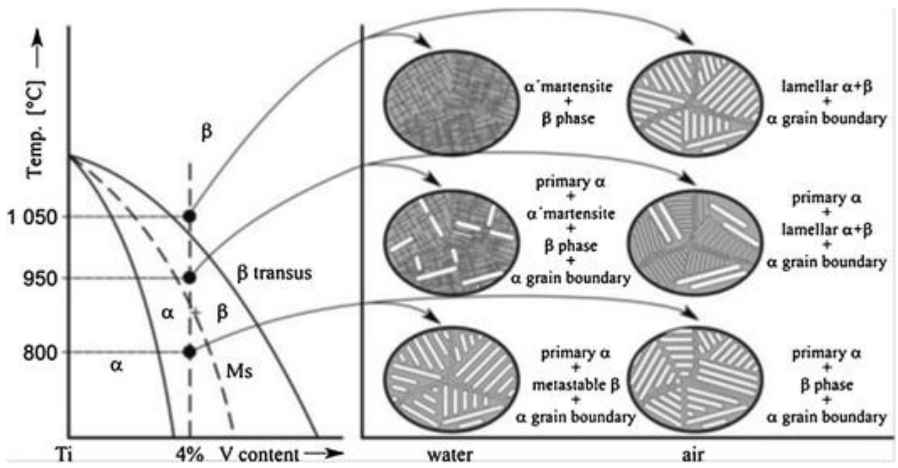

Figure 2.2 : Titanium alloy Ti-6Al-4V phase diagram [14].

The other parameters are considered as the second important parameters such as the squeeze time, weld time, hold time, and off-time. Squeeze time is recognized as the sufficient time to develop the amount of electrode force, the time in which the current flows is called welding time. When the solidification is processed, the time required to finish it is called hold time while the force is still applied. The later is off time, the time which is required by the electrodes to switch to the next weld, and off-time is the time needed for the electrodes to move to the next weld [16]. Figure 2.3 shows the part of a typical RSW machine. In the process, the welding current is flowing through the electrodes, transferred to the materials while the materials are held at once at the same time by both above and below electrodes, give it a tight grip on the materials. This process is conducted in the whole welding time cycle. Determining the amount of welding time in which the current flows is deeply dependent upon the material type, thickness, and the welding tip cross-sectional area [17].

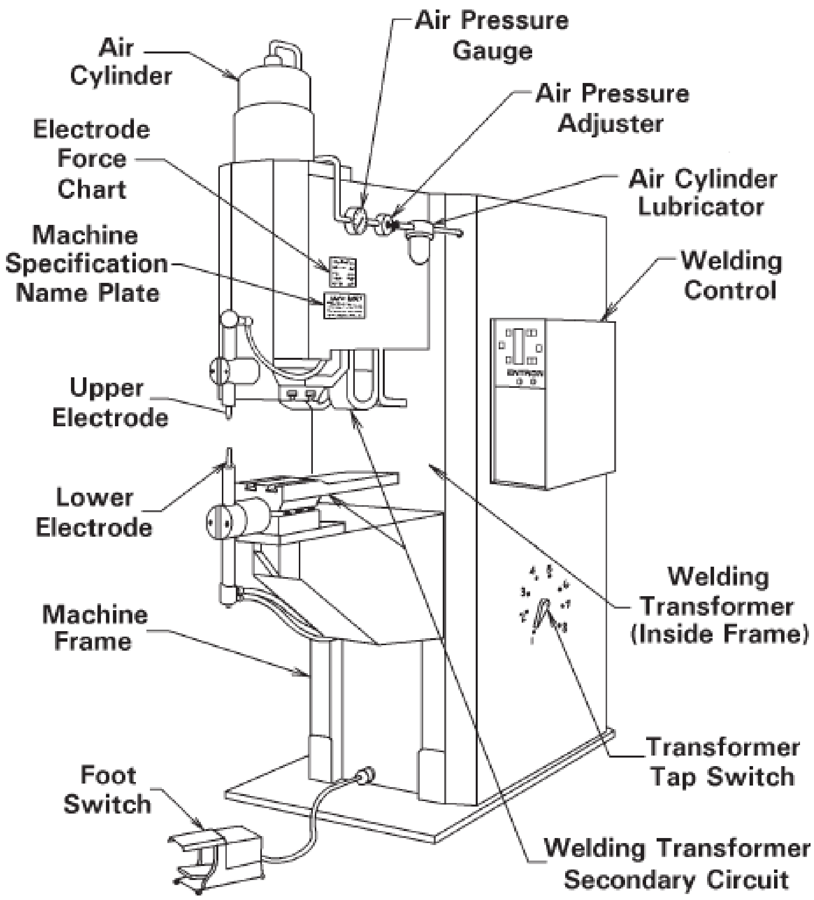

Figure 2.3 : Parts of typical RSW machine [17]

Figure 2.4 depicts an obvious and complete diagram of the RSW process. The various sections of the RSW machine are labeled for clarity [17].

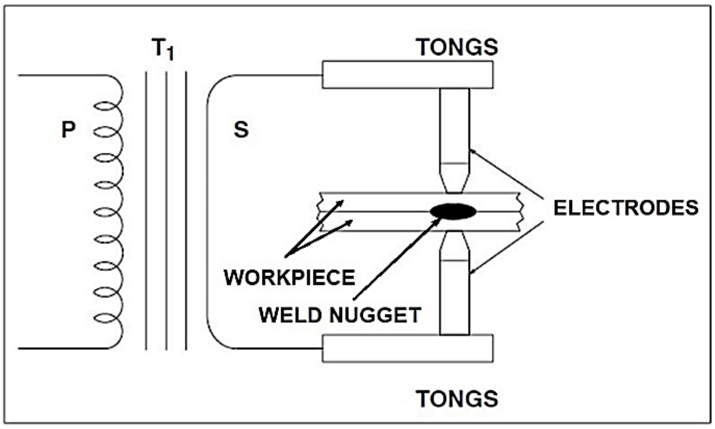

Figure 2.4 : The RSW machine with work

The other important factor is the material resistance which contributes to the name of RSW. As explained before, the weld joint is obtained after the welding current flows and hits the materials as both of the materials are clamped by the electrodes. The material's base metal resistance generates the localized heating spot in the materials. This localized heating spot joins the materials together and the weld is produced subsequently. This is what makes the RSW different from other welding methods because, the localized heating is occurred on the surface of materials and penetrates the internal part of the materials contact. Figure 2.5 exhibits the comparison between RSW and gas tungsten-arc welding (TIG) weld joint [17].

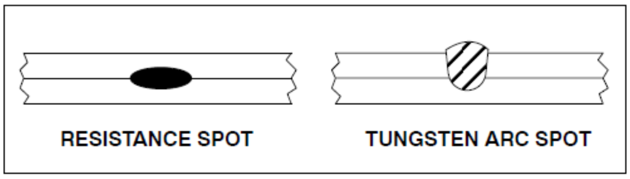

Figure 2.5 : Resistance and TIG spot weld comparison [17]

Only one side of the gas tungsten-arc spot is created. In the RSW, the electrodes on both sides of the workpiece are usually used to make a joint. The RSW process can be achieved in any direction of the manufacturing process and particularly in any position required. In the entire case, certainly, the current must flow, else the weld will not be possible. During the welding process, the electrode points press against the workpiece, keeping the component in close and intimate contact. Keep in mind that the RSW machines aren't meant to be used as force clamps to hold workpieces together while welding [17].

Weld cycle or time may be relatively simple and utilize just the aforementioned times, but they can often be much more complex as shown in Figure 2.6. Modern machine controllers offer the ability to customize and precisely control each of the parameters indicated in the figure. RSW works extremely well for welding the relatively thin sheets that are so common in automotive manufacturing. In addition, incredibly fast welding times combined with the self-clamping nature of the process make it an ideal process for high production robotic welding on which the automotive industry relies heavily [16].

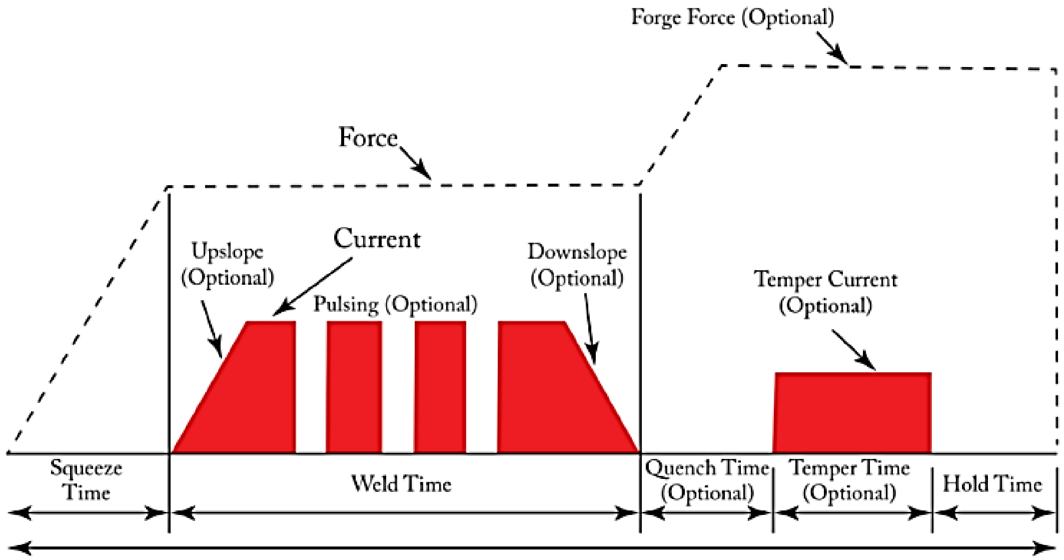

Figure 2.6 : Spot welding cycle [16]

The RSW cycle compare to the development of weld nugget can be seen in Figure 2.7 The following are the basic criteria that influence the amount of heat generated:

1. The welding current (the heat generation is made based on the amount of welding current, subsequently the higher the welding current the more heat will be produced).
2. The length of time spent welding (the welding time contributes to the heat generation proportionally when the heat transferred is constant).
3. The welding force (the higher welding force will give lower contact resistance, which under normal circumstances, the heat will be produced).

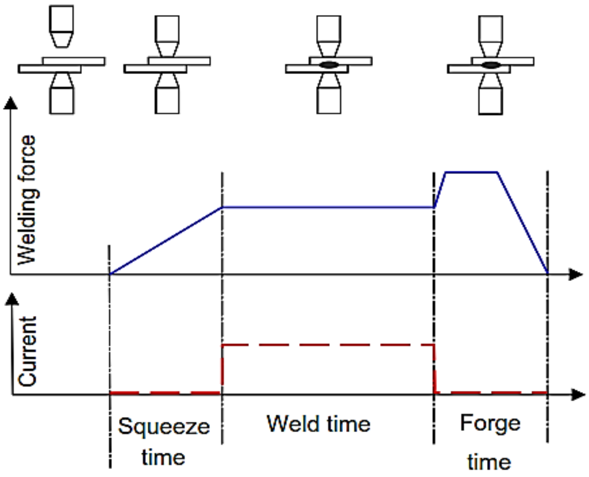

Figure 2.7 : The RSW nugget growth [18].

2.2.1 Heat Generation and Solidification

Heat generation associated with the RSW process is more complicated than just the simple heating of a conductor associated with the passage of electrical current. Where the sheets come into contact with each other, there is the greatest resistance to current flow. Because of this, a weld nugget can develop and expand precisely where it is required between the sheets [16]. When power and heat are assumed to be synonymous, Ohm's Law may be modified. When current is conducted through a conductor, heat is generated due to the conductor's electrical resistance to current flow. As *Q* indicated as the heat, calculated from the amount of welding current *I* which flows through and the electrical resistance *R*, the basic formula for generating heat can be given in the equation (2.1) [17]:

$$\boldsymbol{Q = I^2 R} \tag{2.1}$$

A sequence of resistances makes up the second section of an RSW circuit, which includes the parts to be welded. The entire cumulative value of this electrical resistance affects the current output of the RSW equipment and the heat generation of the circuit. The important aspect is that, while the current value remains constant throughout the electrical circuit, the resistance values might vary substantially at various places. At any point in the circuit, the heat created is proportional to the resistance [17]. In Figure 2.8 it can be figured out the proportions of the time or cycles during welding start to the end. Start from the squeeze time when the pressure from the welding force is started to be applied. The welding current will flow in the bigger proportions of all. The development of the weld nugget will be continued in the hold time and the off-time finally the opportunity to switch to another spot welding is given.

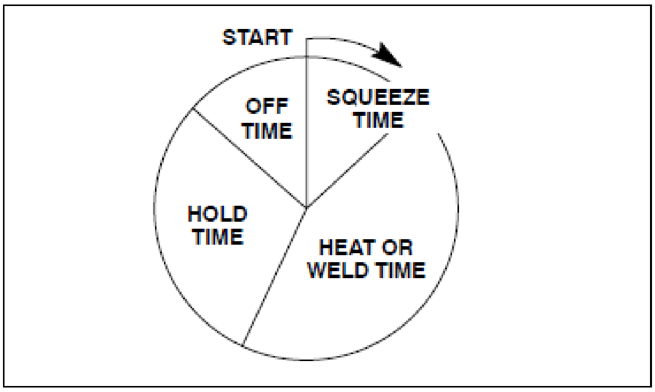

Figure 2.8 : Spot welding time cycle [17]

All of the RSW machine parts including the tongs, the flexible cables, the electrode tips, and the transformer are built with the least amount of resistance possible. RSW machines are made to efficiently deliver the welding current to the weldment. The most relative resistance is needed at the weldment. That is, it is connected to the rest of the welding circuit. In the work area there are six major points of resistance, which are:

1. The meeting point between the top workpiece surface and the electrode surface.
2. The top workpiece
3. The top and bottom interface of the workpiece
4. The bottom workpiece.
5. The meeting point between the bottom workpiece surface and the electrode surface.
6. The electrode tips resistance

When the solidification process occurs, the resistance which is the main factor in the formation of the heating localization affects the process significantly. These resistances, which are connected sequentially, each inhibit the flow of electricity from the electrodes to the material. The amount of resistance is greatly affected by the heat transferability of the material, its electrical resistance, and the thickness of the joint material at the weld joint. Especially at the 3 points which are the junction between the electrodes and the combination of the two materials [17].

The heating localization process requires thousands of amperes at almost every RSW condition. An amperage of that magnitude will create a large amount of heat in a short time when flowing through a high resistance. A handle that is strong enough and tough is very important to produce a good RSW connection when the RSW process occurs. The welding time factor is also very essential especially in most single pulse RSW processes and is the only parameter that can be controlled. Controlling current is frequently cost-prohibitive. In many instances, it is also unpredictable. Time is also a crucial aspect in The RSW. The majority of resistance spot welds are completed in a fairly short amount of time. Since the alternating current is commonly utilized in welding, processes may be based on a 60 cycle time (sixty cycles = one second). Previously, the heat generation formula was utilized. The formula is completed with the addition of the time element T and the heat losses K as follows in equation (2.2) [17]:

$$\boldsymbol{Q = I^2RTK} \tag{2.2}$$

It's crucial to keep track of time. If the time element is too lengthy, the melting (and possibly boiling) temperature of the base metal in the joint may be exceeded. Because of the gas porosity, this could result in poor welds. The unexpected event such as an expulsion from the molten metal ejection during welding is also possible particularly with higher heat input in a short time, which could weaken the weld by reducing the cross-section of the junction. In addition, shorter welding time reduces the risk of excessive heat transfer in the base metal. Welded part distortion is reduced, and the heat-affected zone around the weld nugget is significantly reduced [17].

As with current and time, the effect of welding force is also something that needs to be considered carefully. The application of welding force to the material has the aim of holding the material in its position so that the RSW process can be carried out at the right point. So that the electrical conductivity and resistance are fairly uniform at the point where the welded connection occurs. Pulling the workpieces together with tongs or electrode tips is not recommended [17]. To keep the good condition of contact resistance, the surface condition must be preserved from any substances including rust and other substances that will differ the resistance values. This surface condition of the sheets will also determine the amount of localized heat in the point that is being welded as well as the applied parameters. When the two sheets are brought together, the surface roughness of each metal will limit the contact area. In these circumstances, when the welding current is transmitted through the sheets, the electron will have no chance other than to pass the narrow area where the surface roughness lies. The current density then will be induced extremely at localized points, which results in extremely increased resistance. Surface asperities or roughness are flattened and contact resistance is reduced when electrode force is applied. As a result of the reduced contact resistance, higher RSW forces will generally result in less heating [16].

The resistance factor decreases as the pressure increases. With the electrode tip in close contact with the base metal, proper pressures will tend to transfer heat away from the weld. The control of welding force or pressure is conformable with the current, the lower applied force or pressure is also followed by the required lesser amount of current and vice versa. A similar case is also applicable for the any of RSW machine types [17]. Oxides, rust, scale, grease/oil, and paint, in addition to surface roughness, increase contact resistance. By breaking up oxides and pushing out other surface contaminants, higher electrode forces will have the same effect as lowering contact resistance as shown in Figure 2.9 [16].

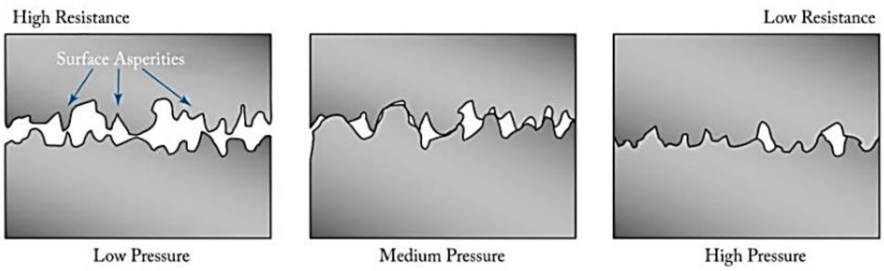

Figure 2.9 : The effect of electrode force on contact resistance [16]

Solidification of a liquid nugget during welding is identical to that of a metal cast and consists of two steps: nucleation of a solid phase and subsequent crystal development, just like ingot mold solidification. Heat dissipation into the base metal and electrodes regulates the crystallization process. The type, size, and orientation of the crystals generated are influenced by the cooling direction and rate, as well as the alloy composition [19].

2.2.2 Weld Quality

The weld and nugget are not the same by definition or measurement, despite their close relationship. A weld is expected to contain all parts of a weldment, including the HAZ, in addition to the nugget. Another point of contention is the distinction between button and nugget diameters. Because metallographic cross-sectioning frequently reveals a nugget's size and shape, a nugget's width is measured rather than its diameter, as shown in Figure 2.10. Other features revealed by cross-sectioning a weldment are also shown in this figure [19]. Different amounts of welding parameters such as welding current will lead to the different results of weld nugget [20]. The example of the different results of the weld nugget is shown in Figure 2.11.

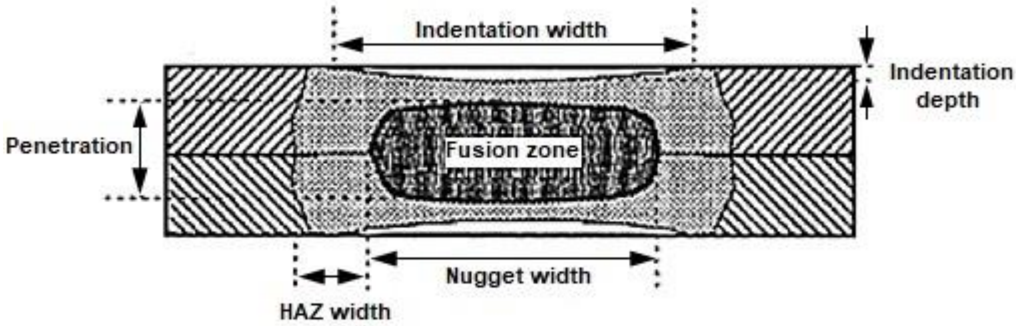

Figure 2.10 : Weld attributes revealed by metallographic sectioning [19]

The shape of welding nugget observation is the easiest way to define the welding quality of joining metals. In terms of the effect of the RSW process, the weld nugget will also bring another microstructure change around it. The fusion zone, HAZ, and the base metal will provide different types of microstructure that will lead to mechanical performance. Other than that, the welding arrangement will also strongly affect the mechanical properties such as the fatigue limit of its weld [21]. Overall optimization of the RSW parameters and the development of a more advanced process system proved to be able to improve the quality of the weld nugget and further investigate its effect on its tensile-shear strength [6].

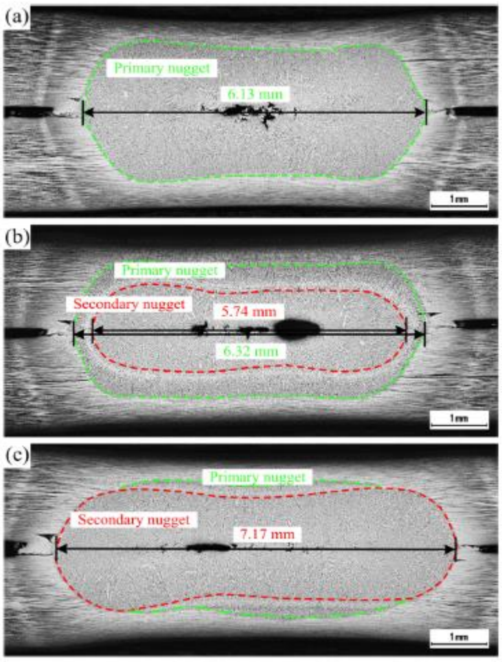

Figure 2.11 : Weld nuggets result of Q&P 980 Steel. (a) Single-pulse weld 7 kA; (b) double pulse weld 7kA-6kA; (c) double pulse weld 7 kA-7.5 kA [20].

However, due to the “hidden” weld position between the sheets or parts being welded, visible examination is not possible in mass industrial outputs with most resistance welding techniques. As a result, maintaining weld quality using RSW procedures is heavily reliant on other methods such as current range and lobe curves as shown in Figure 2.12 and Figure 2.13.

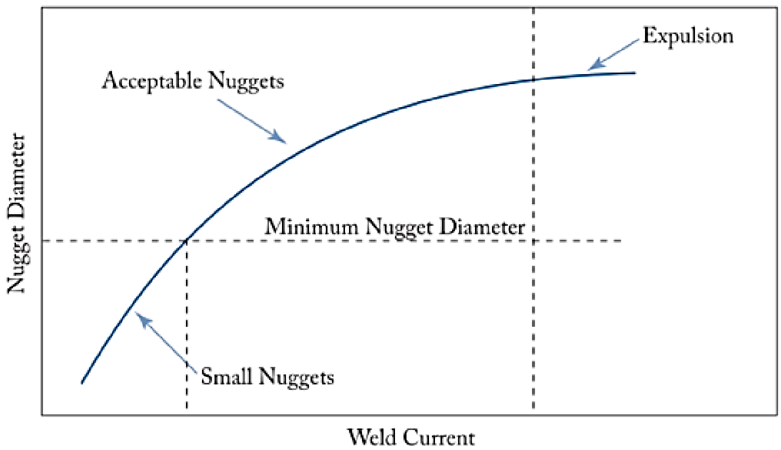

Figure 2.12 : Current range curve [16]

Podržaj et al. concluded that when it comes to the quantity of heat created during RSW, there are two extremes: expulsion happens when the heat generation is exceeded the necessary to form an appropriate weld and a cold weld or there is no created weld nugget if the heat generation is less than the necessary to form an appropriate weld. The heat generation should be in the range between the point of cold weld and expulsion which is called appropriate weld area. Due to the condition when the higher necessary heat generation will increase the weld nugget strength, then the developed heat generation in the range closer to the expulsion range is preferable. In addition, the adequate combination of RSW parameters during welding without any disruption or expulsion is contributing more to an acceptable weld as can be seen in Figure 2.13 [22].

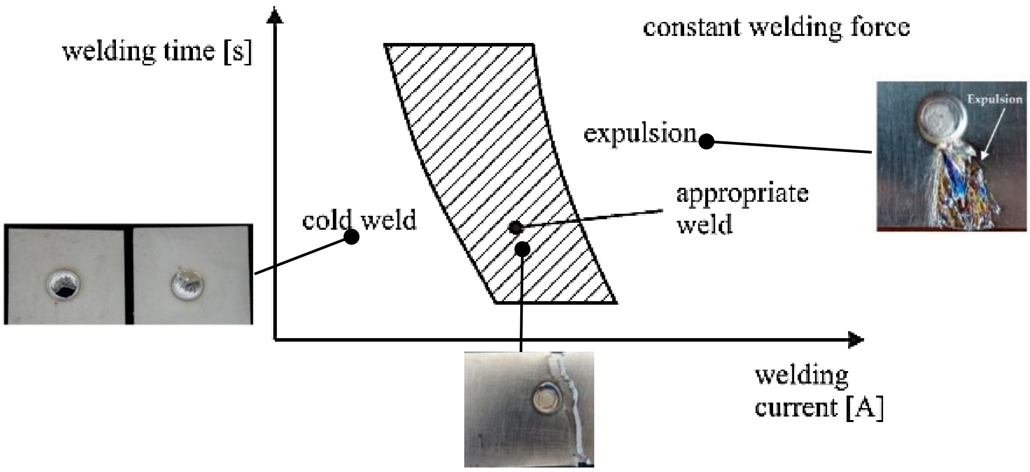

Figure 2.13 : The RSW weld zones/lobe curves [22].

2.3 Titanium and Its Weld Properties

The extended use of materials in such of the specific area that is required some high strengths and good fatigue condition make Titanium alloy is the best choice to be taken. It is also having good weld-ability and heat resistant as well as is corrosion resistant. Welding has the most impact on material characteristics. The minimized contaminant in the surrounding welding environment is also a priority to be fulfilled to get excellent results. In defining the final qualities of welded joints, alloy composition, welding method, and subsequent heat treatment are all critical factors. So, to understand the properties transformation, it must be collected the data about the basics of titanium alloy properties based on proper standards before it is welded. And also for the proper selection of which titanium alloy will be used for the research, certain reasons must be analyzed.

2.3.1 Physical & Mechanical Properties

In the industrial world, titanium is recognized as a low-density metal with 4.5 gr/cm^3 of density, lower than plain steel with 7.85 gr/cm^3 of density. Titanium's properties such as strength can be refixed by either alloying process or the deformation process. Titanium may passivate, making it resistant against many corrosion substances and solutions such as chlorides and mineral acids. Some titanium products such as commercially pure titanium and certain titanium alloys are considered biocompatible with the human body. Many products can be produced from titanium and titanium alloys which gives valuable product quality. These include the applications in chemical and petrochemical industries, maritime settings, and also biomaterials due to their exceptional corrosion resistance and biocompatibility, as well as their high strength. Several of Ti-6Al-4V products are shown in Figure 2.14.

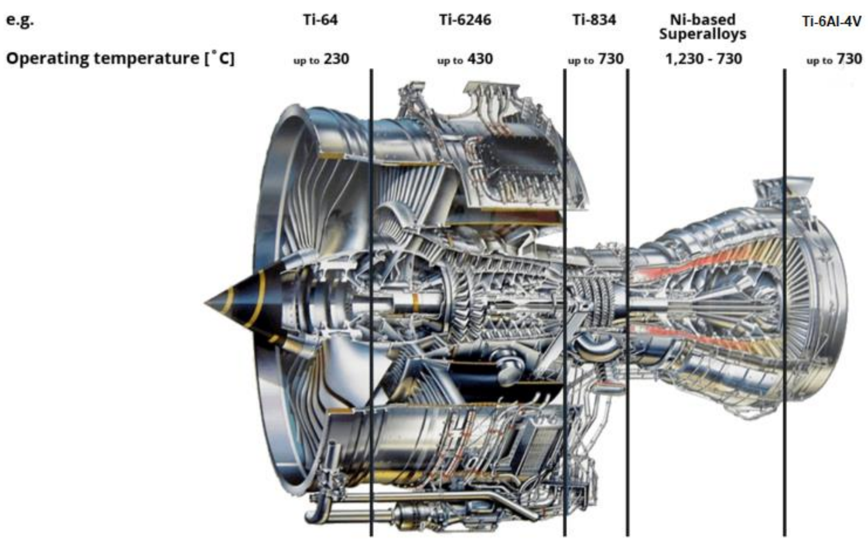

Figure 2.14 : Several Titanium alloy Ti-6Al-4V products

At extremely low to very high temperatures, different titanium alloys exhibit a combination of high strength, stiffness, excellent toughness, low density, and great corrosion resistance, allowing weight reductions in aircraft constructions and other high-performance applications [23]. Mechanical characteristics including yield or ultimate strength to density (strength efficiency), fatigue crack development rate, and fracture toughness, as well as production concerns like welding and forming needs, are crucial. For structural titanium alloy applications, these parameters usually dictate the alloy composition, structure (alpha, alpha-beta, or beta), heat treatment (some form of either annealing or solution treating and aging), and level of process control chosen or recommended [23].

Industrial sectors provide the titanium alloy Ti-6Al-4V, utilize it, and shipped it for almost more than 50 years back from the entire titanium types. Various compositions, such as Ti-4Al-3Mo-1V, Ti-7Al-4Mo, and Ti-8Mn, have seen intermittent use throughout the history of the titanium industry. Various titanium alloys have been developed, but they have never been widely used commercially. One of the most applicable titanium alloys with unique properties is Ti-6Al-4V. This alloy has an imprescriptible capacity to be produced in a variety of small or large-size mill products. In addition, the Ti-6Al-4V mill products are suitable to be processed into more complex hardware or general products. This gives commercially viable in the more dynamic industrial demands. Hence, this wrought titanium alloy is acclaimed to be the most popular among others to be chosen as a standard alloy for measuring the others. Ti-6Al-4V is also the typical alloy for castings that need to be extremely strong. It has also been tested in P/M processing. For many years to come, Ti-6Al-4V will be the most widely used titanium alloy [23].

ASTM described Titanium alloy in Grade to differ among various of its material types according to its alloy and unalloyed condition based on the standard of ASTM B-265. Ti-6Al-4V meaning that, it is Grade 5 - Titanium alloy (6 % aluminum, 4 % vanadium). Titanium alloy grade 5 or Ti-6Al-4V has 130 ksi or 895 MPa of tensile strength with 120 Ksi or 828 MPa of Yield Strength making it one of the strongest alloys among others [4]. This benefit of course making Ti-6Al-4V the first choice among other titanium alloys as base materials of various industrial common products. Especially for a product that is required high strength and ductility but must be light, having good corrosion resistance as well as heat resistant at the same time such as vehicle muffler, engine part, and gas engine turbine blade.

Regarding the RSW research for titanium sheet, Kahraman et al conducted research using 1.5 mm of commercially pure (CP) titanium sheet (ASTM Grade 2), while the parameters of electrode force (2 kN, 4 kN, and 6 kN), welding cycle (5, 15 & 25 cycles) and weld environments (air and controlled argon atmosphere) also set for 18 samples, concluded that the welding time increasing was reciprocal with the amount of electrode force and weld nugget tensile-shear strength as can be seen in Figure 2.15. Compared with the other parameters, during welding it was discovered that the welding time was verified to be the most vital and had the most influential effect on the weld nugget strength, and the welding environment was put otherwise as to the least of them [7].

Zhang et al. [6] conducted research using 1 mm (thickness) of titanium alloy Ti-6Al-4V sheet with the variations of welding current (7, 8, 9, 10, & 11 kA), welding time (4, 8, 12, 16, & 20 cycles) and electrode force (2, 3, 4, & 5 kN). The research discovered the sample's weld nugget strength increased rapidly in tune with the increase of tensile loads, at this point the maximum tensile load was achieved as shown in Figure 2.16a.

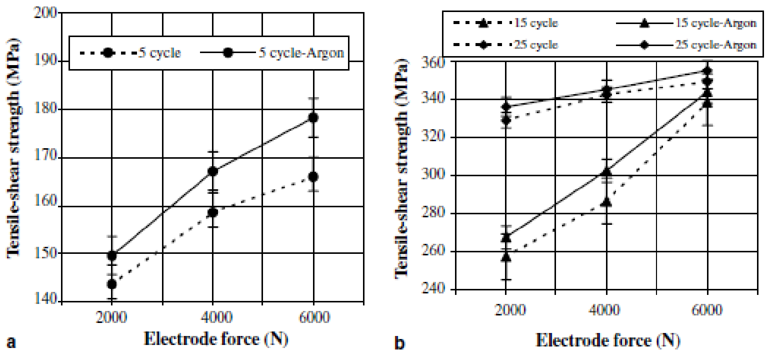

Figure 2.15 : Tensile-shearing test data: (a) 5 cycle weld time and (b) 15 and 25 cycle weld time [6]

As its large contribution to the heat generation, the welding current effect had been discovered as the parameter which gave the greatest impact to the weld nugget strength and size. Controlling its value is affirmatively favorable in the weld nugget quality transformation such as bigger nugget width (W) and the indentation depth. But exceeding it's necessary causing several undesirable expulsions and deeper indentation, lowering the weld nugget strength subsequently. As shown in Figure 2.16b, a linear welding strength curve is shown in line with the increase of welding time but at some point, it was constantly maintained, which exhibits a corresponding effect in the response of weld nugget width (W) development [6].

The reverse weld nugget width (W) response was shown by electrode force, only an initial point it responded as increasing as seen in Figure 2.16c. The remained curve decreased narrowly following the increase of electrode force, leaving the conclusion biased that the higher force should respond otherwise as the electrode tip shape is known as cone generally. However, the validity was owned by the weld nugget height (H). When the electrode force increased, the samples' tensile loads were dramatically reduced due to the deeper depression, resulting in constantly reduced weld nugget height (H) [6].

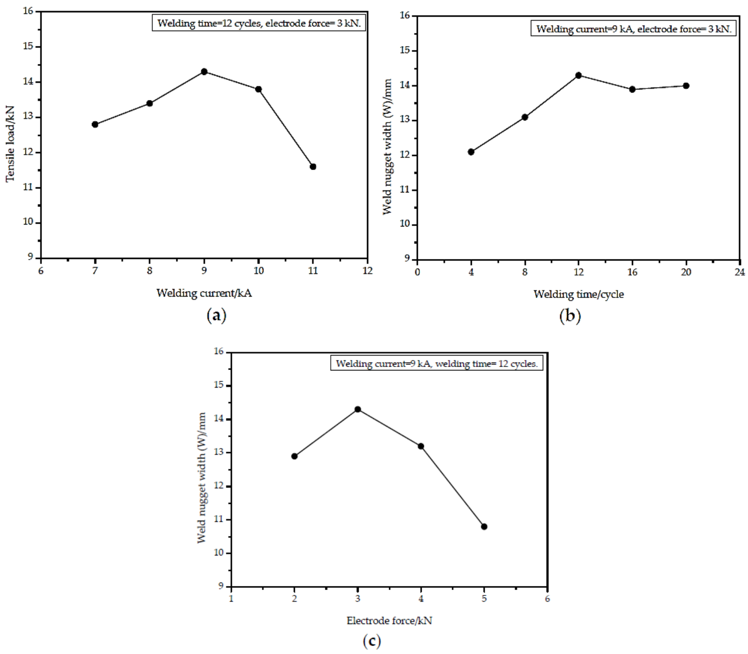

Figure 2.16 : Relations between welding parameters and tensile shear load and weld nugget width: (a) Welding current; (b) welding time; and (c) electrode force [6].

The sample width and weld diameter are also essential to affect the maximum displacement as well. The most valuable factor influencing the energy absorption in the weld is the weld diameter. The next in line is the width effect with less significant impact but still appropriate to support the process, followed by the width and diameter relationship factor and also with the width and length adjustment. To gain more reliable conclusions for the effect, the most common tested strength measurements such as energy, peak load, and maximum displacement in the mechanical testing method are considered to be conducted at once as the indicators for the research based on the experimental and statistical investigation [24]:

1. In the result of tensile-shear testing, the width of the sample was considered the most affected dimension.

2. As observed, the overlap of the sample was less critical and could be determined similarly with the sample width for simplicity.

3. Even though it was discovered that the sample length was supposed to be long enough to avoid its impact during the testing, but this dimension was also discovered less influential than the previous two. It was also considered that 150 mm was found sufficient as 25 mm was used to give clamping space, nevertheless, it was observed as longer than any of the specifications or standards

4. When establishing essential sample sizes for different gauges of materials, the weld diameter should be taken into account.

2.3.2 Chemical Properties

Titanium is a non-magnetic metal with excellent heat-transfer characteristics. Its lower coefficient of thermal expansion than steel and almost less than 50 percent of aluminum, gives it the advantage to withstand the extreme environment in response to a change of high temperature. The restriction of applicable temperature for reshaping and processing titanium and its alloys is still preserved even though they have a greater melting point compared with steel. It is as low as around 427°C (800°F) until 538°C to 595°C (1000°F to 1100°F). The composition of its alloys is still dominantly considered as the affecting factor of the selection. At temperatures up to 760^{o}C (1400 ^{o}F), titanium aluminide alloys show their potential. The commercially pure titanium (CP) meets the minimum criteria for corrosion resistance. In the United States, unalloyed titanium is often manufactured to ASTM standard specifications B 265, B 338, or B 367 in grades

1, 2, 3, and 4. These grades differ in terms of oxygen and iron concentration, which influence strength and corrosion resistance, respectively [23].

Titanium and titanium alloys display a swinging resistance against the harsh environment of widely various chemical exposures. It generates thin passive oxide film, invisible but deterrent to protect its base metal. The tenacious and cohort TiO_2 is the primary content in this film, its chemical stability proves essential to instantaneously heal itself when it is accidentally and mechanically damaged in the presence of even minor amounts of oxygen or water (moisture). This metal is even unaffected and maintains its capability to provide firm protection contrary to the upcoming oxidizing or acidic assault. In aqueous chlorides (e.g., brines, seawater) environment titanium is particularly well-known for its high resistance to localized attack and stress corrosion. As well as the other halides and wet halogens (e.g., wet Cl_2 or Cl_2^- sat. brines). This is also confirmed in the hot, highly-oxidizing, acidic solutions (e.g., FeCl3 and nitric acid solutions) where most commercial metals such as steels, stainless steels, copper, and nickel-based alloys can be severely damaged [86].

The other popular titanium alloy capabilities are their distinctive resistance against any accidental collision, erosion, or cavitation which are commonly generated by any liquid flowing and turbulent fluids. A similar case can be applicable and comparable in the weldment zones, castings and any forging process, because the same protective oxide surface film is developed and exist on most titanium alloys. Titanium alloy's usable resistance is limited, especially as the temperature rises in the range of moderate to high acid solutions such as HF, HCl, H_2SO_4, HBr, and H_3PO_4 at all expected concentrations. These are rather considered to be a reason why titanium alloys are more resistant to a wider variety of chemical conditions and temperatures than other metals such as aluminum, nickel-based alloys, copper, steels, and even stainless steel [86].

2.3.3 Microstructures

Titanium crystallizes in two different ways. One of them, at the room temperature of commercially pure titanium, is recognized as (α) phase with a hexagonal close-packed (HCP) structure. Then another phase is a transformed body-centered cubic (BCC) structure called beta (β) which transforms at 883 ^{o}C (1621 ^{o}F). The production arrangement and titanium alloys properties are based on this crystallographic management through the set up of alloying elements, weldments, or thermomechanical processing. These phases also serve as a useful classification system for titanium mill products. As a result, the classification is trippingly differed using the presence of α alloys, β alloys, or α+ β alloys amount in the material [5].

Aluminum and tin are among the elements found in α alloys. These -stabilizing elements function by either preventing or creating changes in the phase transformation temperature. α alloys have a highly creep resistance property which are rather considered as favorable in the high-temperature process than β alloys. α alloys are appropriate for cryogenic applications because they lack a ductile-to-brittle transition, which is a property of the β alloys [5].

α alloys have acceptable strength, toughness, and weldability, but they are less forgeable than β alloys [87]. As a result of the latter trait, there is a higher likelihood of forging faults. These issues can be mitigated by smaller decreases and frequent reheating. Heat treatment cannot be used to strengthen α alloys, and certainly unlike β alloys. They are most commonly employed in the annealed or recrystallized state to remove residual stresses from working [5].

As the most common and widely used type of titanium alloy, Ti-6Al-4V has fairly unique formability [20]. Although it tends to be difficult to anneal and shape, some heat treatment applications have proven to be well applied to the α + β alloys. At normal temperatures, α + β alloys can account for between 10 and 50% of the total phase depending on the composition at room temperature. This phase is quite dispersed and in its function will then support the nature of the α and β phases. Especially in β phase control which is often done, it can improve the quality of the properties. One of them is the aging process at a temperature of 460-650^{o}C which was previously preceded by solution treatment. This process can refine the α and β phases, especially changing the β phase for the better.

During the process, some β stabilizer alloys is added, a two-phase sistems are usually required and used. This may result in the retention of some β phases below the transus temperature until room temperature is reached. So that when the room temperature is reached, the β phase will be stabilized by a relatively small concentration of β stabilizer. Along with the addition of β phase stabilizers to the process, the percentage of the β phase will also increase at room temperature. From this, it can be described that α + β alloys with a large amount of α stabilizer and a small amount of β stabilizer have a unique ability to stabilize the phases, especially the β phase. Some of the transitions among the various heat treatment conditions can be seen in Figure 2.17.

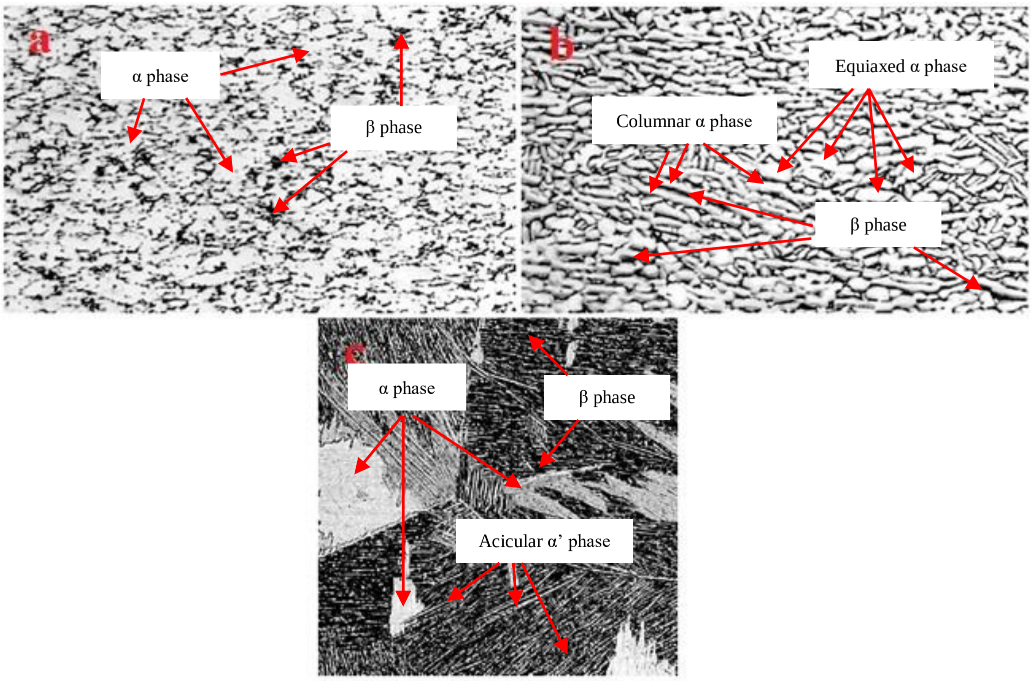

Figure 2.17 : (a) Ti-6Al-4V 100X Alpha-beta alloy 8mm (0.031 in.) sheet 788°C (1450°F)/15 Min., Air Cool (Mill-annealed condition); (b) Ti-6Al-4V 200X Alpha-beta alloy38mm (1.5 in.) plate 788°C (1450°F)/15 Min., Air Cool (Mill-annealed condition); (c) Ti-6Al-4V 100X Alpha-beta alloy38mm (1.5 in.) bar 1016°C (1860°F)/20 Min., Air Cool (Transformed-beta condition) [86].

Heat treatment, which involves quenching from a high α + β temperature and then aging at a somewhat lower temperature, can greatly strengthen two-phase titanium alloys. The quenching prevents the β phase change that would typically happen with gradual cooling. The aging cycle enables fine particles to precipitate from the metastable, giving it a stronger structure than the annealed α + β phase [86].

Transition elements such as vanadium, niobium, and molybdenum are found in β alloys, and they tend to lower the temperature of the α phase transition to β favors the growth of the BCC phase. They offer better forge ability than α alloys over a larger range of forging temperatures, and β alloy sheets can be cold formed in the solution-treated state. β alloys are hardenable and heat treatable. Solution treatment followed by aging at temperatures ranging from 450 to 650°C (850 to 1200°F) is a popular thermal treatment. In the retained, finely dispersed particles arise as a result of this treatment [5].

Kahraman et al concluded that the twinning display was rather observed clearly in the fusion zone as the deformation effect than the shearing, according to the microstructural study of resistance spot weld titanium sheet ASTM Grade 2. High pressure and welding duration were also found to promote twinning [7]. As shown in Figure 2.18, when the weld is held for the lower electrode force, the twinning form is not visible, and certain pores occur. When the electrode force is raised, however, the amount and dimension of twinning increases and the pores vanished.

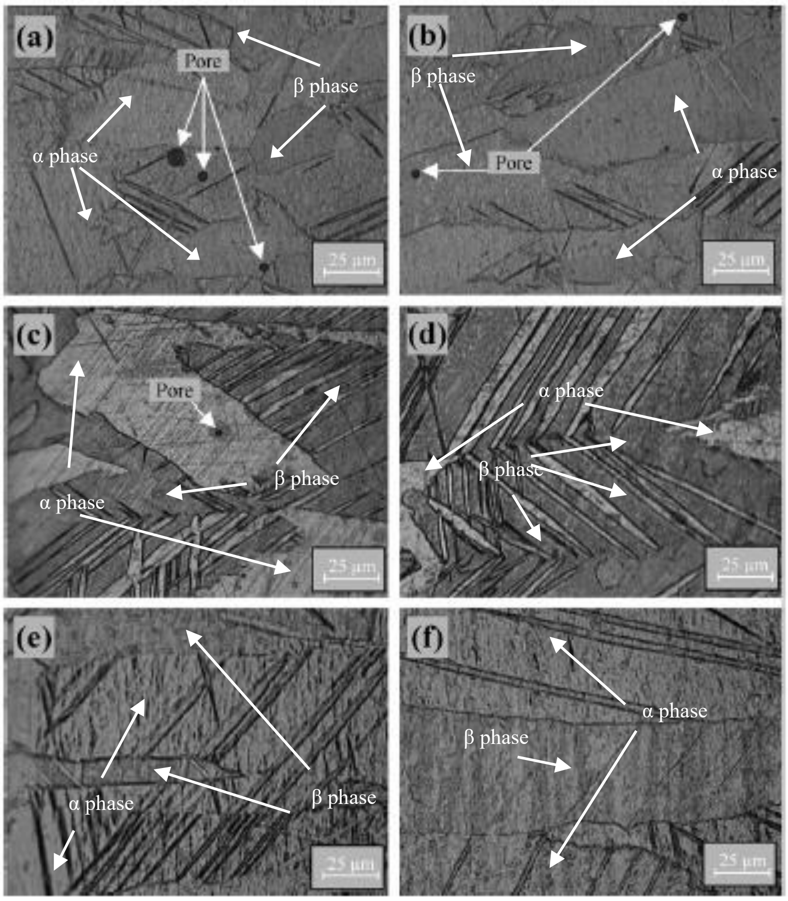

Figure 2.18 : Optical microscope images of the weld nugget of resistance spot welded joints joined at: (a) 2000 N, 15 cycle (b) 2000 N, 15 cycle-Argon (c) 4000 N, 15 cycle (d) 4000 N, 15 cycle-Argon (e) 6000 N, 15 cycle (f) 6000 N, 15 cycle-Argon [7].

Zhang et al on Ti-6A-4V discovered that the β phase was confirmed to be completely transformed into a coarse acicular α' and formed martensitic structure with the needle-like form in the fusion zone and also severely observed in the HAZ as shown in Figure 2.19, resulting in the fusion zone has the maximum hardness. The almost similar characteristic of the increased hardness is also discovered in the HAZ as its microstructure was consist of a mix of primary α, primary β, and a transformed of the β phase to fine acicular α ' phase. But the HAZ hardness was observed lower than the fusion zone but higher than the base metal [6].

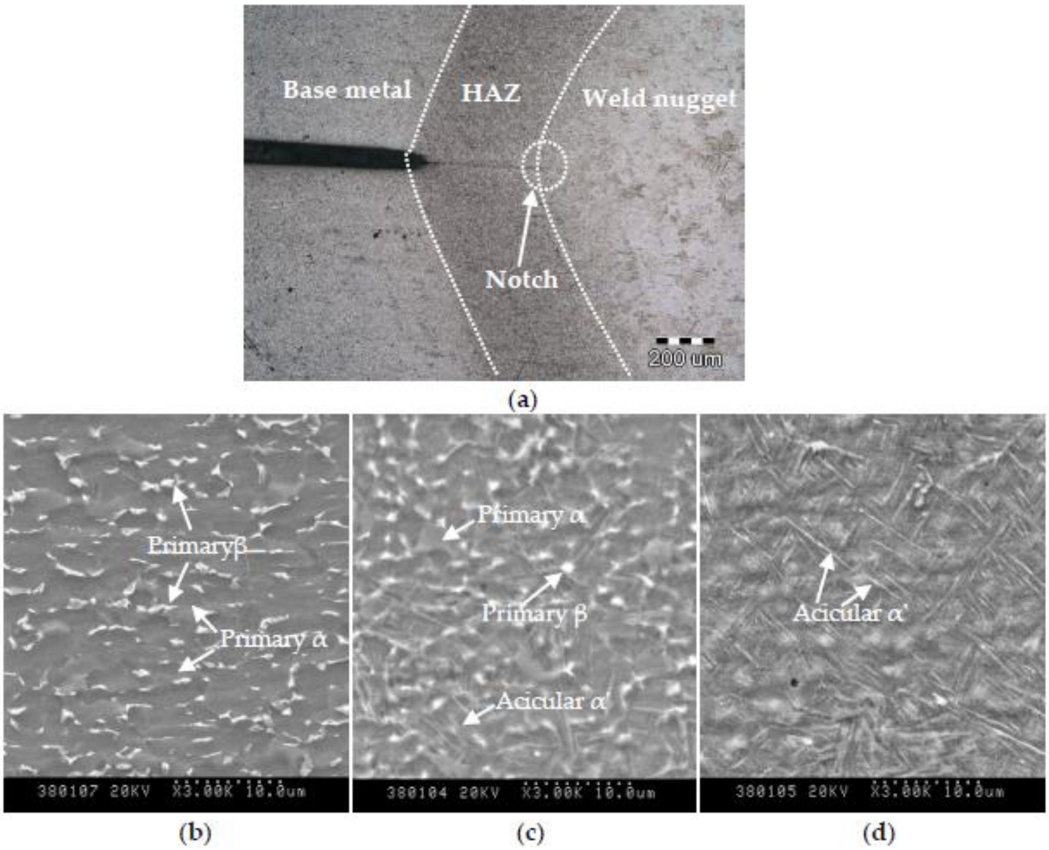

Figure 2.19 : Microstructure of: (a) Three zones (b) base metal (c) HAZ (d) weld nugget zone [6].

2.3.4 Hardness Distribution

The application of hardness testing allows for the evaluation of a material's qualities, such as strength, ductility, and wear resistance, and so aids in determining if a material or material treatment is adequate for the intended purpose. Kahraman et al conducted hardness testing to test the hardness distribution along with the base metal, HAZ and weld nugget cross-sectional as shown in the area as shown in Figure 2.20, then concluded that the hardness values for weld nugget were observed as the highest among all, followed sequentially by the HAZ and base metal. as shown in Figure 2.21 [7].

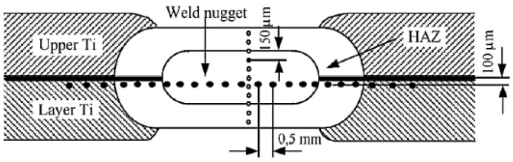

Figure 2.20 : Hardness measurement areas on the welded sample [7].

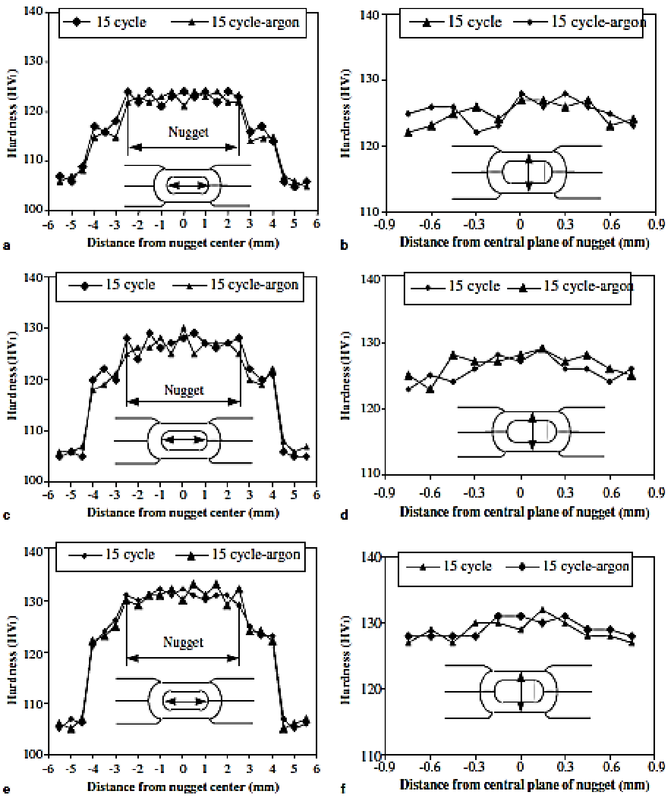

Figure 2.21 : Hardness of: (a) 2000 N, 15 cycle (b) 2000 N, 15 cycle-Argon (c) 4000 N, 15 cycle (d) 4000 N, 15 cycle-Argon (e) 6000 N, 15 cycle (f) 6000 N, 15 cycle-Argon samples welded at different parameters [7].

While Zhang et al concluded the same thing that both the weld nugget area and HAZ hardness are superior that in the base metal as shown in Figure 2.22, resulting in the transformed β phase into acicular martensite α' phase in the weld nugget and the combination of primary α, primary β, and a transformation of the β phase to fine acicular α' phase in the HAZ [6].

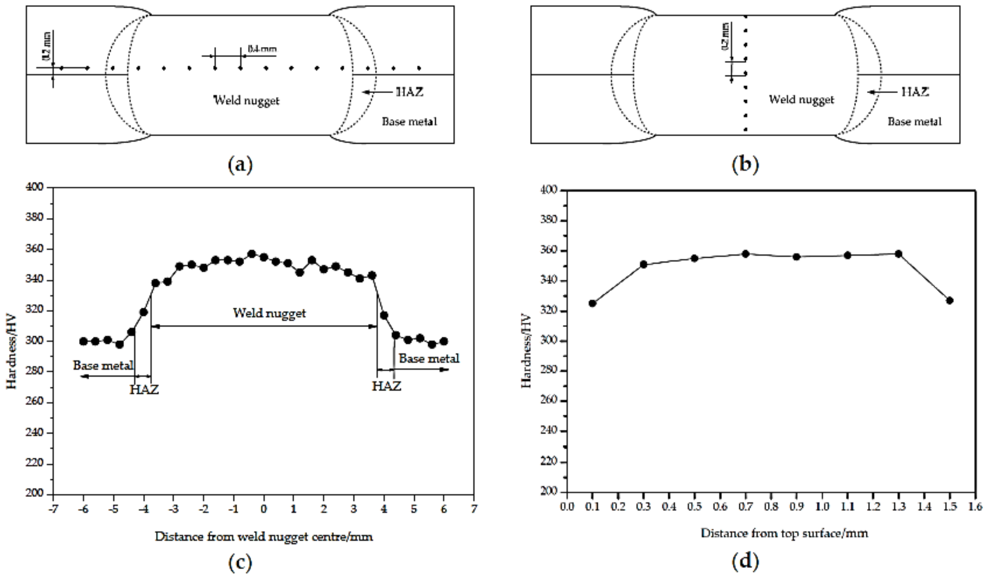

Figure 2.22 : a) Horizontal measurement location (b) vertical measurement location (c) horizontal hardness distribution (d) vertical hardness distribution [6].

2.3.5 The Optimization

In the previous studies, the outcomes for the study of the RSW parameters effect into titanium alloy Ti-6Al-4V weld properties are discovered as lack of information about the results. The list of the previous study can be observed in Table 2.1. The other limitation is that most of the studies did not use a design of experiment (DOE) in the approach, especially to find out the optimum level of RSW parameters. Whereas, this DOE will be helpful not only to find out the optimum level but also to define the most significant affecting parameters. The regression model can also be drawn from the DOE model, hence, the mathematical model is the outcome of this process. The characteristic of the microstructure was also discussed restrictively. The previous investigation didn't mention the clear transition between the β phase into the α' phase with the involvement of the RSW parameters changing. There was also a lack of information about the relationship among the expulsion, failure mode, microstructure, and hardness values. No, hesitate that the improvement in these matters such as applying DOE in the process, deeper discussion in physical and mechanical properties are giving sufficient better outcome and also better discussion matter.

The corrosion resistance transformation as the effect of localized heat input during the RSW process is also a pretty rare discussion matter in the previous studies. Although, the changing of the weld nugget behavior to regenerate passive anti-corrosion film in the surface is essential to be analyzed due to its benefit in the titanium alloy products. The thin or less dense anti-corrosion film in the weld nugget is susceptible to corrosion reaction particularly pitting corrosion. Where this type of corrosion is found common the RSW coarser grain boundaries, even in the atmospheric air condition [93]. This is a challenging question and also creates room for improvement, where this analysis about corrosion resistance study is no doubt will be essential to figure out.

Table 2.1 : Some of the investigation for RSW parameters effect on material properties and corrosion behavior

Year	**Author**	**Project Title**	**Finding**	**Limitation**
2005	Kahraman et al.,	The influence of welding parameters on the joint strength of resistance spot-welded titanium sheets	➢ The resistance spot welded samples tensile-shearing strength rose when welding duration and electrode force were increased ➢ The welding time had the greatest impact on the tensile-shearing strength of the welded samples, whereas the welding environment had the smallest impact.	➢ The welding current is constant, the variation of welding parameters focused on electrode force and welding cycle ➢ The study held into two different welds environments: air and controlled argon
2006	Vural et al.,	Effect of Welding Nugget Diameter on The Fatigue Strength of The Resistance Spot Welded Joints of Different Steel Sheets	➢ The increase of weld current also increases the nugget diameter of three combinations of welded joints in this study ➢ A similar steel sheet joint has a greater endurance limit than the dissimilar steel sheet joint.	➢ The variation of welding parameters only focused on weld current ➢ The study considered the effect of weld nugget diameter on the fatigue strength
2010	Shi et al.,	Effects of Welding Parameters on The Characteristics of Magnesium	➢ The RSW with cover plates is feasible to weld magnesium alloy	➢ The study is considered on one material of welded joint

Year	Author	Project Title	Finding	Limitation
		Alloy Joint Welded by Resistance Spot Welding with Cover Plates	➢ Adjusting electrode force and down-sloping time can inhibit pore formation	➢ A high number of weld current is needed due to the application of cover plate
2013	Pandey et al.,	Optimization of Resistance Spot Welding Parameters Using Taguchi Method	➢ The S/N ratio's response to tensile strength reveals that the welding current is the most important parameter controlling weld tensile strength, whereas holding time and pressure are comparably less important. ➢ According to the ANOVA approach, welding current holding time and pressure contribute 61%, 28%, and 4% to tensile strength, respectively.	➢ The study is lack experiments ➢ The testing method only consist of tensile-shear testing results, it doesn't mention the effect of microstructure and hardness distribution
2016	Long et al.,	Effect of Holding Time on Microstructure and Mechanical Properties of Resistance Spot Welds Between Low Carbon Steel and Advanced High Strength Steel	➢ The geometrical center of the total thickness is where the solidification line of the uneven thickness weld nugget is found. ➢ The results show that extending the holding time improves the weld joints and has an impact on the failure mode.	➢ The number of simulations using FEA is limited to two samples ➢ This study considered a wide range of holding time
2017	Zhang et al.,	Characteristics of Resistance Spot Welded Ti6Al4V Titanium Alloy Sheets	➢ The higher welding the more decrease tensile load. The more increase welding time, the more increase tensile loads.	➢ It comes with no design of experiment so that the number of experiments is low

Year	Author	Project Title	Finding	Limitation
			The more increased electrode force the more increase tensile load but at a certain point if it's continued to be increased the tensile load decreased ➢ The hardness results show that the weld nugget and HAZ are harder than the base metal	➢ The selection parameters of electrode force are less than the welding current and welding time so it does not correspond
2018	Anijdan et al.,	Optimization of Spot-Welding Process Parameters in Dissimilar Joint of Dual-Phase Steel DP600 and AISI 304 Stainless Steel to Achieve the Highest Level of Shear-Tensile Strength	➢ Variation of welding parameters highly affected to dissimilar spot-welding result ➢ Hardness profile on heat-affected zone shows different results between two different material interfaces	➢ The number of experiments is low due to the selection of the Taguchi method ➢ The study considered the small diameter of the welded zone
2018	Mansor et al.,	Microstructure and Mechanical Properties of Micro-resistance Spot Welding Between Stainless Steel 316L and Ti-6Al-4V	➢ Welding current is the most influenced welding parameter on this dissimilar type of welded joint steel ➢ Element composition analysis of the welded joint was observed	➢ This study is considered on a thin of thickness which is rarely applicable ➢ The optimum variation of welding parameters only to conduct the present experiment of this study
2018	Hafez et al.,	The Effect of Welding Atmosphere on The Pitting Corrosion of AISI 304L Resistance Spot Welds	➢ Depending on the type of shielding gas and heat input during welding, RSW nuggets of AISI 304L stainless steel	➢ AISI 304L austenitic stainless steel with a thickness of 1 mm was used in the experiment.

Year	Author	Project Title	Finding	Limitation
			display several sorts of pit morphologies and pit diameters. ➢ The corrosion pitting resistance of stainless steel welded nuggets deteriorates as RSW heat input is increased. ➢ At extremely low heat input, both argon and nitrogen have no discernible influence on the pitting resistance of spot-welded nuggets. ➢ The CPP experiments indicate that nuggets welded under argon have a higher corrosion potential than those welded under nitrogen or air with low heat input.	➢ The welding current was varied from 3.3 to 7.1 kA in this investigation, while the squeezing time, holding time, and welding duration, as well as the electrode force, were held constant at 5, 30, and 35 cycles and 1.2 kN, respectively.

2.3.6 The Mathematical Model

The mathematical model is used to translate problems from one application field into traceable mathematical formulations, which can then be analyzed theoretically and numerically to provide insight, answers, and advice for the original application. Generating a mathematical model can help the possible future research and also make it easier to do. Linear regression is used to determine the mathematical model of the weld nugget diameter and the tensile-shear maximum load in this research.

The most basic linear model has only one independent variable and asserts that when the value of the independent variable grows or decreases, the real mean of the dependent variable changes at a constant pace. As a result, the equation of a straight line is the functional connection between the real mean of Y_i, represented by $\mathcal{E}(Y_i)$, and X_i as expressed in equation (2.3) [88].:

$$\boldsymbol{\mathcal{E}}(\boldsymbol{Y_i}) = \boldsymbol{\beta_0} + \boldsymbol{\beta_1 X_i} \tag{2.3}$$

Where,

$\mathcal{E}(Y_i)$: The functional connection between the real mean of Y_i

β_0 : The intercept, the value of $\mathcal{E}(Y_i)$ when $X = 0$

β_1 : The slope of the line,

X_i : The rate of change in $\mathcal{E}(Y_i)$ per unit change

The dependent variable's observations Y_i are considered to be random observations from populations of random variables, with each population's mean determined by $\mathcal{E}(Y_i)$. To produce the statistical model, the divergence of an observation Y_i from its population mean $\mathcal{E}(Y_i)$ is taken into account by adding a random error ϵ_i in equation (2.4):

$$\boldsymbol{Y_i} = \boldsymbol{\beta_0} + \boldsymbol{\beta_1 X_i} + \boldsymbol{\epsilon_i} \tag{2.4}$$

i = 1,2,…,n denotes the observational unit. The n observations on the independent variable are referred to as the X_i, and they are considered to be error-free measurements. That is, the observed X_i values are taken as a collection of known constants. Both the Y_i and the X_i are paired observations, and both are measured on each observational unit [88].

The multiple regression model is utilized if the response Y_i is impacted by more than one predictor variable and it is also linked with the mathematical model for this study. The investigator has control over these variables, but the yield may be influenced by uncontrolled factors such as those related to the environment. A linear model relating the response Y_i to several predictors has the form of equation (2.5):

$$\boldsymbol{Y_i = \beta_0 + \beta_1 X_1 + \beta_2 X_2 + \cdots + \beta_3 X_3 + \epsilon} \tag{2.5}$$

The regression coefficients are the numbers β_0, β_2, …, β_k. As ϵ allows for Y_i variance that is not explained by the x-factors. This random fluctuation might be attributable in part to unknown or unobserved factors that influence Y_i. So, while the Y_i model is linear in terms of β parameters, it is not necessarily linear in terms of X_i. Thus the model is expressed by the equation (2.6).

$$\boldsymbol{Y_i = \beta_0 + \beta_1 X_1 + \beta_2 X_1^2 + \beta_3 X_2 + \beta_4 sin\, X_2 + \epsilon} \tag{2.6}$$

Are included in the designation *linear model* [89].

As a reference Gawai et al., 2019 discovered that during experimentation, regression analysis on produced data yielded the mathematical model indicated by equation *x*. In the relationship between the nugget diameter and the parameters, the regression equation is determined and expressed in equation (2.5). It is seemingly that the welding pressure is giving more effect to the nugget diameter development as expressed by the equation (2.7) [90].

$$\textbf{\textit{Nugget dia.}} = \mathbf{2.56 + 0.0075}\ \textbf{\textit{Weld Cycle}} + \mathbf{0.330}\ \textbf{\textit{Current}} - \mathbf{0.390}\ \textbf{\textit{Pressure}} \tag{2.7}$$

The generated regression equation for tensile strength is much affected by welding pressure founded from its variable's coefficient. The expressed formulation is given by equation (2.8) [67]:

$$\textbf{\textit{Tensile Strength}} = \mathbf{160 + 3.91}\ \textbf{\textit{Weld Cycle}} - \mathbf{6.59}\ \textbf{\textit{Current}} + \mathbf{9.5}\ \textbf{\textit{Pressure}} \quad (2.8)$$

2.3.7 Corrosion Behavior

In order to understand the corrosion condition of the Ti-6Al-4V weld nugget, it needs to be analyzed the corrosion rate and pitting corrosion behavior against the welding parameters to find the optimum one. Titanium alloys have a unique corrosion resistance mechanism as well as stainless steel by generating thin, invisible but very strong and protective surface oxide called TiO_2. This film provides outstanding resistance against various widely harsh chemical environments especially acidic assault [86].

In the RSW, the weld nugget area properties including its strength are commonly influenced by heat generation, in addition, the microstructure is also gradually transformed by the combination of thermal process and significant cooling rates. Furthermore, the stainless steel surface is heated locally, resulting in the formation of a colored oxide film known as heat tinting. The heat-tinted region's corrosion resistance is decreased, and they are more vulnerable to pitting corrosion than the unaffected base material [91].

It is considered necessary that weld nugget corrosion rate and the most common corrosion type must be analyzed regarding the RSW parameters to obtain the optimum design of Titanium alloy Ti-6Al-4V against possible corrosion events in the future. The electrochemical reaction is recognized widely as the most basic corrosion reaction. A chemical process that involves the transfer of electrons is known as an electrochemical reaction. It's also an oxidation-reduction chemical process. Because metallic corrosion is nearly always an electrochemical process, understanding electrochemical processes at their most fundamental level is critical [92]. For example, from the anodic reactions, if the current generated from this process of metal can be found, then the current would be possibly converted into corrosion rate using Faraday's law [92].

Pitting is the most frequent kind of localized corrosion, in which tiny amounts of metal are removed from specific places on the surface by corrosion, resulting in severe craters or pits. In the RSW nugget, the weld nugget has a different characteristic than the base metal. The localized heating area which becomes the weld nugget will serve as the anode as it has a lesser corrosion protection layer than the base metal. The base metal itself will be the cathode. Commonly in most RSW products, the base metal area will be larger than the weld nugget. This condition is fit for pitting corrosion to occur when the cathode area (damaged coating) is larger than the anode area (exposed metal) [93]. A thorough penetration or a large undercut of the thickness of a metal item is eventually caused by the depth of a pit. The breadth of the pit may widen over time, but not to the same degree as the depth. Most of the time, the corrosion product covers the pit entrance, making it difficult to identify during the inspection. Figure 2.23 reveals the mechanism of the pitting process in a broken mill scale that is becoming the cathode [91].

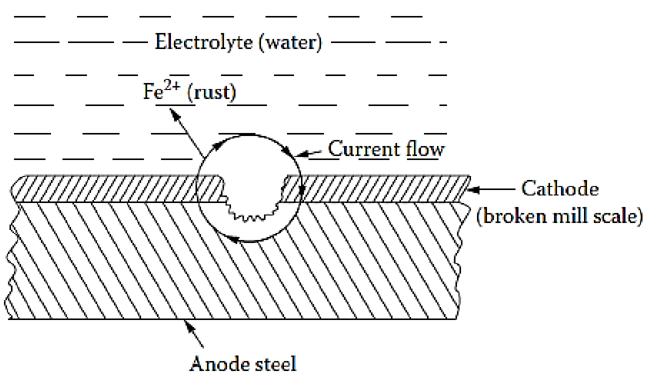

Figure 2.23: Formation of the pit from a break in mill scale [91].

Even if there is plenty of sound material left, pitting can induce structural failure due to localized weakening effects. The reduction of properties or damage presence like stress corrosion cracking, fatigue failure, brittle failure, etc. in the material or weld nugget may also be produced caused by the pits. The different potential when there is an electrical contact between dissimilar metals, or between concentration cells is also the major mechanism that produces and promotes pitting. These result in an electric current flowing from the metallic anode to the adjacent cathode through the water or over moist steel [91].

The previous study that closely engaged the study of corrosion on titanium alloy was the investigation of the gas shielding such as argon and nitrogen influence for austenitic stainless steel welds of 1 mm AISI 304L corrosion resistance improvement and the effect on pitting corrosion. Even though different, the AISI 304L also has high corrosion resistance like titanium alloy. The cyclic potentiodynamic polarization (CPP) was the method selected to conduct the investigation with 3.5% NaCl as the solution. The process was held to reveal any phenomenon in the weld nugget re-passivation of film resistance and against pitting corrosion that hit the fusion zone area. Pictures which are shown in Figure 2.24 revealed the optical observation upon various weld nuggets in the fusion zone during the CPP test in which the pittings were spotted in various dimensions.

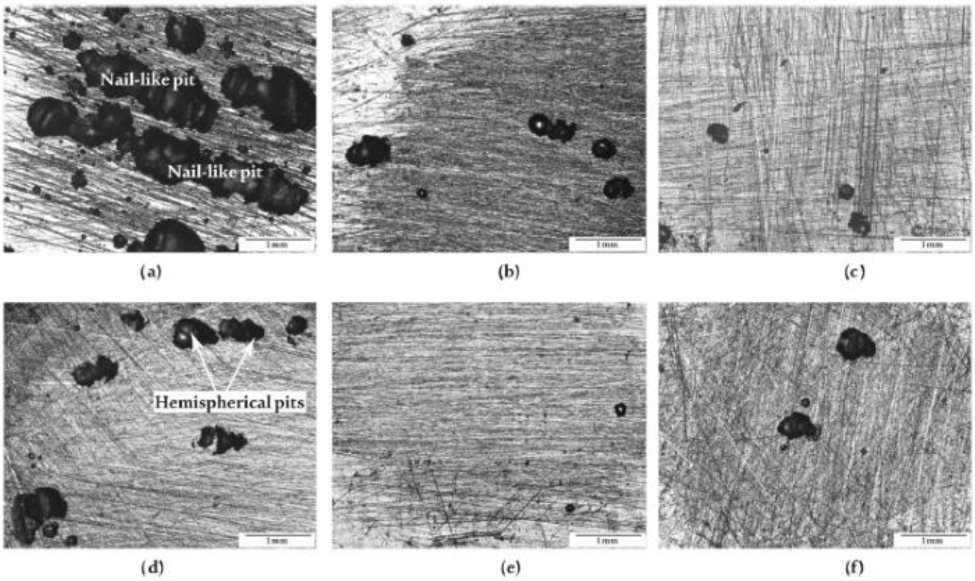

Figure 2.24 : Pitting morphologies on the nugget surfaces after CPP test: (a) Spot welded with high heat input on air. (b) Spot welded with high heat input on nitrogen. (c) Spot welded with high heat input on argon. (d) Spot welded with low heat input on air. (e) Spot welded with low heat input on nitrogen. (f) Spot welded with low heat input on argon [93].

The pit morphologies were displayed within the range of the largest size to the smallest and from the nail-like until hemispherical pits, all were captured optically [93]. Furthermore, the findings indicated that most of the large and deep nail-like pits were observed shattered in the weld nugget of the RSW process without any shielding gas or held in atmospheric air condition. The other RSW processes which used nitrogen and argon in various low and high heat inputs showed less amount and smaller hemispherical Pitts. The type of shielding gases and the amount of heat input as the RSW parameters result were appeared to be much influence for the generation of pits type whether it was large or small, shallow or deep. Figure 2.25 shows a high-magnification SEM picture that shows the pit started by breaking down the passive layer on the welded surface [93].

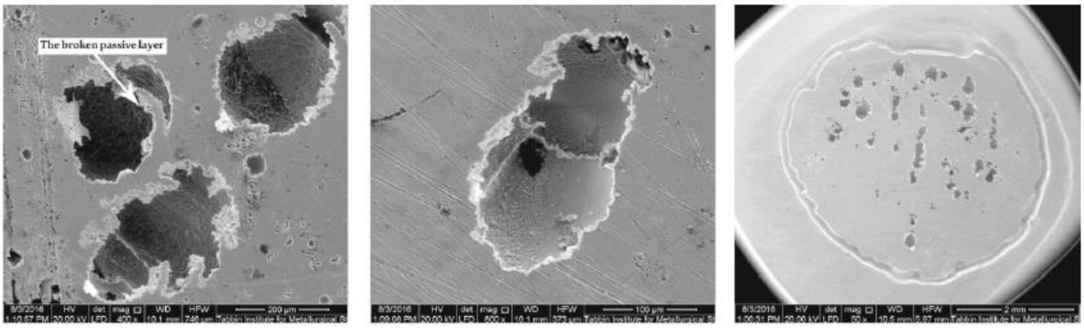

Figure 2.25 : SEM of the nugget pits after CPP test [93].

A significant comparison between the base metal of AISI 304L with the other various weld nugget in a constant welding time of 30 cycles is depicted in Figure 2.27. The comparison was likely forwarded in the positive direction or hysteresis similarly for all curves in the CPP test results. These results were generated particularly caused by the passive current or in another way can be called the anodic current of the backward scan is valued greater than its value in the forward scan. Furthermore, it was clearly shown by the reverse polarization curves that the re-passivation potential was not indicated that it was regenerated instantaneously in the forward polarization scan's breakdown potential and corrosion potential zone, or in other words, it was constantly damaged. This indicated that the breakdown of the passive film gave significant changes in the weld nugget resistance capability and after it occurred, the weld nuggets were unable to re-passivate [93].

A higher negative corrosion potential was observed occurred in the reverse polarization curves. Their curves crossed the forward polarization curves cathodic section and were recognized as an obvious indicator. The plot of polarization results is denoted in Figure 2.26. The corrosion current density (i_{corr}), the corrosion potential ($E_{corr.}$) and the pitting corrosion potential ($E_{pitting}$) are the required values to determine the susceptibility [94]. The sample's surface morphology transformation is seemingly plenty affecting this matter, particularly in high current density during the long time of scanning for the forward polarization scan. It can be described from the curves that the highest pitting corrosion potential ($E_{pitting}$) has adhered in the base metal zone. The other weld nuggets experienced corrosion resistance lowering and subsequently the corrosion potential ($E_{corr.}$) was overseed to have decreased.

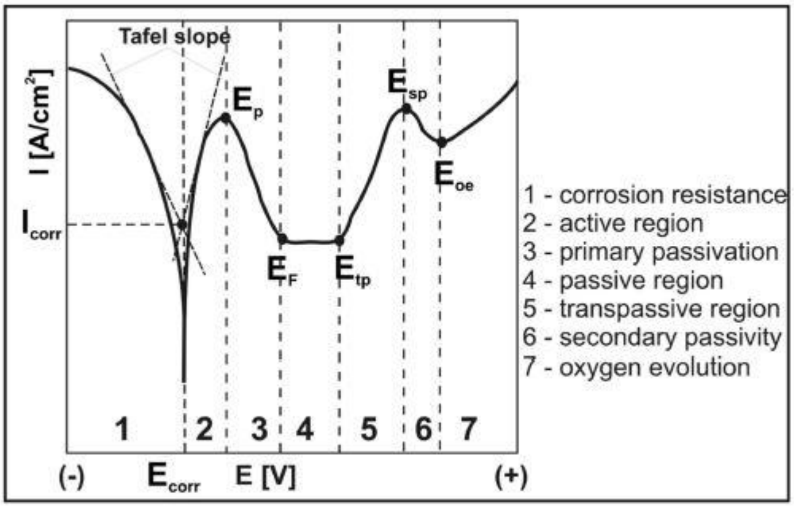

Figure 2.26 : The hypothetical polarization curve scheme [94]

However, the indicator of pitting corrosion resistance tenacity did not rely on the value of anodic current which is already visible that the weld nuggets had lesser anodic current than the base metal zone. The potential difference between $E_{pitting}$ and $E_{corr.}$ (described as $\Delta E_p = E_{pitting} - E_{corr.}$) is mainly used to determine the indicator of the corrosion resistance transformation. This indicates the capability of the material to protect its body by the passive film from the initial pit that is generated in the localized corrosion process. The higher resistance of the material to resist pitting is indicated by the higher amount of ΔE_p during the CPP test. The curves in Figure 2.27 describe that the base metal which has the higher ΔE_p is superior among all weld nuggets, leaving the weld nuggets are vulnerable and susceptible in any pitting corrosion design [93].

The CPP with a 3.5 percent of NaCl solution results revealed that the high heat input during RSW contributed as the very influential factor to decrease the weld nugget corrosion resistance against any pittings, compared with other weld nuggets with the lower heat input. It was also discovered that the heat input also gave a relationship with the weld nugget's shape and dimension.

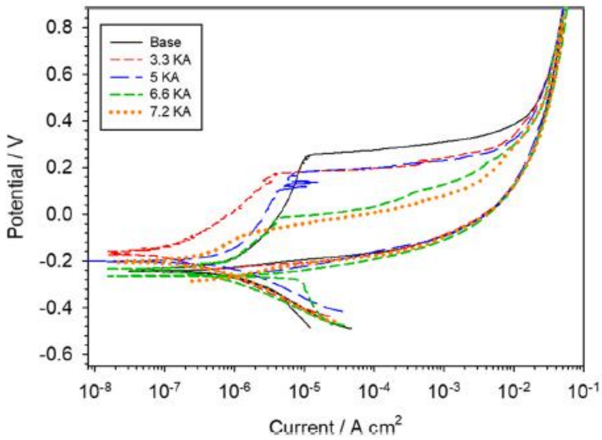

Figure 2.27 : Cyclic potentiodynamic curves for AISI 304L spot-welded nuggets, with different heat inputs [93].

This relationship also expressed that the heat-tinted oxide was dominantly probed circling the weld nugget, its size and color were depended upon the amount of heat input applied on the weld nugget. The low amount of heat input was explicitly predisposed to transform the weld nugget in smaller size accompanied with light yellow color surround it as depicted in Figure 2.28. But increasing the amount of heat input is gradually transforming the weld nugget into a larger size and turned color of the heat-tinted oxides to dark blue [93].

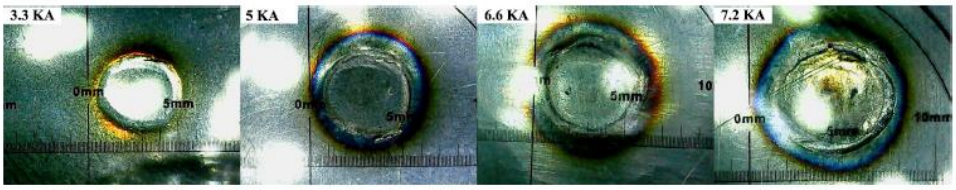

Figure 2.28 : The display of various weld nuggets from various welding currents [93].

The contribution of heat-tinted oxides in reducing the weld nugget corrosion resistance is appeared to be confirmed as having no hesitancy. Increasing the heat input increased dendritic thickness/width (close with the fusion border) as appeared in Figure 2.29 which describes the microstructure of the weld nugget [93]. High amount of heat input related is to this phenomenon, causing the delayed cooling rate, coarsening the grain in the fusion zone gradually.

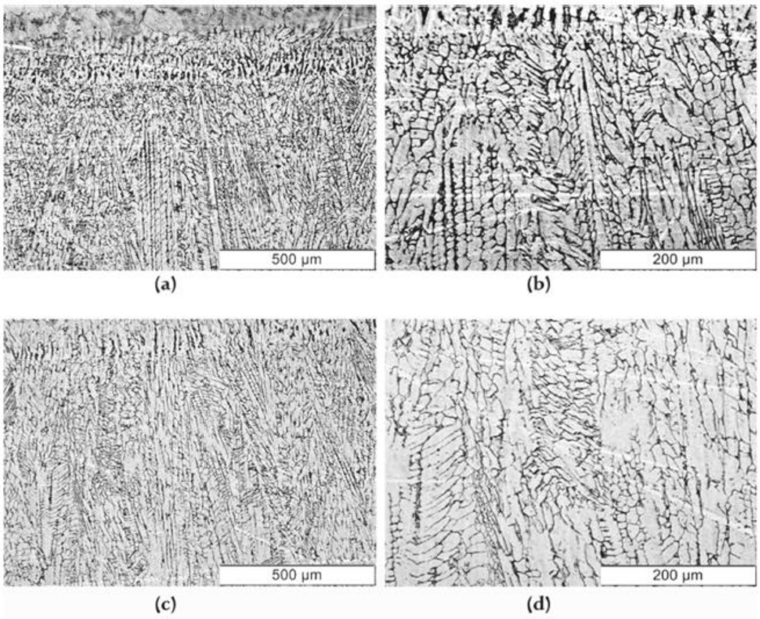

Figure 2.29 : Microstructure of the spot-welded nugget with different heat inputs. Electrolytic etching with NaOH solution a, b at 5 kA and 35 cycles, and c, d at 7.2 kA and 35 Cycles [93].

The coarser grain of δ-ferrite allows the thin passive film upon the fusion zone to become unstable, making its disintegration simpler. Furthermore, high residual strains caused by high heat input may also impact pitting corrosion susceptibility. According to Lu et al., excessive heat input is expected to affect alloying element exclusion and the creation of Cr-depleted zones, leading to the breakdown of localized corrosion resistance [95]. A similar investigation may be applicable for Ti-6Al-4V with the approaching of the similar corrosion resistance mechanism between AISI 304L and Ti-6Al-4V. It was well known that Ti-6Al-4V also created the thin layer of TiO_2 on the surface to prevent any corrosion [86] as on the stainless steel as well. But the other properties such as microstructure, stiffness, density, etc. are perhaps affecting different conclusions in the end. The selection of the test method, chemical solution, and sample size are appeared to be essential to be considered to enhance the accuracy of results.

2.4 Chapter summary

This chapter contains a general explanation of the welding process, its types, specifically discusses resistance spot welding (RSW), the influence of its parameters on the quality of weld nuggets and their effect on Ti-6Al-4V properties. RSW is quite popular today as an effective and efficient welding method on the metal sheets. The heat transferred by the electrode to the metal which is the main factor in metal joining can be controlled by optimizing the main parameters, namely welding current, time and force. For titanium alloy sheet, especially Ti-6Al-4V which is the object of this study, welding with the RSW method is very suitable, besides being quite effective, it can also create joints with high strength. The Ti-6Al-4V microstructure consists of an α phase with Ti as its main component contributing to increase strength and a β phase with Al and V elements as its main components contributing to increase ductility and weldability. In sufficient heat, it can partially transform the β phase into an acicular α' phase which can increase the weld strength thereby creating an appropriate weld. The level of hardness in the fusion zone with a significant number of transformations from β phase to α' phase gives a higher hardness value in the fusion zone than HAZ and base metal. In the corrosion field, the thin film created by the oxidizing Ti element to form TiO_2 compounds which actually provides quite effective protection against corrosion on the Ti-6Al-4V surface. However, it is necessary to further investigate whether heat exposure in the localized heating area during the RSW process can reduce the corrosion resistance ability. So far, no studies have been conducted to investigate this. In the study of the effect of RSW on corrosion of metals such as stainless steel AISI304L, which has the same anti-corrosion film formation pattern, it was proven that increasing heat during the RSW process can reduce the corrosion resistance ability of weld nuggets.

CHAPTER 3

METHODOLOGY

3.1 Chapter Overview

This chapter describes the methodology of how the data is obtained to encounter the research objective. The methodology overview is generally explained by the methodology section that shows a brief step by step of research study explanation. This study is divided into five main phases. In the first phase, the material and equipment preparations are conducted. The samples were cut using cold cutting such as the EDM to avoid early microstructure transformation before welding. The cuts are done according to the standard measurement. After the cuts, all of the samples were polished to clear the surface area. In this phase, the equipment is also inspected and checked particularly the RSW machine. The possible dressing for the RSW electrodes is also considered due to maintaining the weld quality.

The second phase consists of the RSW trial for the free samples, designing the design of the experiment based on the L9 orthogonal array of the Taguchi method (RSW parameters as the variables), and conducting the RSW experiment for 9 samples. The trial was done to ensure the performance of the RSW machine and to get a proper welding position for the experiment. The RSW parameters which were used as the Taguchi variables consist of welding current, time, and force. The third phase is for welding result characterization. In this phase, the physical and mechanical properties of the weld nugget were investigated. The tensile-shear testing was carried out to get the maximum load as the response of the Taguchi table for ANOVA and multiple regression analysis. This ANOVA gives the optimum level parameters as the best result from the Taguchi variables and also the most significant parameter in the RSW affecting the weld nugget tensile-shear strength. The multiple regression analysis established the mathematical models with tensile-shear maximum load and welding diameter as the dependent variables. The confirmation test will be taken to ensure the result of optimum level sample tensile-shear strength is the best of the Taguchi variables. To obtain the microstructure images, the optimum level sample was cut in the center to get the cross-sectional area using cold cutting of EDM. The sample was etched first to get obvious grain boundaries in the sample's cross-sectional area. The microstructure images of base metal, HAZ & fusion zone were captured using the SEM. The hardness values were also tested using this sample and were conducted using Vicker's microhardness testing method. From these entire results, a structural analysis was conducted to interpret the scientific relationship from the whole weld nugget physical and mechanical properties results.

The fourth phase was corrosion testing to get the investigation result of weld nugget corrosion rate and pitting susceptibility. The optimum level sample was used, but the RSW parameters were varied again for the most significant parameter of the ANOVA result, while the others were left constant. The test was conducted using potentiodynamic polarization testing. Form this test the pitting point and corrosion rate was achieved to view the relationship between the parameters variation with its corrosion response. To get clear images of the pitting existence from the sample's cross-sectional area, optical microscopy was utilized to support the hypothesis. The last phase of this study is comprehensive data analysis and concluding. The methodology process is illustrated in Figure 3.1. Based on the methodology process flow, the first, second, and third objectives are achieved by completed phases I, II, and III while the fourth objective is obtained by completing phase IV.

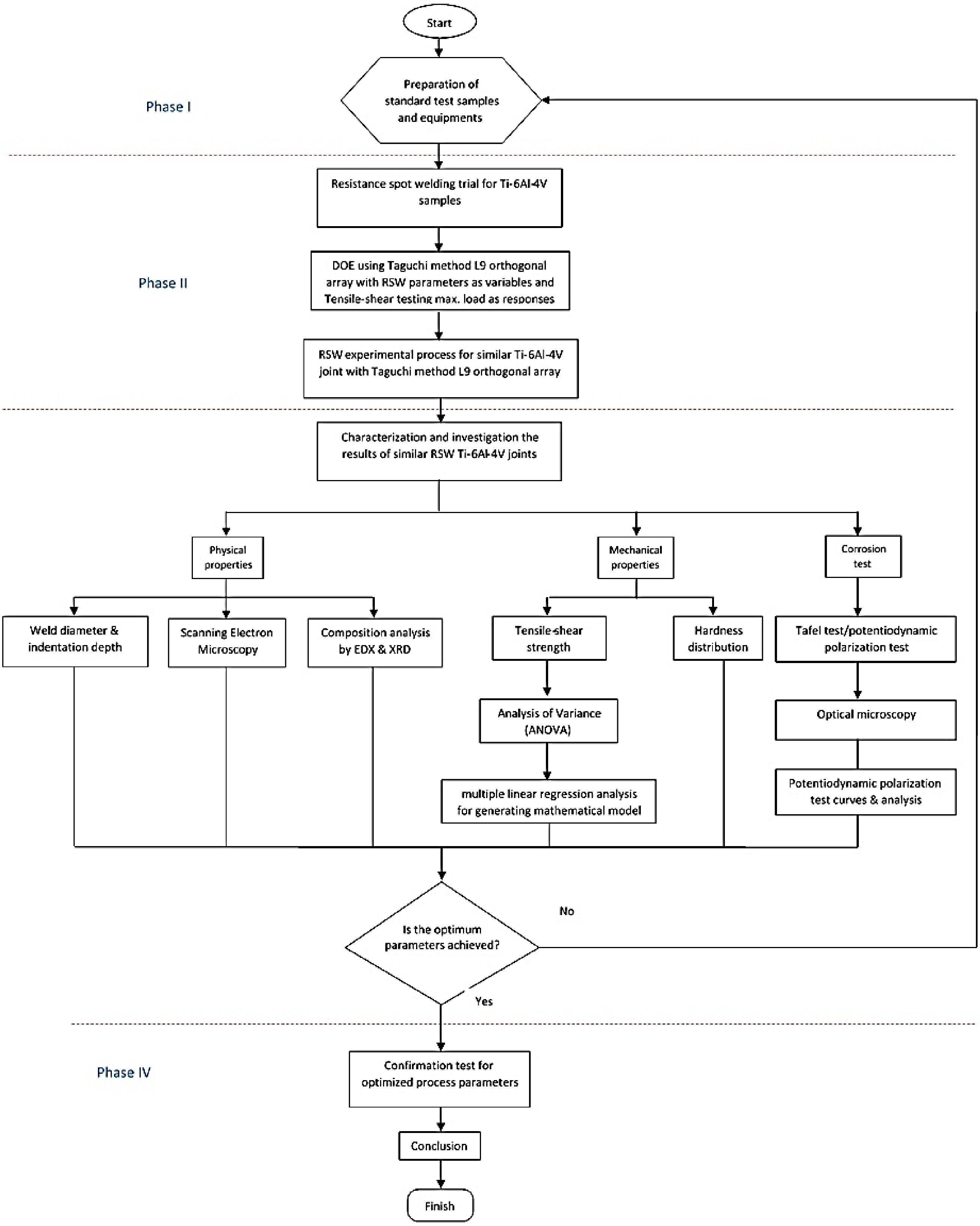

Figure 3.1 : Methodology process flow

3.2 Research Design

The Design of Engineering (DOE) is an effective method for discovering novel processes, getting a better understanding of current processes, and improving these processes to achieve the greatest results. DOE is an experimental method in which the effects of several factors are investigated at the same time by conducting experiments at varying levels of the factor [96]. The Taguchi Method will be used to design the experiment of this study. Dr. Genichi Taguchi developed the Taguchi design as a methodology set, by which at the design stage the manufacturing processes and materials' inherent variability can be taken into account [97]. The Taguchi design is much more effective than a fractional factorial design because the design is simply focused on orthogonal (balanced) experimental combinations and is quite similar to the DOE but different from the DOE in terms of processes [98]. The effect of several parameters can be determined efficiently with matrix experiments using the Taguchi method and the analysis of variances was employed to find the significance of the factor effects.

The level of the full factorial design is shown in Table 3.1 Three levels of control factors are referred to as low, medium, and high. Weld strength was taken as the output variable; welding Current, welding time, and electrode force were taken as input parameters for observing the weld strength.

Table 3.1 : Level of the Factor of Taguchi Method.

Control Factor	Level 1	Level 2	Level 3
Welding Current (kA)	8	9	10
Welding Time (Cycle)	28	30	32
Electrode Force (kN)	3	4	5

While the parameters of squeeze time, hold time and off time will be made constant for 35, 15 & 0 cycles respectively. Table 3.2 shows the experimental design of this study in which the maximum load of tensile-shear testing & corrosion rate would be collected by using the Taguchi method. The Taguchi method L9 was chosen to conduct the experiment and to analyze the tensile-shear, microstructure, hardness, corrosion on this research at once, and to validate the data results, repeatability of the experiments also required and chosen 3 times. The L9 was chosen because it gave effective measurement with less samples and levels are sufficient to discover the optimum parameter. In this method required 9 levels of experiments but with 3 repeatability which required 27 samples for tensile-shear testing, and also 1 sample to analyze the microstructure and hardness distribution (for the optimum level of parameters only regarding the tensile-shear testing result). While for the corrosion will be analyzed only at the 3 different level parameters based on the optimum level as a result of the Taguchi method.

Table 3.2 : Experimental Design Using The Taguchi Method Design of Experiments

Experiments	**Welding Current (kA)**	**Welding Time (cycle)**	**Welding Force (kN)**
1	8	28	3
2	8	30	4
3	8	32	5
4	9	28	4
5	9	30	5
6	9	32	3
7	10	28	5
8	10	30	3
9	10	32	4

3.3 Experimental Activities

The activities of this study involve 4 main phases. The first phase is the preparation of the standard test sample for titanium alloy Ti-6Al-4V. The second phase is the experimental procedure of the RSW according to the design of the experiment. The third phase is determining the mechanical and physical properties of the welded joint. This phase consists of determining tensile-shear strength, microscopy analysis, SEM, EDX, hardness distribution, weld nugget diameter, and corrosion examination (corrosion rate and pitting susceptibility). The last phase is data analysis using analysis of variance and mathematical model of the RSW experiments.

3.3.1 Sample Preparation

In this study, the material used for the experiment is titanium alloy of Ti-6Al-4V ASTM Grade 5 sheet with 3 mm of thickness. Geometric factors are also very important to generate better weld and tensile-shear testing results. Zhou et al. [24] determined critical sample sizes for RSW by analyzed the dimensional factors which have a significant impact on the weld strength measurements. On the maximum displacement, the sample width had a significantly greater impact than other factors. Because of this matter, ASTM standard D1002 was adopted as a result of approaching because the dimensions according to it (length, width, overlap, and area in test grip) was corresponded, particularly for tensile-shear testing, and described as the lap joint sample as can be seen in Figure 3.2.

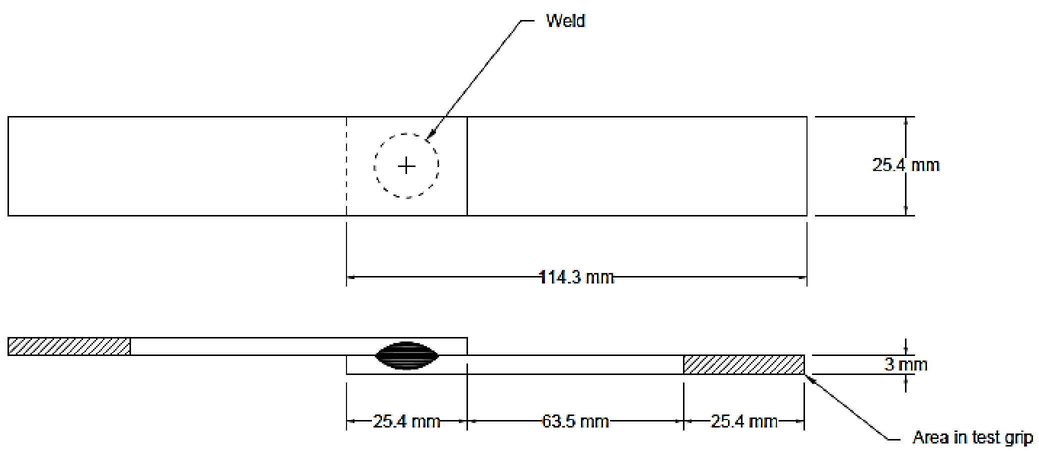

Figure 3.2 : Sample dimension based on ASTM D1002 standard [102].

Weld diameter is determined based on the equation (3.1):

$$\mathbf{d = a\sqrt{t}} \tag{3.1}$$

where,

d = weld diameter

a = a constant range between 3 and 6

t = sheet thickness

This formula is similar to the Koenigsberger [103], as for ”a” is a constant range between 3 and 6, then a constant value of 5 is chosen then according to the formula on the above the weld diameter is 8 mm. To cut the 3 mm Ti-6Al-4V sheet properly without having microstructure transformation, less heating cutting or cool cutting must be performed. To obtain the optimum cutting, the EDM cutting was performed for the samples. The visual display for the samples after the cut is shown in Figure 3.3.

The thickness of the sample also affected the amount of heat generation due to its greater resistivity. This required deeper penetration in order to achieve a suitable weld nugget to the inside of the sample. The shape of the lap joint also helped conformity when tensile-shear testing was carried out using a tension-testing machine, so that the sample was properly gripped on the machine grip and facilitates the testing process.

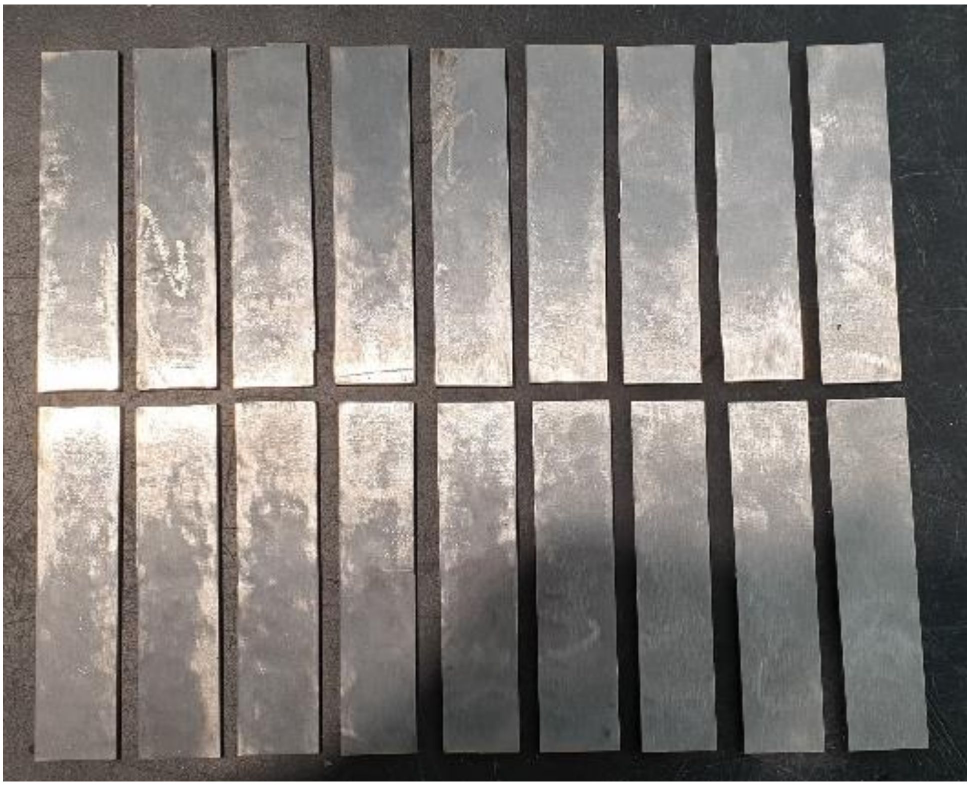

Figure 3.3 : The RSW samples after EDM cutting

3.3.2 RSW Machine and Procedure

The RSW machine that was used for this experiment is Daiden Spot Welder Type SL-AJ 35-600 as can be seen in Figure 3.4. The machine used has sufficient capacity to perform RSW up to a maximum welding current of 14.9 kA and a maximum welding force of 5.4 kN. This machine is available at the Workshop at Universiti Teknologi Petronas (UTP). The RSW machine standard operating procedure (SOP) is described in APPENDIX A. The welding result could be imperfect, it depends on the positioning and setting up the parameters. Some of the expulsions could defy the excellent shape and rejected the results. Focusing and keep on the SOP track is also the key to experiment success. Their assistance during the experiment was also sometimes unavoidable needed but was not taken precedence. The weld nugget results are shown in Figure 3.5.

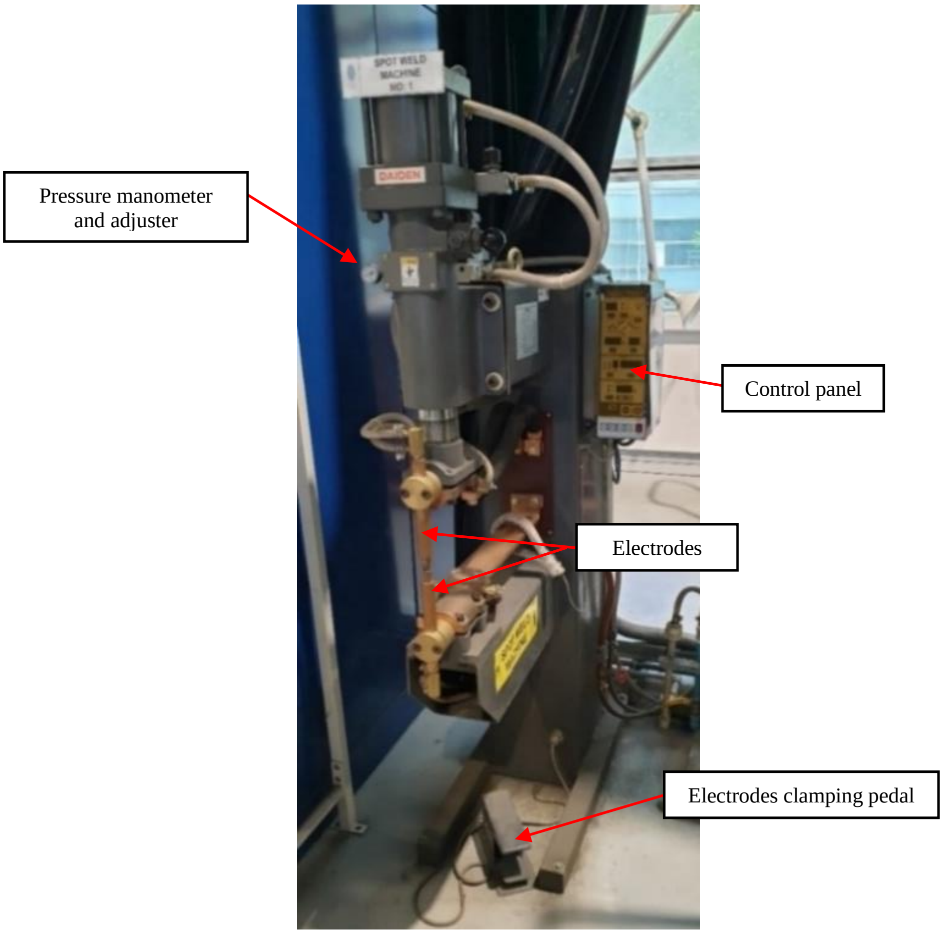

Figure 3.4 : The RSW machine that was used for the experiment

The specification of the machine is described below:

- Brand : Daiden
- Type : SL-AJ 35-600
- RTD Capacity : 35 kVA (AT50%DUTY CYCLE)
- Max. Input : 91 kVA
- Phase : Single
- Pri. Voltage : 415V
- Max. Sec. Curr : 16600 A
- Max. Weld Curr : 14900 A
- Frequency : 50 Hz
- Throat.Dim : 212x600 mm
- Duty Cycle : 7.3%
- Max. Pressure : 5.4 kN
- Weight : 275 kg
- Mach.No. : R3122YWKA00161001
- Date : 2003.5
- Manufacturer : Daihen Industrial Machinery Corporation, Daihen Corporation

Figure 3.5 : The weld nuggets appearance on the samples top view

3.3.3 Tensile-Shear Testing

For tensile strength measurement, the ASTM E8/E8M standard is chosen. This standard of the tensile-shear testing method specifies the procedures at room temperature for determining specific properties such as materials reduction area, tensile strength, yield strength, elongation, and yield point elongation in any material shape. Unless otherwise indicated, the room temperature for experimenting should be between 10 and 38°C (50 and 100°F). The numbers are expressed in SI units. Each of the system must be operated separately from the other for the reason that the values in each system are considered not exact counterparts. Non-compliance with the standard may occur if the two systems are combined [105]. The Ti-6Al-4V samples were tested in the tensile-shear testing machine each. The machine that is used to testing according to this ASTM standard of E8/E8M is Zwick/Roell, Amsler HA50 as can be shown in Figure 3.6.

The four main methods are considered to be utilized to test the yield strength such as Extension-under-load (EUL), Offset technique, Halt-of-the-Force Method, and Autographic Diagram Method (ADM), the last two methods are applicable particularly for materials with discontinuous yielding [105]. Figure 3.7 shows the arrangement of the sample in the tension testing machine.

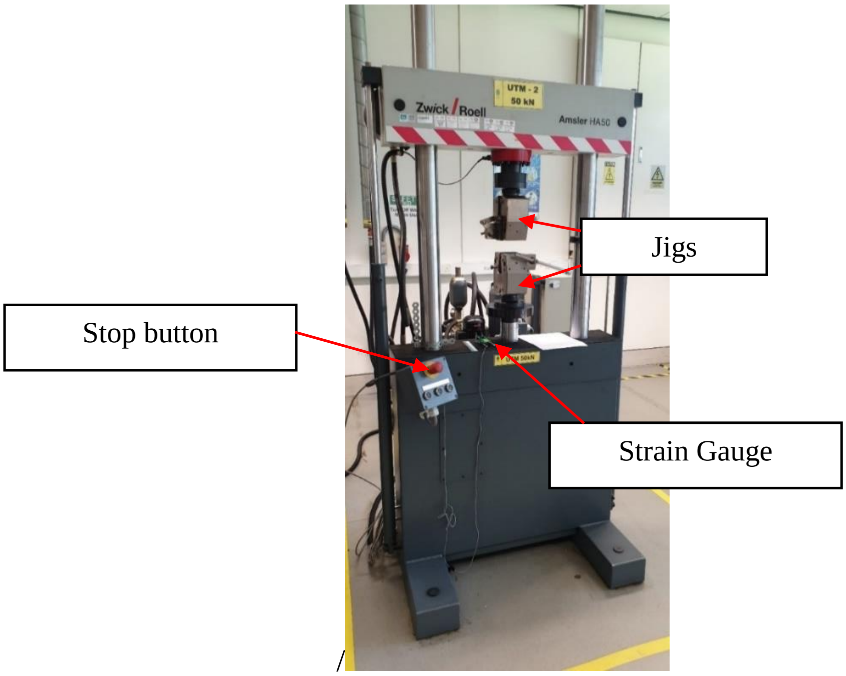

Figure 3.6 : The tension testing machine.

Highlights:

Jigs : Used to clamp the sample upper and lower and transfer the force to the sample to pull the sample until its failed

Strain gauge : Used to measure the strain during the testing and record it or transfer it into the computer to be ploted

Tensile testing set-up :

1. Insert the sample in the jigs, make sure no slip on the grips
2. Attached the strain gauge in the sample, make sure it is centered in the weld nugget
3. Input the gauge length size in the software about 25 mm
4. Input the ram speed in the software around 60 mm/menit
5. Run the test with clicking the run button in the software

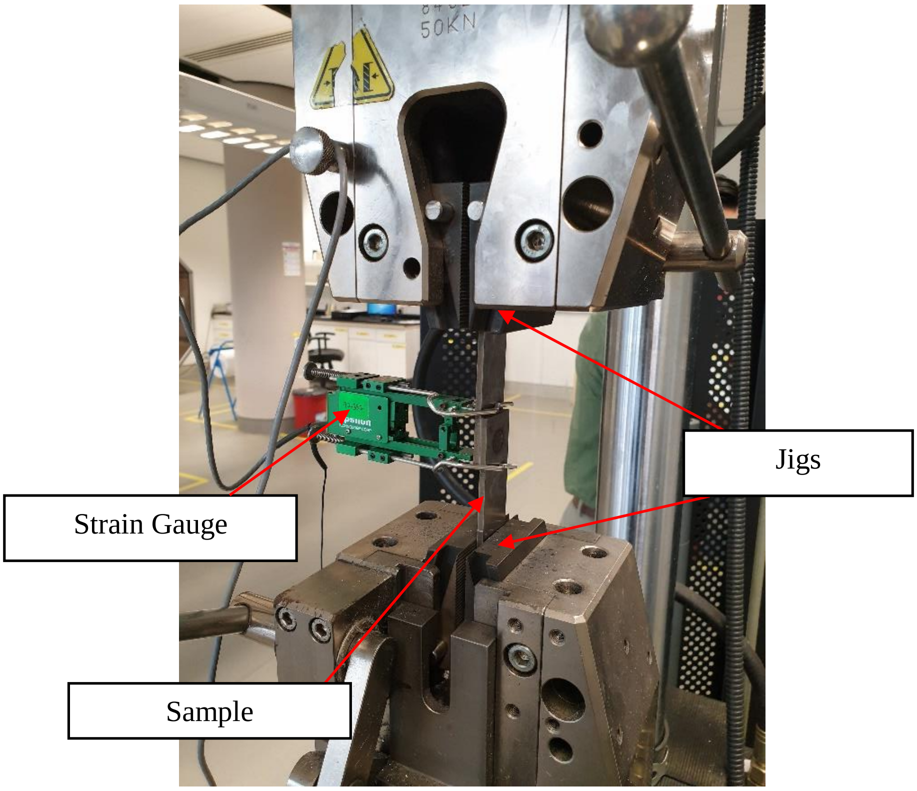

Figure 3.7 : The tensile-shear testing set up for the sample.

The peak load and yield strength are the other responses as the most relevant test findings. By definition, the yield strength, or commonly denoted as YS or Sy [FL–2], n, is the stress at which plastic elongation of the material is regarded to have started, according to the convention. This stress can be expressed as (a) a defined departure from a linear stress-strain relationship, (b) the total extension achieved, or (c) maximum or minimum engineering stresses observed during discontinuous yielding. In order to indicate the material can withstand the Su [FL–2], n is used and described as the highest tensile stress. The initial sample's cross-sectional area value with the largest force is applied during a tension test to rupture and is used to determine the tensile strength [105]. The typical stress-strain diagram is shown in Figure 3.8 and becomes the basis of reference for the stress-strain relationship in the post-testing result.

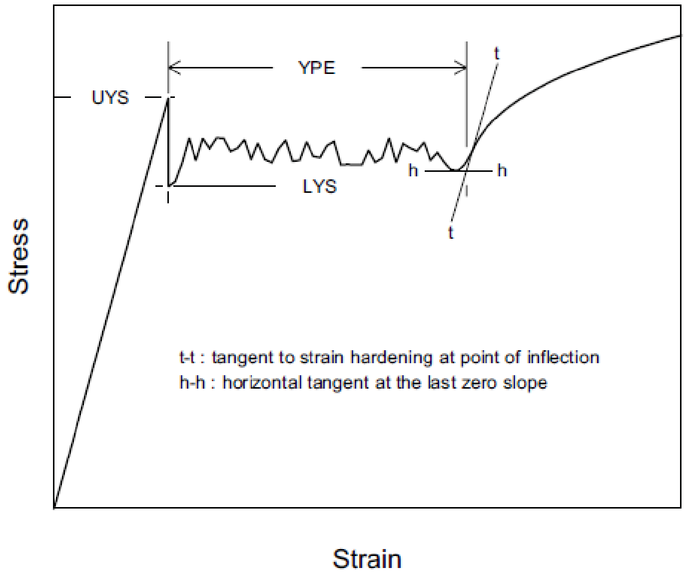

Figure 3.8 : Typical of Stress-Strain Diagram Showing Yield Point Elongation (YPE) and Upper (UYS) and Lower (LYS) Yield Strengths [105].

3.3.4 Microetching, SEM, EDX, and Microscopy

The micro etching is conducted for micrographic purposes to see the development of microstructure before and after the welding between the base metal and the weld microstructures. The ASTM E407-07 as a standard practice for micro etching metals and alloys is selected to conduct this experiment. Chemical solutions and techniques for etching metals and alloys for microscopic inspection are covered in this practice.

There are also safety precautions and other bits of information [106]. Before etching the preparations were required such as sample mounting, grinding, and polishing. The mounting was conducted using hot press mounting with implement 1000 automatic mounting press machines as shown in Figure 3.9. The hot mounted sample is shown in Figure 3.10.

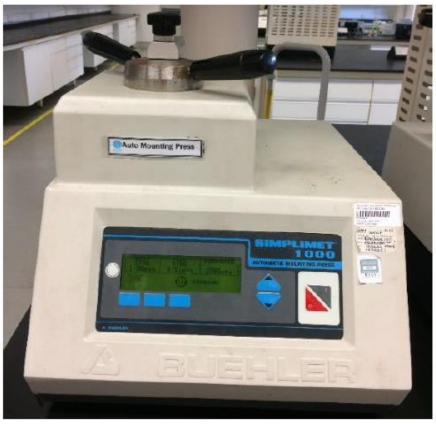

Figure 3.9 : Auto-mounting press machine (hot mounting machine).

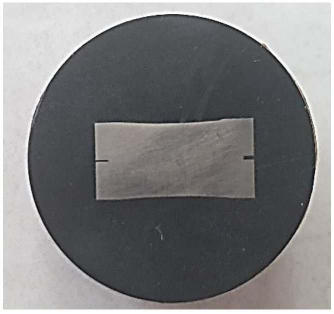

Figure 3.10 : The hot mounted sample

To get a clear image of microstructure, the sample surface area must be clean and slick. The first process to be conducted was the grinding process, this process was required to shape the flat and smooth surface. This surface was accomplished by sequentially grinding from the small size of grinding paper to the big size such as 180, 220, 320, 400, 600, 800, 1200, and 4000. The grinding machine which was used to serve this process was Buehler MetaServ 250 twin grinder-polisher machine as shown in Figure 3.11. This machine also served the polishing process. The polishing process was performed to remove any scratches and damages after the grinding process and also to get a clear and slick surface.

Figure 3.11 : Grinder and polisher machine.

The etching process was the next in line to be performed to made clear grain boundaries on the surface. The tint etch was used to conduct this practice, due to a thin oxide, sulfide, molybdate, chromate, or elemental selenium layer on the polished surface, an immersion etchant generates color contrast, typically selective to a specific ingredient in the microstructure. This shows the structure as a function of layer thickness owing to differences in light interference effects which is also recognized as a stain etch [106].

The approach is the vapor-deposition interference layer method, which is a technique for generating increased contrast between microstructural components, generally in color, using thin films produced by vacuum deposition of dielectric substances (such as TiO_2, ZnO, ZnTe, ZnS, or ZnSe) Owing to light interference effects (also known as the "Pepperhoff technique"), with a given refraction index [106]. For Titanium-based Ti-6Al-4V, the solution of Kellers Etch was applied, those are swabbed for 10-30 s as a standard procedure [106]. The swabbing method was selected to reveal a much clearer microstructure reckoning the highly anti-corrosion behavior of Ti-6Al-4V. The composition of Kellers Etch is shown in Table 3.3.

Table 3.3 : The composition of Kellers Etch

Etchant	Composition	Concentrations	Conditions
Kellers Etch	Distilled water	190 ml	10-30 second swabbing method, Use only fresh etchant
	Nitric acid	5 ml	
	Hydrochloric acid	3 ml	
	Hydrofluoric acid	2 ml	

The microstructure obvious images were acquired using the SEM process. The SEM standard used was ISO/TC 202/SC 4 for Scanning Electron Microscopy (SEM) & for EDX analysis, the standard of ASTM E1508 - 12a (2019) Standard Guide for Quantitative Analysis by Energy-Dispersive Spectroscopy is used. The SEM works by creating a picture by scanning a concentrated electron beam over the surface. When electrons in a beam contact with a sample to observe more about the surface topography and composition, they produce a variety of signals that may be utilized. The SEM was conducted using EVO LS15 ZEISS SEM as shown in Figure 3.12. While in the EDX, when an electron beam collides with an atom's inner shell, it knocks an electron out of the shell while leaving a positively charged electron-hole. This would disclose the amount of materials composition in the spectrum in question.

Figure 3.12 : EVO LS15 ZEISS SEM.

The microscopy analysis was performed for viewing the pitting images after the polarization process. Using LEICA LM DM Optical Microscope as shown in Figure 3.13 with a sharp lens and simple utilization procedure, the Pitt images were easily captured. The tiny Pitt images were required to be viewed from a small-scale microscope lens. The Pitts were sometimes straggling around the fusion zone area and shaped with irregular size. This requires a lens with a small one around 20x magnification.

Figure 3.13 : LEICA LM DM Optical Microscope.

3.3.5 Hardness Testing

The hardness is essential to know the material wear resistance and related strongly with the material microstructure. Gaining accurate results is essential, so the standard must be used to accommodate its compliance. The ASTM E92-17 standard test methods for Vickers Hardness and Knoop Hardness of metallic materials are used to conduct the testing to ensure the hardness distribution through the weld, HAZ, and the base metal [107]. In this particular research, the Vickers test method is used. This method was developed by Robert L. Smith and George E. Sandland in 1921 in Vickers Ltd. This method was discovered as the alternative to another hardness testing method that is The Brinell [108]. The main reason for this method selection is that The Vickers method principle is applicable for any of materials and it is easier to use. This standard covers the entire specification of the machine to be used and also every step of procedures outlined inside [107]. Besides the measurement, the calculation expression after the measurement is also user-friendly and avoids any complications. Figure 3.14 shows the equipment that is used to undergo the Vickers hardness testing.

Figure 3.14 : The Vickers hardness testing equipment.

The test was carried in the test forces range from 1 gf to 120 kgf. In the operation, the force levels which are the measurement levels are given in the units of kilograms-force (kgf) as specified by the International System of Units (SI). The SI standard also specifies the units of length in millimeters (mm) or micrometers (μm). The application of these units is supported for decades as the information or plunged into the articles as the reliable reporting values. Those reasons alone maintain the unit's reputation and are continuously being applied in scientific research due to historical precedent and continuing popular usage [107]. Figure 3.15 shows the display during the Vickers hardness measurement.

Figure 3.15 : The Vickers hardness measurement

The Vickers calculation is quite simple, the n diagonal measurement is conducted on a standardized test block as part of a performance verification to indicate the repeatability R in the performance of a Vickers hardness machine at each hardness level, given the specific verification conditions. The % range of n diagonal measurements concerning the measured average hardness value is used to assess repeatability as expressed in equation (3.2) [107]:

$$\boldsymbol{R} = \mathbf{100} \times \left(\frac{\boldsymbol{d_{max}} - \boldsymbol{d_{min}}}{\bar{d}}\right) \tag{3.2}$$

where,

d_{max} = the longest diagonal length measurement made on the standardized test block,

d_{min} = the shortest diagonal length measurement made on the standardized test block, and

$\bar{d}$ = the average of the n diagonal length measurements made on the standardized test block.

3.3.6 Potentiodynamic Polarization Testing

The standard used for this method is ASTM G59. The experiment to measure the polarization resistance of the samples procedure is outlined by this standard. The others such as the equipment specification, calibration, and methodology validation are also described well in the standard. The repeatability is also essential, it is discussed intensely and applied for both corrosion potentials and polarization resistance measurements. The equipment standard and condition issues are also valuable to ensure the accuracy and continuity of the test such as the condition of potentiostats, measuring device, reference electrodes, scan generators, electrochemical cells, and recording device. This standard also helps to ensure or as the main guidance for the equipment's capabilities can be maintained for working properly [109].

Before the potentiodynamic polarization process was conducted, the sample preparations have been done to ensure the correct installation in the equipment. To get a clear view of the pitting corrosion in the weld nugget, all samples will be cut to get the cross-sectional areas of the weld nuggets. The EDM wire-cutting machine was used to perform this matter, so the weld nugget microstructure was preserved due to less heat generated in this process. The final prepared samples are shown in Figure 3.16. The samples were then attached with the copper wires as the electrodes to be connected with the potentiostat and ensured that they were strong enough or attached properly.

Figure 3.16 : Prepared samples for potentiodynamic polarization process.

The attachments were conducted during the RSW process because the copper wires were impossible to be soldered using tin into the Ti-6Al-4V samples. The samples were then mounted using cold mounting with resin and ensured there is no hollow space that the solution would enter.

The 1.0 M NaCl test solution was provided as stated in Test Method G5 using American Chemical Society reagent grade acid and distilled water. 900 mL of test solution is required for the typical test cell. Within 1^{o}, the temperature must be kept at $30^{o}C$. Sequential good polishing till 1200 grit SiC paper should be used in the sample preparation to ensure surface cleaning. The calculation was done to the sample's surface area to the closest 0.01 cm^2 and also the removal of the area beneath the gasket (typically 0.20 to 0.25 cm^2). The sample was degreased using a solvent such as acetone and washed with distilled water right before immersion. Between rinsing and immersion, there was kept in very little time between them [109]. The polarization result plot and the polarization diagram can be seen in Figure 3.17 and Figure 3.18.

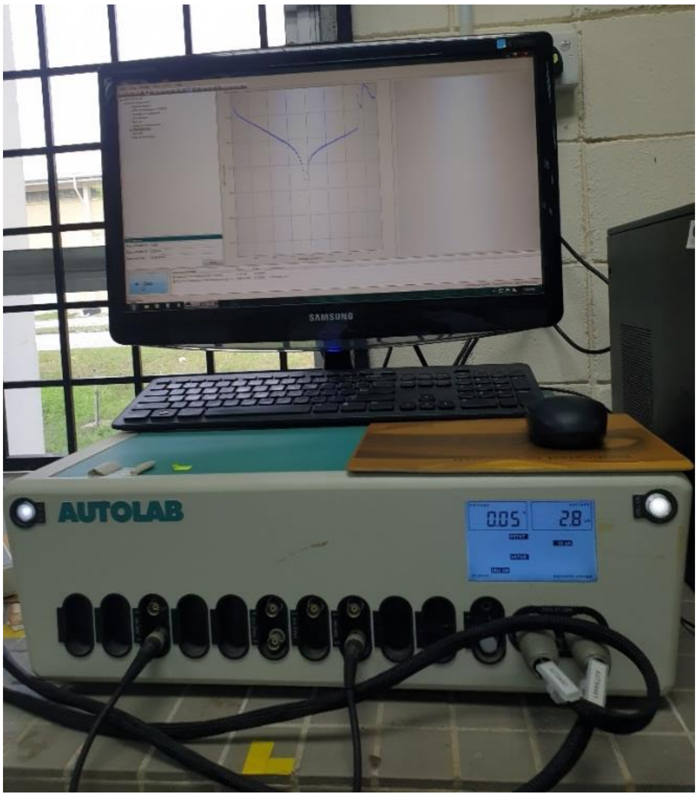

Figure 3.17 : The used potentiodynamic polarization device installed with the PC and monitor.

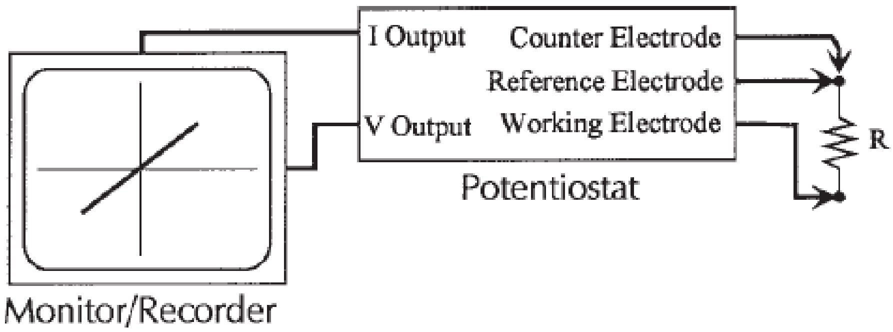

Figure 3.18 : Arrangement for Testing of Electrical Equipment (Potentiostat, X-Y Recorder) [109].

The polarization process can be seen in Figure 3.19. The diameter of the tip was prepared not to exceed 1 mm. After 5 and 55 minutes of immersion, the recording was conducted for the potential E_{corr}. Applying a voltage was 30 mV lower than the 55-minute corrosion potential.

Figure 3.19 : Polarization process.

The anodic potential was begun to be scanned at a sweep rate of 0.6 V/h one minute after applying the -30 mV potential (within 5%). The recording was conducted for a potential that was 30 mV higher than the corrosion potential after 55 minutes. The results are shown in the monitor for Ecorr. Calc. (V), Ecorr. Obs. (V), jcorr, icorr, corrosion rate, polarization resistance, and the curves.

3.3.7 Standard Practice for Calculation of Corrosion Rates and Related Information from Electrochemical Measurements

Even though the software had shown almost all of the measurement output but theoretically, the calculation was carried based on the ASTM G102, this procedure was intended to assist in the conversion of electrochemical data into consistent corrosion rates. For most engineering alloys, calculation techniques for translating corrosion current density data to mass loss rates or average penetration rates are provided. Furthermore, some conversion instructions for polarization resistance values to corrosion rates are also obtained [109].

To convert a measured or estimated current value to current density, the equation below (3.4) was used [109]:

$$\boldsymbol{i_{cor}} = \frac{\boldsymbol{I_{cor}}}{\boldsymbol{A}} \tag{3.4}$$

Where:

i_{cor} = corrosion current density, μA/cm^2

I_{cor} = total anodic current, μA, and

A = exposed sample area, cm^2

This computation was done automatically in computerized polarization equipment once the sample area is input into the computer software as well as after the polarization was done [110].

The following method was used to compute the alloy's equivalent weight. Considered a unit mass of oxidized alloy. The electron equivalent for 1 gram of an alloy, the Q is thus is expressed as equation (3.5) [109]:

$$\boldsymbol{Q} = \sum \frac{\boldsymbol{nifi}}{\boldsymbol{Wi}} \tag{3.5}$$

Where:

fi = the mass fraction of the i^{th} element in the alloy

Wi = the atomic weight of the i^{th} element in the alloy

ni = the valence of the i^{th} element of the alloy

As a result, as shown in equation (3.6), the alloy equivalent weight, EW, is the reciprocal of that amount [110].

$$\boldsymbol{EW} = \frac{\boldsymbol{1}}{\sum \frac{\boldsymbol{nifi}}{\boldsymbol{Wi}}} \tag{3.6}$$

3.4 Chapter Summary

This chapter has described the experimental setup and standard preparation for the RSW process. It also provides the standard methods used to identify and investigate the mechanical properties, physical properties, and corrosion tests. The statistical analysis to determine the level of the optimum parameter with tensile-shear strength response is calculated using Minitab 19 software. The design based on the Taguchi method calculation will determine the ANOVA and also can be drawn into multiple regression to get the mathematical models. The optimum level sample was prepared by grinding, polishing, and etching before microstructure analysis which was taken by the SEM. The standard preparation particularly for etching took several seconds longer than usual metal reminding that Ti-6Al-4V has excellent corrosion resistance capability. The microstructure images were taken on three parts of the cross-sectional area which were the base metal, HAZ, and the fusion zone. This would help the analysis became obvious to compare the three zones which were affected by the welding force and heat input variables: welding current and welding time. The samples were attached to the copper wire and stabilize in the 1M NaCl solution before the test began. The potentiodynamic polarization method as one of the very effective and common methods was used to identify the corrosion rate and pitting susceptibility. The calculations were carried out based on the i_{corr}, E_{corr}, and E_{pitt} as the results from the polarization process. The microscopy analysis was also conducted to capture the pitting images in the sample's cross-sectional area after the polarization test.

CHAPTER 4

RESULTS AND DISCUSSION

4.1 Chapter Overview

This chapter discusses the influence of RSW parameters into the weld nugget. The physical properties were observed to determine the influence of the parameters into the weld nugget diameter. The optimum parameters were analyzed using ANOVA with the tensile-shear strength as its response. The multiple regression analysis was used to generate the mathematical models of weld nugget diameter and tensile-shear strength. The microstructure and the concentration of Ti, Al & V components were taken by SEM and EDX analysis. Their correlation is also analyzed and highlighted. In the corrosion test, the potentiodynamic polarization results help to correlate the influence of heat input into the corrosion resistance transformation on the weld nugget surface. The pitting morphologies were taken by microscope to observe the amount of pitts in the weld nugget.

4.2 Weld Nugget

The measurement positions for weld nugget diameter were taken in 5 positions, as shown in Figure 4.1, and were determined its average.

Table 4.1 shows the appearance results for weld nuggets in various samples with different RSW parameters. The weld nugget appearances for all of the samples are completely close to the round shape, with the dark blue color on the nugget edge. It proves that the electrodes are in good condition and the heat was generated properly. Figure 4.2 shows the measurement of weld diameter and also the indentation depth from each sample with various parameters. The indentation depths were measured using a micrometer.

The weld nugget growth is influenced by the combination of the heat input and the applied welding force. Initially, the clamping effect from the welding force applied from both sides of the samples by the welding electrode keeps the sample immobile and helps localize the heat input. The heat input is generated by the combination of welding current and time, where the value is also influenced by the material and welding electrode resistivity. It is shown in Figure 4.2 that the weld diameter is not significantly increasing in the same welding current value, although the welding force and the welding time are increased. But it is subsequently increased significantly when the welding current is increased.

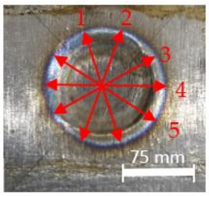

Figure 4.1 : Weld nugget measurement positions.

From the heat input equation can be drawn that weld nugget growth has a very close relationship with the amount of heat input and its variables particularly welding current. The increase of the welding current will increase the heat input value subsequently [30].

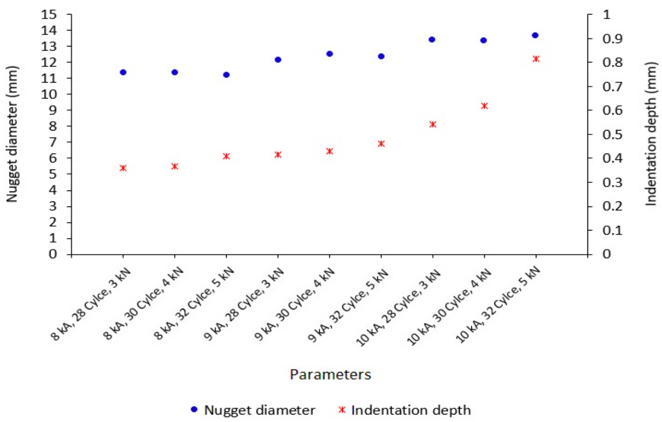

Figure 4.2 : Weld nugget size

At a constant sample's resistivity, the welding current is more influenced for the weld nugget growth in particular the nugget diameter than the welding time and force, because the high welding current will give a wider melting zone and sufficient penetration to the localized welding area around the weld nugget [98]. The smaller nugget width/diameter can ensue when a low welding force is applied thus will cause the increase of current density and reducing the contact area in the faying layer [30]. Medium welding force is rather sufficient to form a maximum nugget diameter than low or high welding force [31].

Table 4.1 : Weld nugget appearance

Exp.	**RSW Parameters**			**Weld nugget appearance**
	Welding Current	**Welding Force**	**Welding Time**	
1	8	28	3	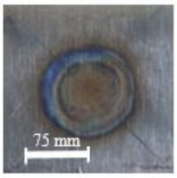
2	8	30	4	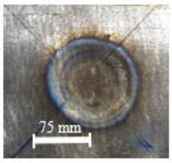
3	8	32	5	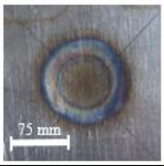
4	9	28	3	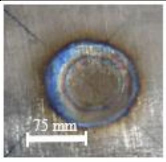
5	9	30	4	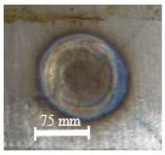
6	9	32	5	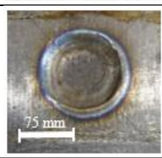
7	10	28	3	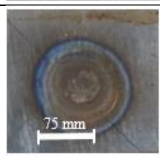
8	10	30	4	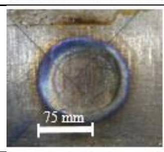
9	10	32	5	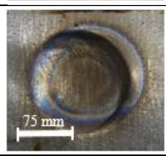

4.3 Taguchi Method for Tensile-Shear Testing Results and Regression Analysis

As the load was increasing the weld nugget suffered excessive stress and started to transform gradually before it was failed. The bending display in the lap joint was one of the phenomena which were observed as seen in Figure 4.3. The tensile-shear test is the most common method used to evaluate the mechanical properties in static conditions.

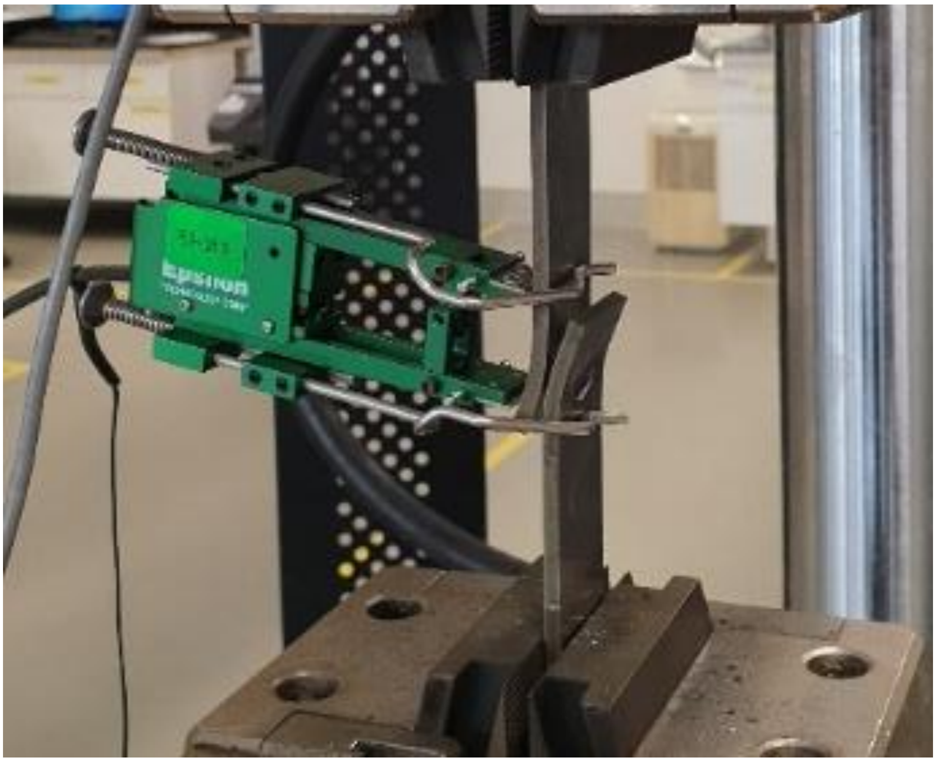

Figure 4.3 : The bending phenomenon in the lap joint during tensile-shear testing.

The final breaking form of the sample's failure in the post-tensile-testing process as shown in Figure 4.4 indicated that the sample has reached beyond the ultimate strength and obtained a fracture. From the tensile-shear testing curve, as shown in Figure 4.5, many data are drawn from the testing results including the maximum stress (peak stress), maximum load (peak load), yield strain, Young's modulus, etc. The indicator was used as the response of the Taguchi method was the maximum load (peak load), as it gives certain information about the tensile strength and corresponded with the weld nugget form and lap joint shape of the sample.

Figure 4.4 : The sample's failure in the post-tensile-shear testing.

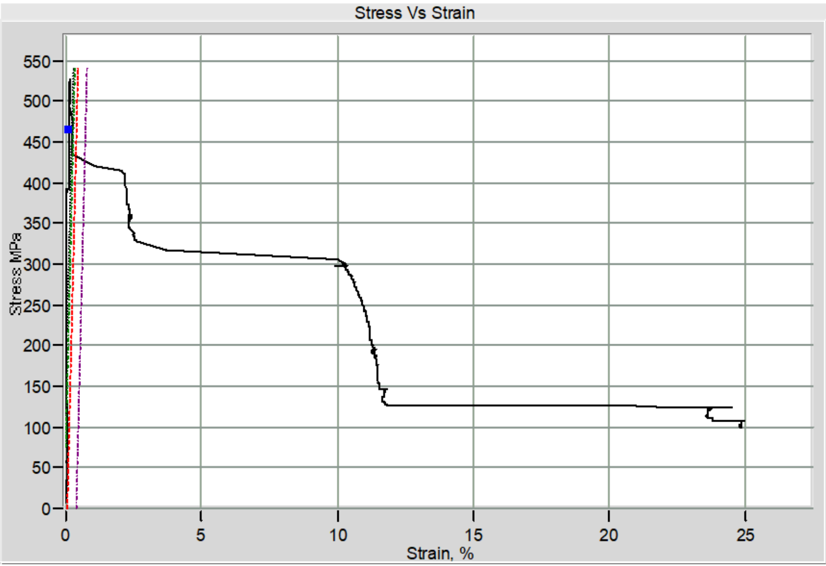

Figure 4.5 : The stress-strain diagram/curve in sample no. 2.

The Taguchi method analysis determines the most significant parameter and the parameter pattern which are affecting the maximum stress of the tensile-shear test. Table 4.2 shows the results for the tensile-shear test for the whole experiment in the L9 Taguchi method. The lowest maximum load is found in the welding parameter of 8 kA welding current, 28 cycles welding time, and 3 kN welding force. The highest stress is found in the welding parameter of 10 kA welding current, 30 cycles welding time, and 4 kN force.

Table 4.2 : Maximum load results of the tensile-shear testing

Exp.	**Current (kA)**	**Welding Time (Cycles)**	**Force (kN)**	**Max. Load (kN)**
1	8	28	3	38 ± 0.6
2	8	30	4	39 ± 0.5
3	8	32	5	40 ± 0.1
4	9	28	4	40 ± 0.2
5	9	30	5	41 ± 0.3
6	9	32	3	43 ± 0.9
7	10	28	5	41 ± 0.4
8	10	30	3	40 ± 0.5
9	10	32	4	40 ± 0.4

In Table 4.3, it can be seen that the delta value of the welding current is the greatest of all parameters. Then followed by welding time and welding force. It can also be seen clearly in the graph in Figure 4.6 that the welding current chart has the most significant graph compared to welding time and welding force. Certainly, based on Equations (2.1) and (2.2), the heat generation is dependent mostly on the amount of current and resistance, since the resistance is constant then the amount of welding current is decisively the main factor to decide the amount of heat input. The value of the combined resistance helps to localize the heat, generating a weld joint in a spot. The force is not affecting either less than welding current and time because its value gives only significant influence to the contact resistance both of the specimens and the electrode. These are the particular reason how the welding current has been put at rank 1 as the most significant parameter which affects the maximum sample tensile load, followed by welding time at rank 2 and welding force at rank 3 as can be seen in Table 4.3.

Table 4.3 : Response for means

Level	**Current**	**Time**	**Force**
1	39.23	39.86	40.80
2	41.75	40.45	40.01
3	40.75	41.42	40.92
Delta	2.53	1.56	0.91
Rank	1	2	3

The high welding current and high welding time are creating more penetration and denser fusion zone. The welding current of 9 kA, welding time of 32 cycles, and welding force of 5 kN are selected as the optimum parameter resulting in the best maximum load as appeared in Figure 4.6.

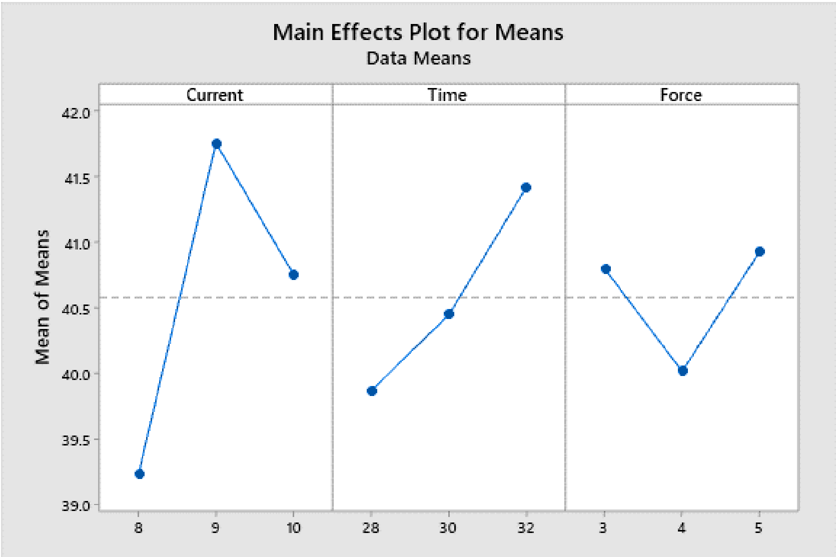

Figure 4.6 : The significant effect plot of RSW parameters into weld nugget strength

Generating a mathematical model can help the possible future research and also make it easier to do. Linear regression is used to determine the mathematical model of the maximum tensile stress and weld nugget diameter as dependent variables. The welding current, welding time, and welding force act as independent variables. After multiple linear regression analyses, the ANOVA with R-sq. at 94.68% is given in Table

4.4. Figure 4.7 shows the normal probability plot for maximum stress and Figure 4.8 shows weld diameter as the response. Thus the regression equation for mathematical models is given in Equation (4.1) & (4.2).

$$\textbf{\textit{Max. Load}} = \mathbf{21.8 + 0.763}\ \textbf{\textit{Current}} + \mathbf{0.389}\ \textbf{\textit{Time}} + \mathbf{0.064}\ \textbf{\textit{Force}} \tag{4.1}$$

$$\textbf{\textit{Weld diameter}} = \mathbf{0.545 + 1.0869}\ \textbf{\textit{Current}} + \mathbf{0.0665}\ \textbf{\textit{Time}} + \mathbf{0.0114}\ \textbf{\textit{Force}} \tag{4.2}$$

Table 4.4 : Analysis of variance.

Source	**DF**	**Adj SS**	**Adj MS**	**F-Value**	**P-Value**
Regression	3	7.1556	2.38518	0.97	0.474
Current	1	3.4915	3.49149	1.43	0.286
Time	1	3.6395	3.63949	1.49	0.277
Force	1	0.0246	0.02458	0.01	0.924
Error	5	12.2407	2.44814		
Total	8	19.3962			

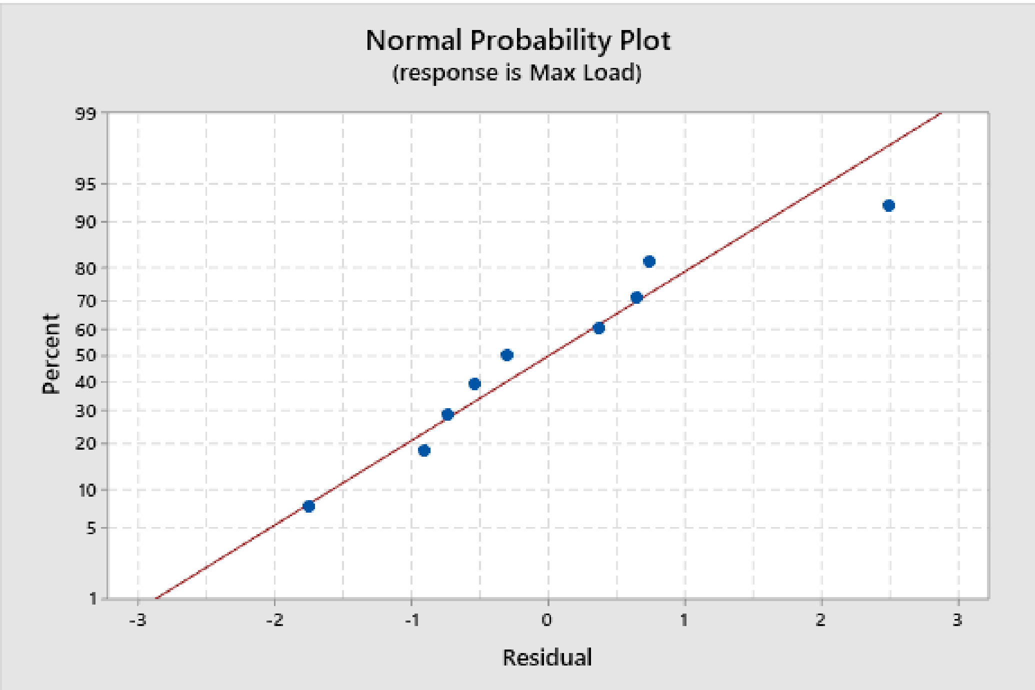

Figure 4.7 : Normal probability plot in the response of Max. Load.

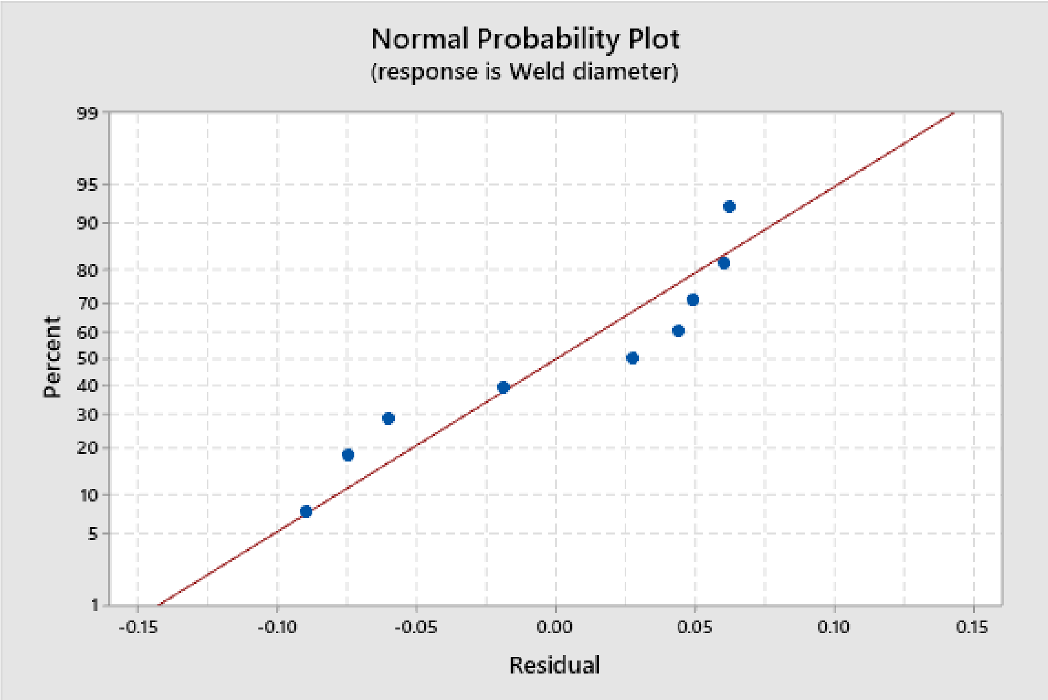

Figure 4.8 : Normal probability plot in the response of weld diameter.

A confirmation test was taken from the selected optimum parameters result, which was given by the ANOVA. From Figure 4.9, it is known that the weld nugget shape was round. The average diameter measurement, which was taken from six circular positions, was 12 ± 0.5 mm.

Figure 4.9 : Confirmation test weld nugget appearance.

The measured indentation depth was 0.45 mm with no expulsion appearing. The values of the tensile-shear strengths are displayed in Table 4.5 and Figure 4.10, showing that the maximum stress of confirmation test is 599.7 MPa and the maximum load is 44.9 kN, which is the highest value among all of the results given in the Taguchi Table as shown in Table 4.5. This indicates that the RSW parameters in the confirmation test are considered as the most optimum level of parameters to produce the strongest joint. As shown in Table 4.5, the yield stress is 595.7 MPa, which was high enough to withstand high stress.

Table 4.5 : Tensile-shear testing results

Sample	Peak Stress (MPa)	Peak Load (kN)	0.2% Offset Yield Stress (MPa)	Modulus (GPa)
1	507 ± 0.5	38 ± 0.6	455 ± 0.1	77 ± 0.9
2	526 ± 0.8	39 ± 0.5	419 ± 0.9	86 ± 0.3
3	534 ± 0.8	40 ± 0.1	525 ± 0.3	91 ± 0.5
4	535 ± 0.6	40 ± 0.2	500 ± 0.3	94 ± 0.7
5	550 ± 0.6	41 ± 0.3	550 ± 0.6	102 ± 0.1
6	583 ± 0.9	43 ± 0.9	530 ± 0.4	113 ± 0.7
7	551 ± 0.6	41 ± 0.4	466 ± 0.9	108 ± 0.5
8	540 ± 0.4	40 ± 0.5	498 ± 0.8	105 ± 0.6
9	538 ± 0.1	40 ± 0.4	537 ± 0.9	101 ± 0.3
Conf. Test	599.7	44.9	595 ± 0.7	118 ± 0.4

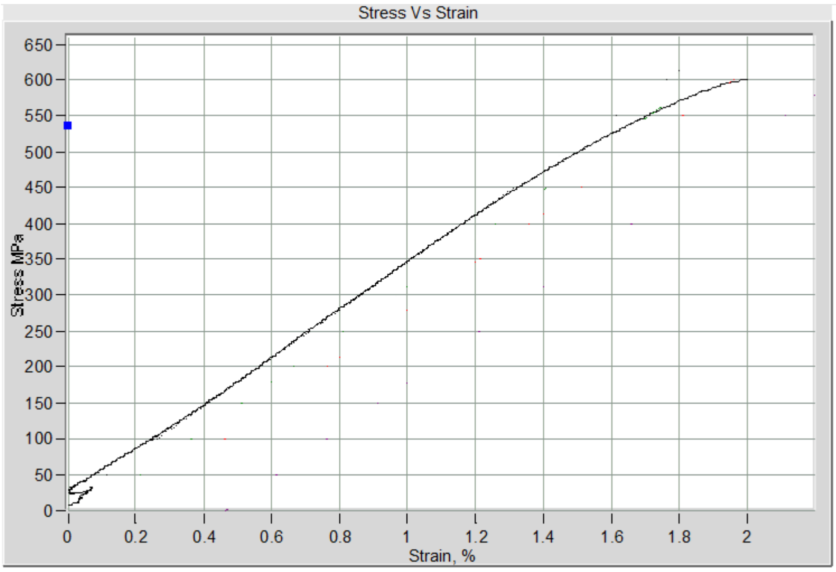

Figure 4.10 : Confirmation test tensile-shear testing result: stress vs strain

4.4 Failure Mode

In the weld nugget physical properties analysis, the failure mode and the fracture mechanism are also important components. Pullout failure (PF), interfacial failure (IF) and partial interfacial mode (PIF), and partial thickness partial pullout (PT-PP) mode are the most common failure mode in the tensile-shear testing results [111]. The weld nugget failure mode was influenced by the fusion zone dimension, the sheet thickness, and the weld nugget hardness to failure location hardness ratio during the tensile-shear testing [113].

As can be seen in

Table **4.6** exp. 1, it is shown that the failure mode was PIF. The low welding current contributed to low heat input and the generation of a fusion zone with low strength, thus resulting in IF mode in the fusion zone [33] because the localized heating only occurred in the small area covered by the welding electrode and resulted in a low heating temperature. It is also related to the generation of a smaller weld nugget diameter and a shallow indentation depth, and the transformation of the microstructure. This created a brittle fracture in the fusion zone after the tensile testing, indicated by the lowest maximum load in Table 4.2.

Table 4.6 exp. 2 shows that the failure mode was still the PIF but the fracture started to move away from the fusion zone and hit the HAZ. A higher welding current helped increase the weld nugget size and the indentation depth, and created a different microstructure, then causing the maximum load to increase. In

Table **4.6** exp. 3-6, the failure modes were changed into PF. The HAZ was seemingly more favorably affected than the fusion zone, except for that shown in

Table **4.6** exp. 6. The fracture location in

Table **4.6** exp. 6 was observed to occur in the base metal, leaving the fusion zone and the HAZ undamaged. In

Table **4.6** exp. 7 & 8, the failure modes were still PF, but the maximum loads were decreased.

Table **4.6** exp. 9 shows that the failure mode changed into a PI-PP with expulsion appearing. The expulsion caused material degradation so that the fusion zone thickness became thinner. This event lowered the weld nugget strength indicated by the decrease of the maximum load during the tensile-shear testing.

An expulsion can be explained as follows: when a higher welding current was given which developed a higher heat input in a short welding time, and expulsion was generated. This expulsion was caused by overheating and degrading the material deposit to the air suddenly [117]. The expulsion created a higher indentation depth in the area which included the fusion zone and the HAZ as well. The significant impact of the expulsion event affected the weld nugget final yield strength. Therefore, the expulsion event is one of the most essential factors to detect and characterize the weld nugget quality assurance [114]. The possible outcome of the expulsion formation can also be generated, when the electrode displacement exceeds the limit of the maximum expansion, leading to an explicit spatter formation [28].

Table 4.6 : Failure modes

Exp.	RSW Parameters			Weld nugget appearance
	Welding Current	Welding Force	Welding Time	
1	8	28	3	
2	8	30	4	
3	8	32	5	

4	9	28	3	

Table 4.7 : Failure modes (cont'd)

Exp.	RSW Parameters			Weld nugget appearance
	Welding Current	Welding Force	Welding Time	
5	9	30	4	
6	9	32	5	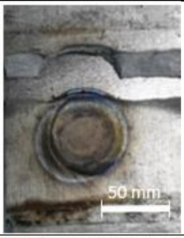
7	10	28	3	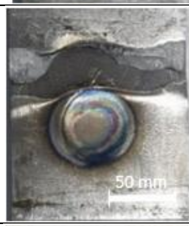
8	10	30	4	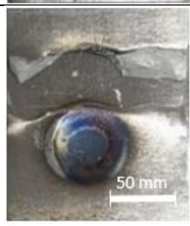
9	10	32	5	

Consideration can be taken, as the expulsion tends to increase when a too low or too high welding force is applied [26]. As can be seen in Figure 4.11, there was a slight expulsion on the side of the weld nugget, and therefore, the indentation depth increased significantly, as shown in Figure 4.2. A massive expulsion created a bigger nugget diameter but with a higher indentation depth. From Figure 4.12, the appearance of weld nugget failure after tensile-shear testing for confirmation test sample can be seen. It is shown that the failure mode was the PF mode mostly in the HAZ and the base metal with no expulsion appearing both in the outside and the inside of the weld nugget. This indicated that the sufficient welding current, welding time, and force had met properly in the range of appropriate weld as depicted in Figure 2.13.

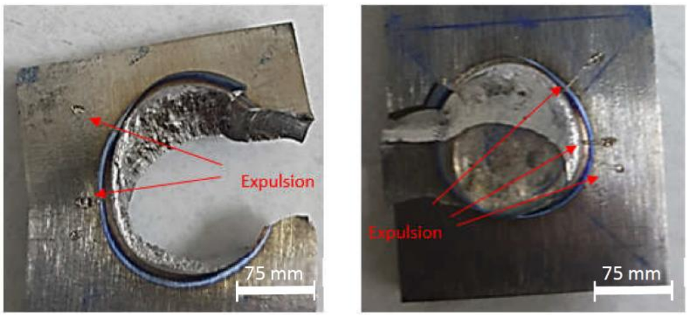

Figure 4.11 : Expulsion under the conditions of a welding current of 10 kA, a welding time of 32 cycles, and a welding force of 4 kN.

Figure 4.12 : Confirmation tensile-shear test failure mode.

4.5 Microstructure, Compositions, and Hardness distribution

The microstructure of Ti-6Al-4V consists of the α, β, or α + β phase. Ti-6Al-4V with the α phase has good strength, toughness, and weldability but has poor forgeability.

Ti-6Al-4V with the β phase is an alloy composed of vanadium, niobium, and molybdenum, which has good forgeability over a wide temperature range [5]. The presence of this alloy is also useful to reduce the temperature transition of the α phase to the β phase, thereby contributing to the formation of a β-phase BCC structure. Figure 4.13 shows the SEM image of the microstructure with a 5000× magnification at three positions, namely base metal, HAZ, and fusion zone. Figure 4.13a shows the base metal microstructure was duplex which consisted of the α phase (light color) and β phase (dark color) and mostly consisted of columnar α and equiaxed α. Figure 4.13b shows that the β-phase stabilizer which had a BCC structure transformed into the α' phase which had a hexagonal close-packed (HCP) structure at the β transus temperature around 980–1000 °C, spread over the HAZ and began to multiply in the fusion zone, as shown in Figure 4.13c.

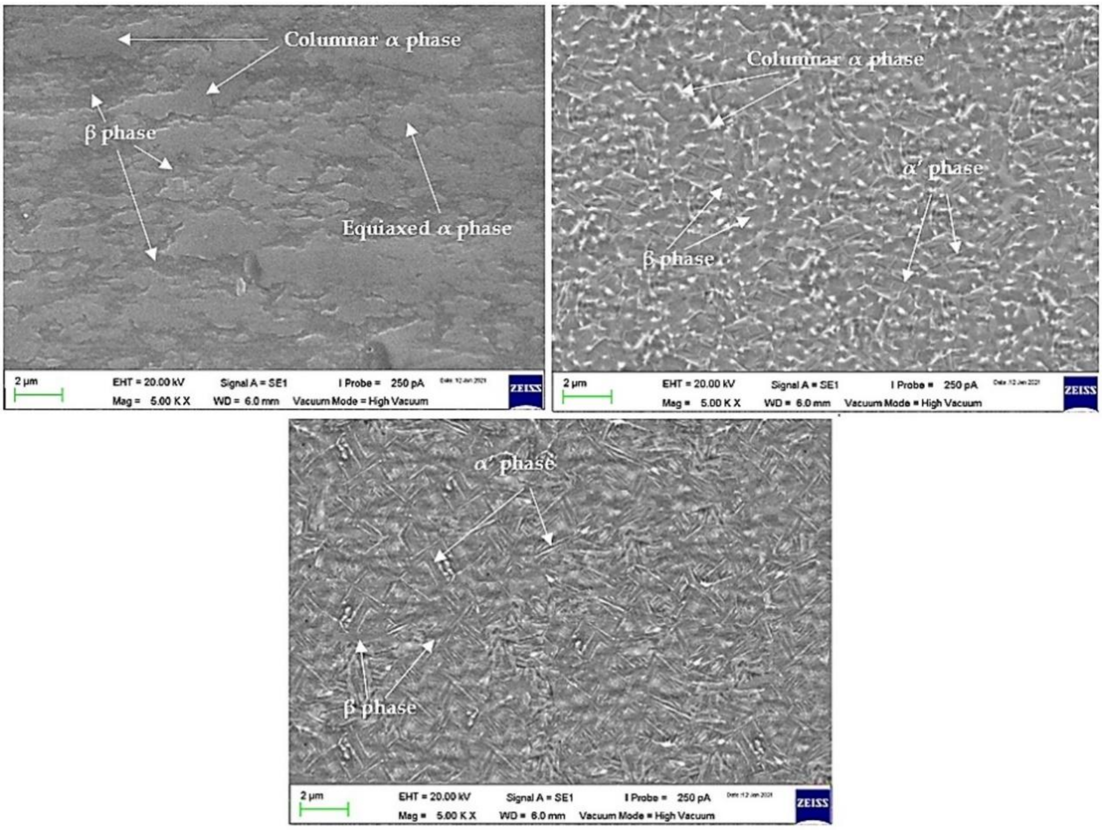

Figure 4.13 : SEM 5.00 K X Mag.: (a) Base metal; (b) Heat affected zone; (c) Fusion zone

The α' phase is known as the supersaturated solid solution of elements in the Ti α phase, which is transformed in a β phase stability temperature range at a rapid cooling rate [118]. At this temperature, a lot of β phases transform into α' phases. Both α and α' phases have HCP structures [120]. The high heating temperature in the fusion zone and the rapid cooling rate (air cooling) that is evenly distributed in the fusion zone compared to in HAZ greatly contributed to many transformations of the β phase into the α' phase. The high temperature spread from the contact center of the electrode with the material radially towards the base metal so that even in a thin HAZ, the α' phase was observed. This would rather coarsen the grain in the fusion zone than in the base metal, which had a lower temperature.

The EDX analysis was applied in the weld nugget cross-sectional area and was taken for 5 spectrums in 5 positions in the base metal, HAZ, and fusion zone respectively. The spectrums were taken in a horizontal position aligned with weld nugget diameter as shown in Figure 4.14.

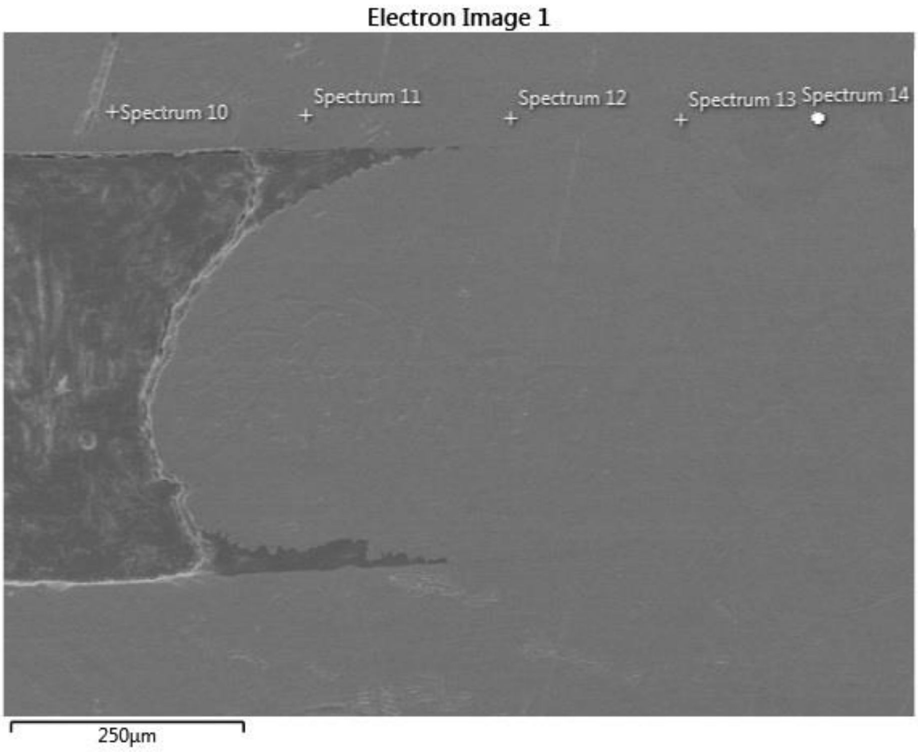

Figure 4.14 : The EDX spectrum positions : spectrum 10 & 11 are base metal, spectrum 12 is HAZ, spectrum 13 & 14 are fusion zone

Figure 4.15 shows the Ti-6Al-4V compositions in each spectrum. As explained before in the literature review, that Ti-6Al-4V is composed of Ti composition which forms the BCC alpha phase and the combination of alpha+beta alloy. This alloy much affects the material zone characteristic. As observed before in Figure 4.13a, the microstructure of base metal is formed from the α phase and β phase. However, in the HAZ in Figure 4.13b started to form the α' phase and began to increase in the fusion zone in Figure 4.13c which was a transformation from the β phase and was supersaturated in Ti α phase. This causes the EDX reading of Wt% of Ti shown in Figure 4.15, especially in spectrum 12, which is the location of HAZ, to be recorded as the highest at 86.1 than in spectrum 10 and 11, which are base metals, which are recorded only 85.1 and 85.7, respectively. In the fusion zone of spectrum 13, the recorded value is even greater, namely 86.3 because the transformation of the β phase to the α' phase is increasing.

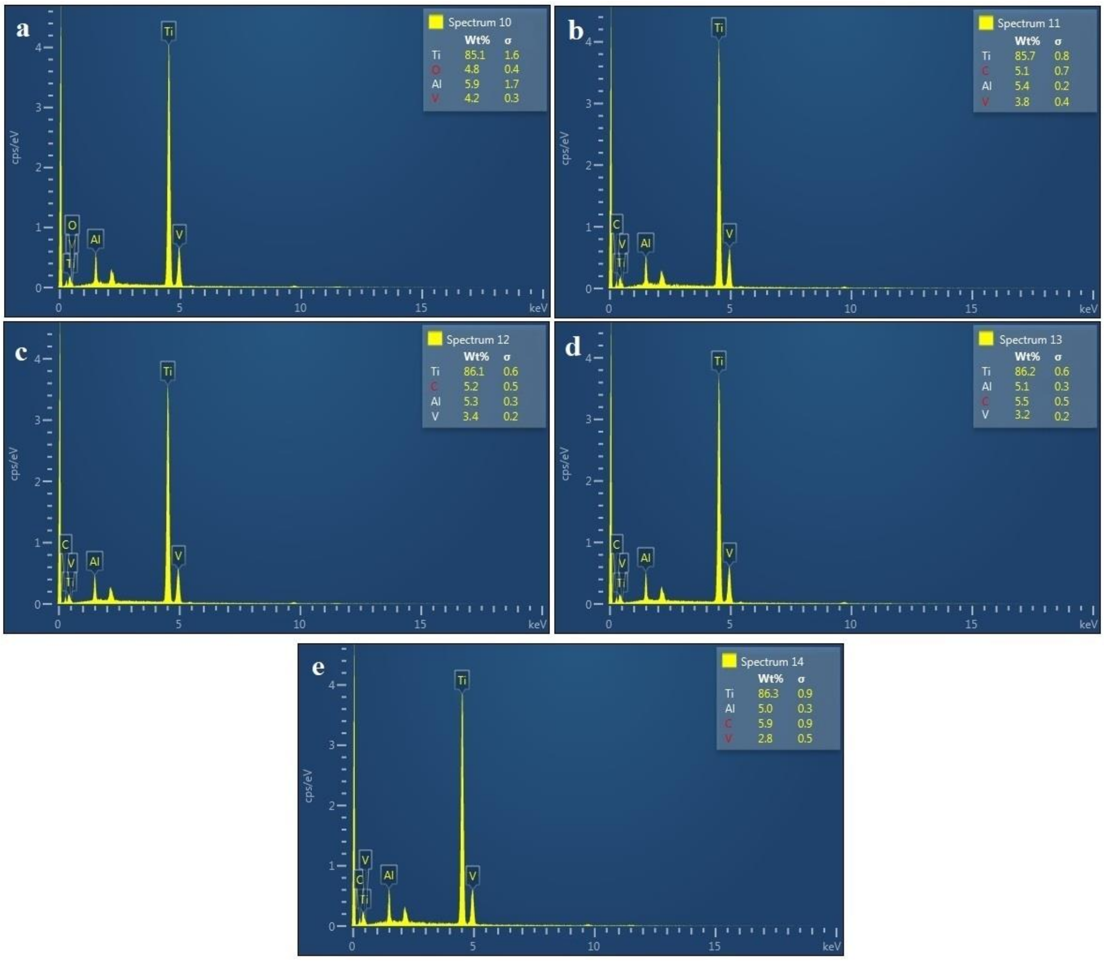

Figure 4.15 : The EDX results for respective spectrum: (a) spectrum 10; (b) spectrum 11; (c) spectrum 12; (d) spectrum 13; (e) spectrum 14

The Wt% of Al and V as the constituent components of the β phase have the opposite value change. The number of β phase that are transformed into α' phase in the

HAZ and fusion zone causes a decrease in value. Spectrums 10 and 11 which are in the base metal have quite large Al and V values, between 5.9 to 5.4 in Al and 4.2 to 3.8 in V. A significant decrease occurs in spectrum 12, 13 and 14 which are in the HAZ and fusion zone i.e. 5.3 to 5.0 at Al and 3.4 to 2.8 at V.

The Vickers microhardness test was performed on a cross-sectional area of the weld nugget at 23 points starting from the base metal towards the fusion zone and across the other side of base metal according to Figure 4.17. The 6 base metal and 2 HAZ points of measurement have 0.6 mm of distance due to its tiny space. The fusion zone has 1.25 mm distance each point. It can be seen that the base metal with a duplex microstructure provided the lowest hardness value of the overall test results with HV = 305 as observed in Figure 4.17.

With the testing getting closer to the fusion zone, the observed hardness values were increased, starting in the HAZ with the acicular α' martensitic population which began to form a lot. The martensitic acicular α' phase can cause an increase in the hardness value. The attainment of β-transus temperature by rapid cooling (air cooling) with a long welding time caused changes to occur. This microstructure transformed the structure from the BCC structure to become the HCP structure, which had a vast increase in volume, generating a highly stressed structure. That is the reason why the martensite microstructures had higher hardness and higher strengths in the fusion zone and the HAZ, which than in the base metal but less ductile and too brittle. The highest hardness value was in the fusion zone with HV = 552.5 as observed in Figure 4.17.

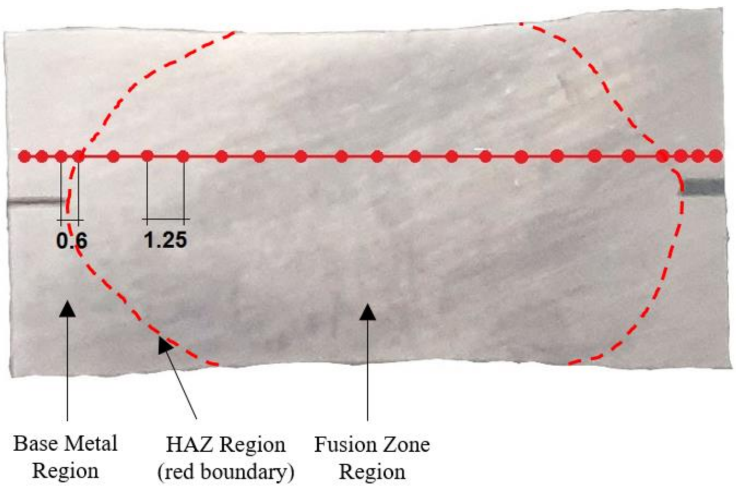

Figure 4.16 : Vickers hardness test points

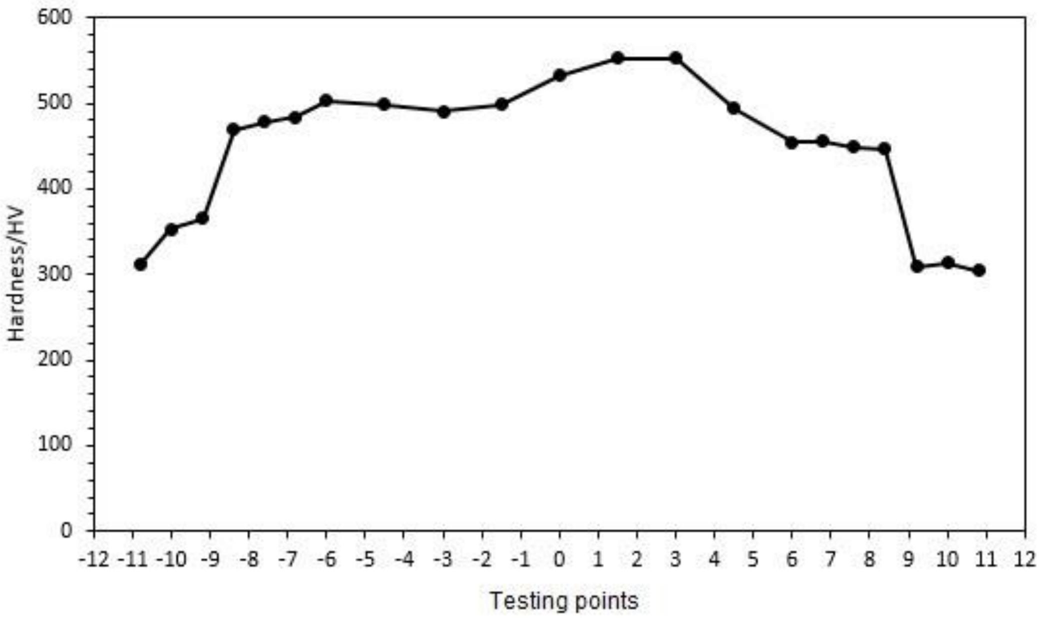

Figure 4.17 : Vickers microhardness test result of optimum parameter.

4.6 Corrosion Rate & Pitting Susceptibility

The welding time and welding force were considered constant at 32 cycles and 5 kN as the most optimum level based on Table 4.2 and the welding currents were varied in 3 parameters. The selected parameter for the welding currents was: 8, 9, and 10 kA. This is because the welding current is the most significant affecting parameter according to Table 4.3 and Figure 4.6. Table 4.8 shows the RSW parameters used for various samples of polarization test. The cutting process to get a weld nugget is discussed in chapter 3. The cross-sectional area of the weld nugget is shown in Figure 4.18.

Titanium and titanium alloys are recognized as materials with extremely high corrosion resistance but in some specific conditions pitting corrosion of titanium can occur [120]. Welding of Ti and titanium alloys changes their structure. It is well known that titanium is a highly reactive metal with a standard electrode potential of -1,63 V, and its corrosion resistance is only due to the formation of TiO_2 passive film.

Table 4.8 : RSW parameters for various polarization test samples

Sample	Welding current (kA)	Welding time (Cycles)	Welding force (kN)
Base metal	-	-	-
Sample 1	8	32	5
Sample 2	9	32	5
Sample 3	10	32	5

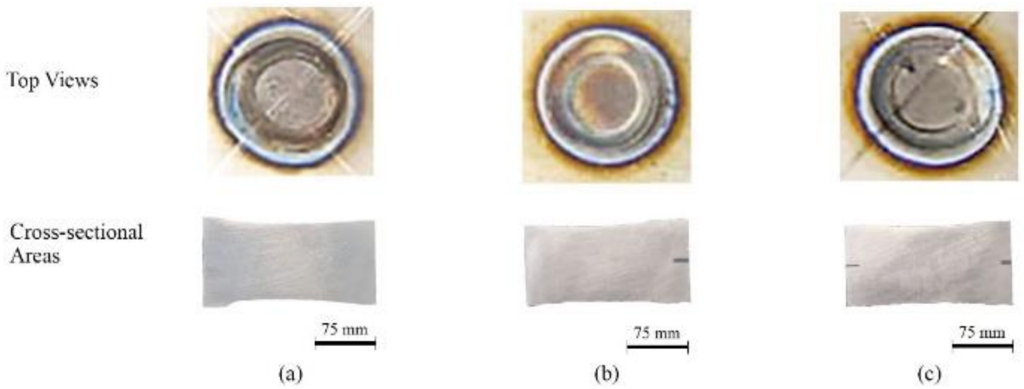

Figure 4.18 : Weld nugget appearances and cross-sectional areas at RSW parameter of (a) sample 1; (b) sample 2; (c) sample 3.

The integrity of this passive film is governed by its structure that depends on the underlying metal structure. For instance, the coarse metal structure is a condition for the formation of a less dense oxide layer and thus for the facilitation of corrosion processes [125]. The passive film can be destroyed by halide ions as they cause its electrochemical dissolution and open-path for aggressive environments through it towards the bare metal surface [126].

Microstructure transformation on the β transus temperature proved to be vital in corrosion resistance reduction in the weld joints [121]. Before testing potentiodynamic polarization to determine pitting susceptibility and corrosion rate, SEM was carried out first on all weld nuggets to preview the microstructure for each sample. In Figure 4.19a, the base metal microstructure is duplex with α phase and β phase. In Figure 4.19b, c, and d the β phase stabilizer which has a BCC structure has transformed into α' phase which has a hexagonal close-packed (HCP) structure at the β transus temperature around 980-1000^{o}C and spread over in the fusion zone [6].

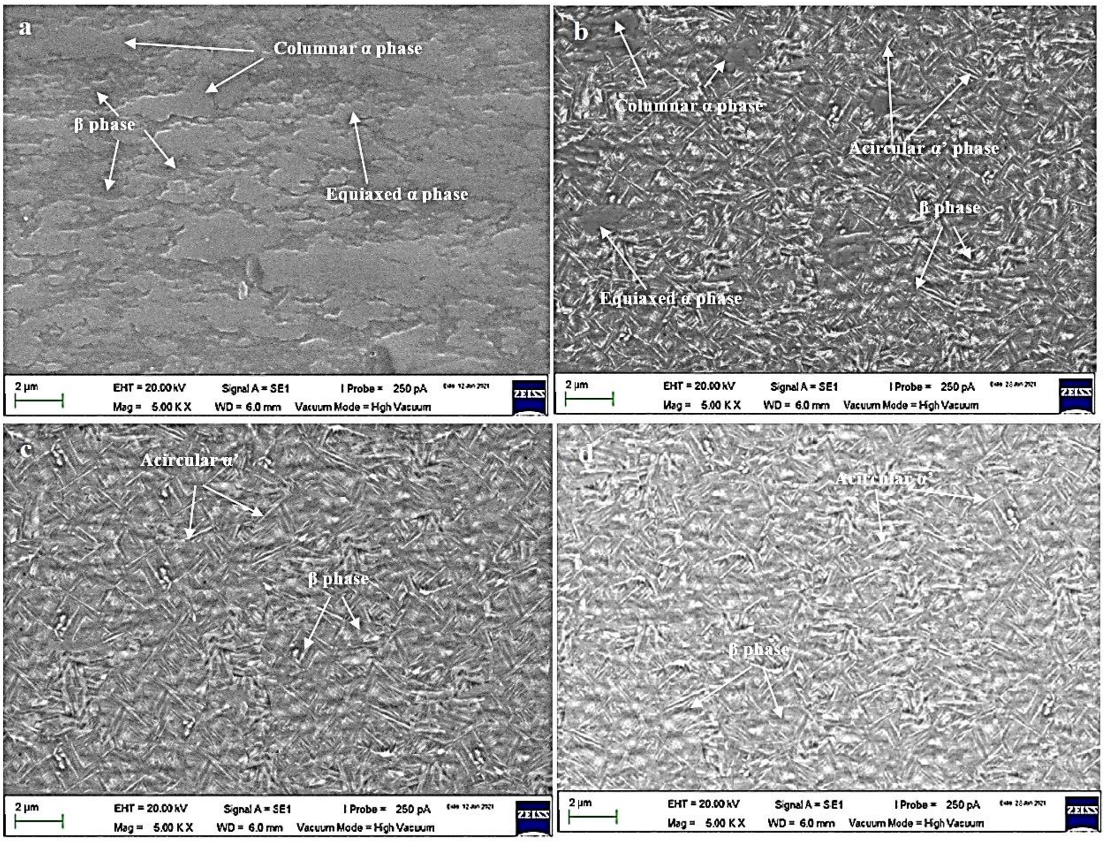

Figure 4.19 : SEM 5.00 K X Mag. of : (a) base metal; (b) sample 1; (c) sample 2; (d) sample 3.

But it appears that in Figure 4.19b and c, there are still about 10% columnar α phase, equiaxed α and β phase which are not transformed to acicular α' at the β transit temperature. This causes the grain size phase to be larger than the acicular α 'scattered around it compared to Figure 4.19d where the majority of the β phase is transformed into acicular α'. The main reason for the difference is that the welding current of 8 kA generated lower heat input than 9 kA and 10 kA so that it causes some acicular α' transformations to be imperfect. Figure 4.20 shows that as the corrosion potential increases, the current density also increases sharply at the $E_{pitting}$ for all samples. It appears that the base metal sample has the highest pitting corrosion potential ($E_{pitting}$) compared to all other samples. Then followed by sample 1, sample 2 & sample 3 sequentially. A cathodic current can result in a reduction of the protective oxide layer, thus activating the metal surface [127]. As the corrosion stability of titanium and its alloys is dictated by the protective properties of the passive layer, highly reducing potentials can have a deteriorating influence on the layer's integrity and corrosion resistance [123].

Sample 3 has the lowest pitting corrosion potential ($E_{pitting}$) compared to the others. However, the indicator of the material's ability to resist pitting corrosion is shown by the difference between $E_{pitting}$ and E_{corr} with $\Delta E_p = E_{pitting} - E_{corr}$ [93]. Table 4.9 shows the results of the corrosion rates for each sample. The grater ΔE_p the greater the pitting corrosion resistance of the material will be. So that it can be seen on the Figure 4.20 curves that base metal ΔE_p is larger than all weld nuggets. The greater the welding time, the smaller the ΔE_p as can be seen on sample 3 curve which has the smallest ΔE_p. So that sample 3 has the smallest resistance to pitting corrosion and also has the highest corrosion rate.

Table 4.9 : Potentiodynamic polarization test results

Sample	**i_{corr}**	**E_{corr}**	**$E_{pitting}$**	**ΔE_p**	**Corrosion rate (mm/year)**
Base metal	4.2236E-08	-0.3159	0.1210	0.4369	0.0000466
Sample 1	2.4487E-08	-0.2043	0.0488	0.2531	0.0000646
Sample 2	1.9012E-08	-0.1701	0.0243	0.1944	0.0000895
Sample 3	1.8073E-08	-0.1797	0.0008	0.1805	0.0001098

Figure 4.21a reveals that there is very little pitting corrosion and little pitting in the base metal. While the weld nugget sample 1 and sample 2 are in Figure 4.21b and c can be observed that the pitting corrosion appears to be more and more with a quite small diameter. This is due to the heat input from the electrode which hits the weld nugget zone so that it changes the grain on the fusion zone microstructure to be coarser and martensitic as observed in Figure Figure 4.21b and c.

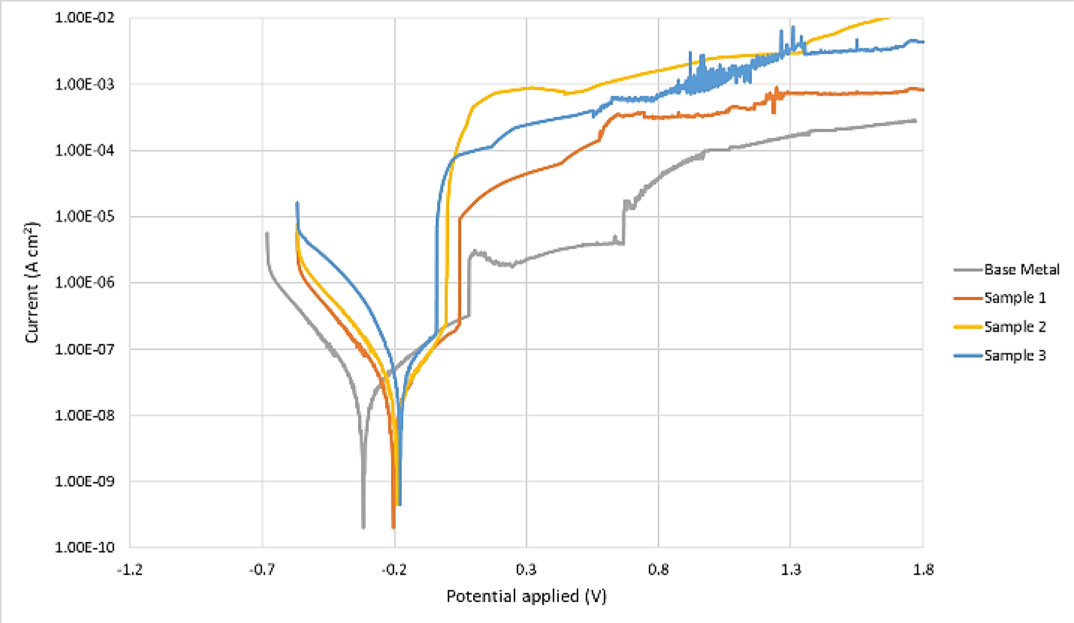

Figure 4.20 : Potentiodynamic polarization test curves.

The worsened corrosion behavior of welds was attributed to their coarsened and transformed structure [12]. Even Figure 4.21d sample 3 shows that there are more pits and the size is getting bigger. The dark scan color of the pits indicates that the pit depth is also getting deeper. The high heat input with longer welding time resulted in a coarsened grain which was indicated by the number of acicular α' which formed a martensitic structure that was evenly distributed in the fusion zone sample 3 and was getting coarser. While the β phase has a BCC structure, the acicular α' phase has a hexagonal-closed packed (HCP) structure with a highly stressed structure. The self-passivation of the fusion zone surface layer is generated at grain boundaries [12]. The finer microstructure allows the regenerating of a denser and thicker surface oxide layer [12]. Otherwise, the coarser microstructure fusion zone prevented itself to regenerates its passive oxide film, thus the thin passive oxide film becomes slight and unstable. This thin film has a high possibility to disperse quickly [93].

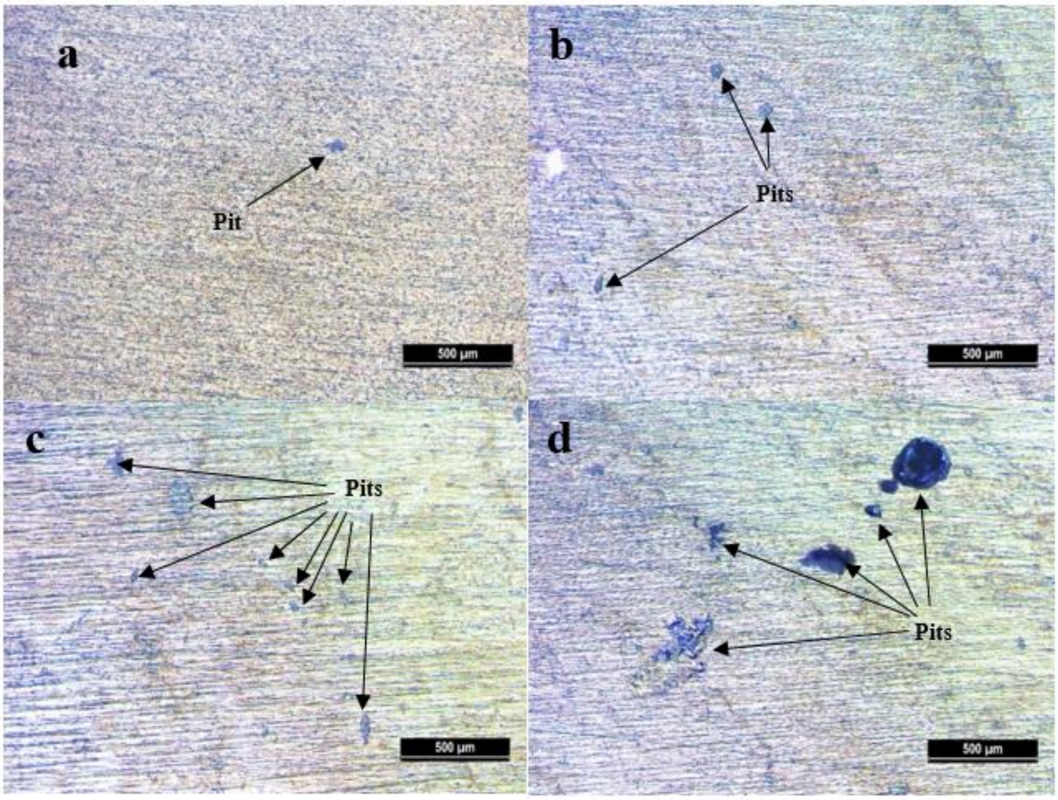

Figure 4.21 : Microscope observations of pitting images post-Tafel test at 20 X Mag.: (a) base metal; (b) sample 1; (c) sample 2; (d) sample 3.

CHAPTER 5

CONCLUSIONS AND RECOMMENDATIONS

5.1 Conclusions

After several experiments, observations, and analyses from the present study, there are following conclusions which can be drawn:

1. From the Taguchi analysis response for means and main effect plots for means are proved that tensile-shear strength is affected significantly by welding current followed by welding time and welding force. The response table for means is pointing to the highest delta value with the medium level of welding current 9 kA as the selected optimum level. This is supported by the highest stage of welding time of 32 cycles and welding force of 5 kN which also created a dense fusion zone. These answer the objective no. 1 to find out the optimum parameters to create a high tensile-shear strength.

2. The lowest welding current created a colder weld. Otherwise, the highest welding current generated expulsion although at this level the deeper penetration was achieved. The higher welding current is increasing the heat input significantly, this causes the wider melting zone in the faying layer of the contact area between the electrode and the sample. The weld nugget diameter and indentation depth tend to grow higher subsequently. The tensile testing maximum load was increasing following the increase of heat input, but an expulsion generated at the stage of the heat input highest level, the melted zone overheated at a short welding time and ejected some material deposits instantly in the air. The weld nugget strength reduction occurred in the highest stage and lowest stage of heat input. These were indicated by the low maximum load results. In these levels, a brittle fracture also attacks the HAZ and the fusion zone. The selected optimum RSW parameters were giving the highest tensile-shear stress with no expulsion appeared in the weld nugget. The highest tensile-shear stress was 599.724 MPa and with the maximum load of 44.979 kN. When the higher heat input was applied, the larger martensitic microstructure with α' phase presence as the transformation from β phase in β

transus temperature was formed with no pores appeared at all. This structure has a hexagonal-closed packed (HCP) as a highly stressed structure causing the fusion zone to have the highest hardness values among all areas. The lowest hardness value was in the base metal with HV = 305 and the highest was in the fusion zone with HV = 552.5. These effects answer the objective no. 2, to investigate the influence of RSW current, time, and force for titanium alloy TI-6Al-4V weld nugget physical & mechanical properties.

3. The multiple regression analysis results showed that the welding current contributed as the highest regression coefficient followed by welding time and force. From the regression, the mathematical models were also generated: Max. Load = 21.8 + 0.763 Current + 0.389 Time + 0.064 Force and Weld diameter = 0.545 + 1.0869 Current + 0.0665 Time + 0.0114 Force. This answers the objective no. 3 to find out the mathematical models related with the RSW parameters. The R-sq. was 94.68%, indicated that the model explained all the variability of the response data around its mean and the model fits the data quite better.

4. The potentiodynamic polarization results showed that sample 1 has Δ Ep = 0.2531, sample 2 has Δ Ep = 0.1944 and sample 3 has Δ Ep = 0.1805. This showed that all of spot-welded nugget samples had lower Δ Ep than the base metal which has Δ Ep = 0.4369. The higher heat input was applied during RSW in a longer welding time coarsened the sample's fusion zone microstructure. The coarser fusion zone microstructure was causing the decrease of fusion zone capability to regenerate thick and dense passive corrosion resistance film than in the base metal and the finer fusion zone microstructure. This effect explains and answers the objective no. 4 related to the effect of welding parameters with the transformation of corrosion resistance and pitting susceptibility.

5.2 Recommendations

There are still several improvements room for this research to fill the gap and lack of various aspects. To overcome this, some of the recommendations are fit to propose and also will probably increase the research quality as well as the outcomes. The recommendations are as follows:

1. The full factorial design can be performed as the design of the experiment to give a wider space of parameter intervals. This will increase the data accuracy even though it will require a larger number of experiments.

2. Applying heat treatment on Ti-6Al-4V samples before RSW will refine the β phase transformation thus will increase the possibility of better weld nugget physical and mechanical properties. This will also increase the possibility of a better weld nugget corrosion rate because the finer grain is obtained.

3. To measure the reduction in stiffness and strength of the Ti-6Al-4V weld nugget, the fatigue test can be applied under repeated loading and also to determine the total number of load cycles to failure.

4. The strong acid solution such as H_2SO_4 or HCl can be used to perform potentiodynamic polarization, therefore the more obvious pitting images can be obtained. This will also increase the corrosion rate data accuracy.

REFERENCES

[1] ASM, Welding brazing and soldering engineering in ASM Handbook, ASM International, Geauga, OH, USA, vol 6, 1993.

[2] H. Fujii, Y. Yamashita, K. Takahashi, "Application of Titanium and Its Alloys For Automobile Parts," *Nippon Steel Technical Report*, no. 88, Jul. 2003.

[3] I. Inagaki, Y. Shirai, T. Takechi, N. Ariyasu, "Application and Features of Titanium for the Aerospace Industry," *Nippon Steel & Sumitomo Metal Technical Report*, no. 106, Jul. 2014.

[4] ASTM B 265-20, Standard Specification for Titanium and Titanium Alloy Strip, Sheet, and Plate, ASTM International, West Conshohocken, PA, USA, 2010.

[5] ASM International Handbook Committee, ASM Handbook Volume 2: Properties and Selection-Nonferrous Alloys and Special-Purpose Materials, ASM International, Geauga, OH, USA, 2001.

[6] X. Zhang, J. Zhang, F. Chen, Z. Yang, and J. He, "Characteristics of resistance spot welded Ti6Al4V titanium alloy sheets," *Metals (Basel).*, 2017, doi: 10.3390/met7100424.

[7] N. Kahraman, "The influence of welding parameters on the joint strength of resistance spot-welded titanium sheets," *Mater.* Des. 2007, doi: 10.1016/j.matdes.2005.09.010.

[8] I. Fatmahardi, M. Mustapha, A. Ahmad, T. L. Ginta, I. Taufiqurrahman, and M. Danish, "Effect of welding parameters on the properties of the Ti-6Al-4V plate resistance spot weld joint," *IOP Conf. Ser. Mater. Sci. Eng.*, 2021, doi: 10.1088/1757-899x/1101/1/012036.

[9] I. Fatmahardi, M. Mustapha, A. Ahmad, M. N. Derman, T. Lenggo Ginta, and I. Taufiqurrahman, "An exploratory study on resistance spot welding of titanium alloy Ti-6Al-4V," *Materials (Basel).*, 2021, doi: 10.3390/ma14092336.

[10] I. Taufiqurrahman, T. Lenggo Ginta, and M. Mustapha, "The effect of holding time on dissimilar resistance spot welding of stainless steel 316L and Ti6Al4V titanium alloy with aluminum interlayer," *Materials Today: Proceedings*, p. 6, Aug. 2020, doi: 10.1016/j.matpr.2020.07.237.

[11] I. Taufiqurrahman, A. Ahmad, M. Mustapha, T. L. Ginta, L. A. F. Haryoko, and I. A. Shozib, "The effect of welding current and electrode force on the heat input,

weld diameter, and physical and mechanical properties of SS316l/Ti6Al4V dissimilar resistance spot welding with aluminum interlayer," *Materials (Basel).*, 2021, doi: 10.3390/ma14051129.

[12] N. V. Ferdinandov, D. D. Gospodinov, M. D. Ilieva, and R. H. Radev, "Structure and Pitting Corrosion of Ti-6Al-4V Alloy and Ti-6Al-4V Welds," 2018, doi: 10.24264/icams-2018.vi.7.

[13] S. Conroy, "Modern Welding," United States: NY Research Press, 2021.

[14] A. Abbas, A. Seif, I. El-Mahallawi, and W. Khalifa, "Microstructure and hardness of subzero quenched and heat treated Ti-6Al-4V alloy," *Minerals, Metals and Materials Series*, 2017.

[15] F. Bozkurt and F. H. Çakır, "An experimental design of spot welding of Ti6Al4V sheets and numerical modeling approach," Weld. World, 2021, doi: 10.1007/s40194-020-01054-3.

[16] M. Kimchi and D. H. Phillips, "Resistance Spot Welding: Fundamentals and Applications for the Automotive Industry," *Synth. Lect. Mech. Eng.*, 2017, doi: 10.2200/s00792ed1v01y201707mec005.

[17] Miller Electric Mfg. Co., "Handbook For Resistance Spot Welding", *www.MillerWelds.com*, 003 335A, Jul. 2005.

[18] A. M. Pereira, J. A. M. Ferreira, F. V. Antunes, and P. J. Bártolo, "Assessment of the fatigue life of aluminium spot-welded and weld-bonded joints," *Journal of Adhesion Science and Technology*, vol. 28, no. 14–15, pp. 1432–1450, Jul. 2014.

[19] H. Zhang and J. Senkara, Resistance welding: Fundamentals and applications. 2005.

[20] X. D. Liu, Y. B. Xu, R. D. K. Misra, F. Peng, Y. Wang, and Y. B. Du, "Mechanical properties in double pulse resistance spot welding of Q&P 980 steel," *Journal of Materials Processing Technology*, vol. 263, pp. 186–197, Jan. 2019.

[21] W. Liu, H. Fan, X. Guo, Z. Huang, and X. Han, "Mechanical Properties of Resistance Spot Welded Components of High Strength Austenitic Stainless Steel," *Journal of Materials Science & Technology*, vol. 32, no. 6, pp. 561–565, Jun. 2016.

[22] P. Podržaj, I. Polajnar, J. Diaci, and Z. Kariž, "Overview of resistance spot

welding control”, *Maney*, United Kingdom, Jan. 2008.

[23] ASM International, Titanium: A Technical Guide 2nd Edition (#06112G), 2000.

[24] M. Zhou, J.S. Hu, and H. Zhang, “Critical Sample Sizes for Tensile-Shear Testing of Steel Sheets,” *The University of Michigan, Welding Research Supplement*, United States, Sep. 1999.

[25] H. T. Lee and Y. C. Chang, “Effect of double pulse resistance spot welding process on 15B22 hot stamped boron steel,” Metals (Basel)., 2020, doi: 10.3390/met10101279.

[26] T. Kobayashi, Y. Mihara, “Numerical simulation of nugget formation in spot welding: Mechanical Design & Analysis Corporation,” *In SIMULIA Community Conference*, Rhode Island, USA, May 22, 2014.

[27] N. T. Williams and J. D. Parker, “Review of resistance spot welding of steel sheets: Part 2 - Factors influencing electrode life,” *International Materials Reviews*, 2004, doi: 10.1179/095066004225010541.

[28] M. Wohner, N. Mitzschke, and S. Jüttner, “Resistance spot welding with variable electrode force-development and benefit of a force profile to extend the weldability of 22MnB5+AS150,” *Weld. World*, 2021, doi: 10.1007/s40194-020-01001-2.

[29] T. Bick, V. Heuler, K. Treutler, and V. Wesling, “Characterization of influences of steel-aluminum dissimilar joints with intermediate zinc layer,” *Metals (Basel).*, 2020, doi: 10.3390/met10040442.

[30] V. Wesling, T. Rekersdrees, S. Keitel, R. Winkler, and S. Schreiber, “Investigations into the resistance spot welding of newly developed sheets made of higher-strength and super-high-strength steels,” *Weld. Cut.*, 2004.

[31] D. Shirmohammadi, M. Movahedi, and M. Pouranvari, “Resistance spot welding of martensitic stainless steel: Effect of initial base metal microstructure on weld microstructure and mechanical performance,” *Mater. Sci. Eng. A*, 2017, doi: 10.1016/j.msea.2017.07.067.

[32] M. Alizadeh-Sh, S. P. H. Marashi, and M. Pouranvari, “Resistance spot welding of AISI 430 ferritic stainless steel: Phase transformations and mechanical properties,” *Mater. Des.*, 2014, doi: 10.1016/j.matdes.2013.11.022.

[33] G. Yu, X. Chen, B. Zhang, K. Pan, and L. Yang, “Tensile-shear mechanical behaviors of friction stir spot weld and adhesive hybrid joint: Experimental and

numerical study," *Metals (Basel).*, 2020, doi: 10.3390/met10081028.

[34] A. M. Saeed, H. Zuhailawati, A. B. Ismail, Z. Samad, and T. Ariga, "Weldability of titanium and nickel with alloy filler addition and different electrodes tip shapes by using micro spot brazing method," *Int J Adv Manuf Technol*, vol. 73, no. 5–8, pp. 591–599, Jul. 2014, doi: 10.1007/s00170-014-5873-9.

[35] C. Ma, D. L. Chen, S. D. Bhole, G. Boudreau, A. Lee, and E. Biro, "Microstructure and fracture characteristics of spot-welded DP600 steel," *Materials Science and Engineering: A*, vol. 485, no. 1, pp. 334–346, Jun. 2008, doi: 10.1016/j.msea.2007.08.010.

[36] M. Pouranvari, S. M. Mousavizadeh, S. P. H. Marashi, M. Goodarzi, and M. Ghorbani, "Influence of fusion zone size and failure mode on mechanical performance of dissimilar resistance spot welds of AISI 1008 low carbon steel and DP600 advanced high strength steel," *Materials & Design*, vol. 32, no. 3, pp. 1390–1398, Mar. 2011, doi: 10.1016/j.matdes.2010.09.010.

[37] X. Wang, Y. Zhang, J. Ju, J. Zhang, and J. Yang, "Characteristics of Welding Crack Defects and Failure Mode in Resistance Spot Welding of DP780 Steel," *J. Iron Steel Res. Int.*, vol. 23, no. 10, pp. 1104–1110, Oct. 2016, doi: 10.1016/S1006-706X(16)30163-7.

[38] J. Xie, Y. Chen, L. Yin, T. Zhang, S. Wang, and L. Wang, "Microstructure and mechanical properties of ultrasonic spot welding TiNi/Ti6Al4V dissimilar materials using pure Al coating," *Journal of Manufacturing Processes*, vol. 64, pp. 473–480, Apr. 2021, doi: 10.1016/j.jmapro.2021.02.009.

[39] M. Ghosh, K. Bhanumurthy, G. B. Kale, J. Krishnan, and S. Chatterjee, "Diffusion bonding of titanium to 304 stainless steel," *Journal of Nuclear 129 Materials*, vol. 322, no. 2, pp. 235–241, Nov. 2003, doi: 10.1016/j.jnucmat.2003.07.004.

[40] C. Velmurugan, V. Senthilkumar, S. Sarala, and J. Arivarasan, "Low temperature diffusion bonding of Ti-6Al-4V and duplex stainless steel," *Journal of Materials Processing Technology*, vol. 234, pp. 272–279, Aug. 2016, doi: 10.1016/j.jmatprotec.2016.03.013.

[41] Y. Zhang, Y. Bi, J. Zhou, D. Sun, and H. Li, "Microstructure and mechanical property improvement of Ti alloy and stainless steel joint based on a hybrid connection mechanism," *Materials Letters*, vol. 274, p. 128012, Sep. 2020, doi:

10.1016/j.matlet.2020.128012.
[42] T. Vigraman, D. Ravindran, and R. Narayanasamy, "Effect of phase transformation and intermetallic compounds on the microstructure and tensile strength properties of diffusion-bonded joints between Ti–6Al–4V and AISI 304L," *Materials & Design (1980-2015)*, vol. 36, pp. 714–727, Apr. 2012, doi: 10.1016/j.matdes.2011.12.024.
[43] Z. Cheng, Z. Ye, J. Huang, J. Yang, S. Chen, and X. Zhao, "Influence of heat input on the intermetallic compound characteristics and fracture mechanisms of titanium-stainless steel MIG-TIG double-sided arc welding joints," *Intermetallics*, vol. 127, p. 106973, Dec. 2020, doi: 10.1016/j.intermet.2020.106973.
[44] C. Luo, Z. Lai, and Y. Zhang, "Improvement of mechanical properties of dissimilar spot-welded joints of additively manufactured stainless steels," *Journal of Manufacturing Processes*, vol. 54, pp. 210–220, Jun. 2020, doi: 10.1016/j.jmapro.2020.03.019.
[45] A. Kumar Mandal, M. L. Meena, A. Kumar Chaudhary, A. Patidar, and B. L. Gupta, "Comparative analysis of resistance spot welded and weld bonded joint of al 6082-T651," 2020, doi: 10.1016/j.matpr.2020.10.446.
[46] M. Shojaee, A. R. H. Midawi, B. Barber, H. Ghassemi-Armaki, M. Worswick, and E. Biro, "Mechanical properties and failure behavior of resistance spot welded third-generation advanced high strength steels," *J. Manuf. Process.*, 2021, doi: 10.1016/j.jmapro.2021.03.047.
[47] L. Burca, I. Mitelea, I. Dragos Utu, and M. Burca, "Resistance spot welding particularities of the nickel alloy Nimonic 80 A," *Mater. Today Proc.*, 2021, doi: 10.1016/j.matpr.2020.11.870.
[48] H. G. Mohammed, T. L. Ginta, and M. Mustapha, "The investigation of microstructure and mechanical properties of resistance spot welded AISI 316L austenitic stainless steel," *Mater. Today Proc.*, 2020, doi: 10.1016/j.matpr.2020.07.258.
[49] Y. Ma et al., "Measurement of local material properties and failure analysis of resistance spot welds of advanced high-strength steel sheets," *Mater. Des.*, 2021, doi: 10.1016/j.matdes.2021.109505.
[50] S. Roth, A. Hezler, O. Pampus, S. Coutandin, and J. Fleischer, "Influence of the

process parameter of resistance spot welding and the geometry of weldable load introducing elements for FRP/metal joints on the heat input," *J. Adv. Join. Process.*, 2020, doi: 10.1016/j.jajp.2020.100032.

[51] X. Cao, Z. Li, X. Zhou, Z. Luo, and J. Duan, "Modeling and optimization of resistance spot welded aluminum to Al-Si coated boron steel using response surface methodology and genetic algorithm," *Meas. J. Int. Meas. Confed.*, 2021, doi: 10.1016/j.measurement.2020.108766.

[52] A. Chabok, E. van der Aa, and Y. Pei, "A study on the effect of chemical composition on the microstructural characteristics and mechanical performance of DP1000 resistance spot welds," *Mater. Sci. Eng. A*, 2020, doi: 10.1016/j.msea.2020.139501.

[53] M. Vigneshkumar, S. Balu Mahandiran, P. Ashoka varthanan, D. Barath, U. Dhyaneswar, and P. Varun, "Challenges and possibilites in the resistance spot welding of dissimilar metals – A review," *Mater. Today Proc.*, 2021, doi: 10.1016/j.matpr.2021.01.238.

[54] A. Kumar Deepati, W. Alhazmi, and I. Benjeer, "Mechanical characterization of AA5083 aluminum alloy welded using resistance spot welding for the lightweight automobile body fabrication," *Mater. Today Proc.*, 2021, doi: 10.1016/j.matpr.2021.01.646.

[55] D. Mishra, K. Rajanikanth, M. Shunmugasundaram, A. P. Kumar, and D. Maneiah, "Dissimilar resistance spot welding of mild steel and stainless steel metal sheets for optimum weld nugget size," *Mater. Today Proc.*, 2021, doi: 10.1016/j.matpr.2021.01.067.

[56] S. Ren, Y. Ma, S. Saeki, Y. Iwamoto, C. Chen, and N. Ma, "Fracture mechanism and strength evaluation of Al5052/CFRP joint produced by coaxial one-side resistance spot welding," *Compos. Struct.*, 2020, doi: 10.1016/j.compstruct.2020.112766.

[57] M. Bemani and M. Pouranvari, "Microstructure and mechanical properties of dissimilar nickel-based superalloys resistance spot welds," *Mater. Sci. Eng. A*, 2020, doi: 10.1016/j.msea.2019.138825.

[58] G. Zhang, Y. Li, and Z. Lin, "Evolution mechanism of geometry morphology for metallic bump assisted resistance spot welded (MBaRSW) joints," *J. Manuf. Process.*, 2020, doi: 10.1016/j.jmapro.2020.09.068.

[59] T. Chen, Z. Ling, M. Wang, and L. Kong, "Effect of a slightly concave electrode on resistance spot welding of Q&P1180 steel," *J. Mater. Process. Technol.*, 2020, doi: 10.1016/j.jmatprotec.2020.116797.

[60] F. Badkoobeh, A. Nouri, H. Hassannejad, and H. Mostaan, "Microstructure and mechanical properties of resistance spot welded dual-phase steels with various silicon contents," *Mater. Sci. Eng. A*, 2020, doi: 10.1016/j.msea.2020.139703.

[61] A. Ghatei Kalashami, X. Han, F. Goodwin, and N. Y. Zhou, "The influence of modified annealing during the galvanizing process on the resistance spot welding of the CMn1.8Si advanced high strength steel," *Surf. Coatings Technol.*, 2020, doi: 10.1016/j.surfcoat.2019.125181.

[62] P. Sivaraj, M. Seeman, D. Kanagarajan, and R. Seetharaman, "Influence of welding parameter on mechanical properties and microstructural features of resistance spot welded dual phase steel sheets joint," 2020, doi: 10.1016/j.matpr.2019.08.201.

[63] P. Ravichandran, C. Anbu, B. Meenakshipriya, and S. Sathiyavathi, "Process parameter optimization and performance comparison of AISI 430 and AISI 1018 in resistance spot welding process," 2020, doi: 10.1016/j.matpr.2020.05.197.

[64] T. Das, R. Das, and J. Paul, "Resistance spot welding of dissimilar AISI-1008 steel/Al-1100 alloy lap joints with a graphene interlayer," *J. Manuf. Process.*, 2020, doi: 10.1016/j.jmapro.2020.02.032.

[65] A. K. Biradar and B. M. Dabade, "Optimization of resistance spot welding process parameters in dissimilar joint of MS and ASS 304 sheets," 2019, doi: 10.1016/j.matpr.2020.02.256.

[66] K. S. Pandya, V. Grolleau, C. C. Roth, and D. Mohr, "Fracture response of resistance spot welded dual phase steel sheets: Experiments and modeling," *Int. J. Mech. Sci.*, 2020, doi: 10.1016/j.ijmecsci.2020.105869.

[67] S. Rahimi and M. Movahedi, "Resistance Spot Welding of Aluminum to Aluminum Clad Steel Sheet: Experimental and Theoretical Analysis," *J. Manuf. Process.*, 2020, doi: 10.1016/j.jmapro.2020.08.026.

[68] V. Ungureanu, I. Both, M. Burca, B. Radu, C. Neagu, and D. Dubina, "Experimental and numerical investigations on built-up cold-formed steel beams using resistance spot welding," *Thin-Walled Struct.*, 2021, doi:

10.1016/j.tws.2021.107456.

[69] G. Park, S. Uhm, and C. Lee, “Effects of in-situ post-weld heat treatment on the microstructure and mechanical properties of the coarse-grained heat-affected zone in a resistance spot weld in medium Mn TRIP steel,” *Mater. Sci. Eng. A*, 2020, doi: 10.1016/j.msea.2020.139477.

[70] S. D. Bhat, V. Vijeesh, P. Acharya, and M. Rao, “Investigation of thin sheet stainless steel resistance spot welds: Effect of weld current on nugget failure and microstructure,” 2019, doi: 10.1016/j.matpr.2020.02.350.

[71] D. Zhao, D. Ren, G. Song, K. Zhao, L. Liu, and Z. Zhang, “Comparison of mechanical properties and the nugget formation of composite ceramic-centered annular welding and traditional resistance spot welding,” *Int. J. Mech. Sci.*, 2020, doi: 10.1016/j.ijmecsci.2020.105933.

[72] G. Chen, W. Xue, Y. Jia, S. Shen, and G. Liu, “Microstructure and mechanical property of WC-10Co/RM80 steel dissimilar resistance spot welding joint,” *Mater. Sci. Eng. A*, 2020, doi: 10.1016/j.msea.2020.139008.

[73] H. Essoussi, S. Elmouhri, S. Ettaqi, and E. Essadiqi, “Microstructure and mechanical performance of resistance spot welding of AISI 304 stainless steel and AISI 1000 series steel,” 2019, doi: 10.1016/j.promfg.2019.02.296.

[74] A. Subrammanian, P. V. Senthiil, D. B. Jabaraj, and D. Devakumar, “Improving mechanical performance of resistance spot welded joints of AISI 409M steel by double pulse current,” 2019, doi: 10.1016/j.matpr.2019.05.181.

[75] L. Qi, F. Li, R. Chen, Q. Zhang, and Y. Li, “Improve resistance spot weld quality of advanced high strength steels using bilateral external magnetic field,” *J. Manuf. Process.*, 2020, doi: 10.1016/j.jmapro.2020.02.030.

[76] C. Rajarajan, P. Sivaraj, M. Seeman, and V. Balasubramanian, “Influence of electrode force on metallurgical studies and mechanical properties of resistance spot welded dual phase (DP800) steel joints,” 2020, doi: 10.1016/j.matpr.2019.09.009.

[77] Q. Qin, H. Zhao, Y. Zhang, J. Li, and Z. Wang, “Microstructures and mechanical properties of Al-Mg2Si-Si alloys resistance spot welded with Al-Si interlayers,” *J. Mater. Res. Technol.*, 2019, doi: 10.1016/j.jmrt.2019.07.043.

[78] Y. Zhang, J. Guo, Y. Li, Z. Luo, and X. Zhang, “A comparative study between the mechanical and microstructural properties of resistance spot welding joints

among ferritic AISI 430 and austenitic AISI 304 stainless steel," *J. Mater. Res. Technol.*, 2020, doi: 10.1016/j.jmrt.2019.10.086.

[79] L. Shi, J. Kang, X. Chen, A. S. Haselhuhn, D. R. Sigler, and B. E. Carlson, "Determination of fracture modes in novel aluminum-steel dissimilar resistance spot welds," 2019, doi: 10.1016/j.prostr.2019.08.047.

[80] C. Luo and Y. Zhang, "Fusion zone characterization of resistance spot welded maraging steels via selective laser melting," *J. Mater. Process. Technol.*, 2019, doi: 10.1016/j.jmatprotec.2019.116253.

[81] V. H. Vargas, I. Mejía, V. H. Baltazar-Hernández, and C. Maldonado, "Characterization of resistance spot welded transformation induced plasticity (TRIP) steels with different silicon and carbon contents," *J. Manuf. Process.*, 2018, doi: 10.1016/j.jmapro.2018.02.005.

[82] H. M. Rao, J. Kang, L. Shi, D. R. Sigler, and B. E. Carlson, "Effect of sample configuration on fatigue properties of dissimilar aluminum to steel resistance spot welds," *Int. J. Fatigue*, 2018, doi: 10.1016/j.ijfatigue.2018.06.009.

[83] L. Shi, J. Kang, D. R. Sigler, A. S. Haselhuhn, and B. E. Carlson, "Microstructure and fatigue behavior of novel Multi-Ring Domed resistance spot welds for thin X626-T4 aluminum sheets," *Int. J. Fatigue*, 2019, doi: 10.1016/j.ijfatigue.2018.08.022.

[84] B. Ma, C. Fan, D. Chen, H. Wang, D. Ma, and F. Zhou, "Experimental study on deformation and fracture of resistance-spot-welded (RSW) overlapping plates impacted at RSW joint by round-nosed bullet," *Int. J. Impact Eng.*, 2020, doi: 10.1016/j.ijimpeng.2020.103663.

[85] M. Ghosh and S. Chatterjee, "Characterization of transition joints of commercially pure titanium to 304 stainless steel," *Materials Characterization*, vol. 48, no. 5, pp. 393–399, Jul. 2002, doi: 10.1016/S1044-5803(02)00306-6.

[86] RMI Titanium Company, Titanium alloy guide, January 2000.

[87] M.J. Donachie, Jr., Titanium: A Technical Guide, ASM International, 1988, p 28.

[88] J. O. Rawlings, S. G. Pantula, and D. A. Dickey, Applied Regression Analysis: A Research Tool, Second Edition. 1999.

[89] A. C. Rencher and G. B. Schaalje, Linear Models in Statistics. 2007.

[90] B. S. Gawai, R. L. Karwande, M. Irfan, and P. S. Thakare, "Mathematical

modeling and optimization of process parameters for tensile strength and nugget diameter in resistance spot welding of HR E-34 steel sheet joint," *Lect. Notes Mech. Eng.*, 2019, doi: 10.1007/978-981-13-2490-1_1.

[91] P. A. Schweitzer, Fundamentals of Corrosion-Mechanisms, Causes, and Preventative Methods. 2013.

[92] P. R. Roberge, Corrosion Engineering. Principles and Practice. 2008.

[93] K. M. Hafez, "The effect of welding atmosphere on the pitting corrosion of AISI 304L resistance spot welds," *Int. J. Adv. Manuf. Technol.*, 2018, doi: 10.1007/s00170-018-1915-z.

[94] N. Makuch, "The importance of phase composition for corrosion resistance of borided layers produced on nickel alloys," *Materials (Basel).*, 2020, doi: 10.3390/ma13225131.

[95] B. T. Lu, Z. K. Chen, J. L. Luo, B. M. Patchett, and Z. H. Xu, "Pitting and stress corrosion cracking behavior in welded austenitic stainless steel," *Electrochim. Acta*, 2005, doi: 10.1016/j.electacta.2004.08.036.

[96] R. Greensmith, V. L. Anderson, and R. A. Mclean, "Design of Experiments - A Realistic Approach.," *Oper. Res. Q.*, 1975, doi: 10.2307/3008227.

[97] J. Stufken and G. S. Peace, "Taguchi Methods: A Hands-On Approach," Technometrics, 1994, doi: 10.2307/1269218.

[98] S. Shafee, B. B. Naik, and K. Sammaiah, "Resistance Spot Weld Quality Characteristics Improvement By Taguchi Method," 2015, doi: 10.1016/j.matpr.2015.07.215.

[99] N. Muhammad, Y. H. P. Manurung, R. Jaafar, S. K. Abas, G. Tham, and E. Haruman, "Model development for quality features of resistance spot welding using multi-objective Taguchi method and response surface methodology," J. Intell. Manuf., 2013, doi: 10.1007/s10845-012-0648-3.

[100] A. G. Thakur, T. E. Rao, M. S. Mukhedkar, and V. M. Nandedkar, "Application of Taguchi method for resistance spot welding of galvanized steel," *J. Eng. Appl. Sci.*, 2010.

[101] U. Eşme, "Application of taguchi method for the optimization of resistance spot welding process," *Arab. J. Sci. Eng.*, 2009.

[102] ASTM D1002-99, Standard Test Method for Apparent Shear Strength of Single-Lap-Joint Adhesively Bonded Metal Samples by Tension Loading (Metal-to-Metal), ASTM International, West Conshohocken, PA 19428-2959, United

States.

[103] F. Koenigsberger, “Design for Welding in Mechanical Engineering”, *Longmans, Gree, and Co.*, pp. 81–91, 1948.

[104] OSHA, Personal Protective Equipment, Occupational Health and Safety Administration, US Department of Labor, OSHA 3151-12R, 2004.

[105] ASTM E8/E8M – 13a, Standard Test Methods for Tension Testing of Metallic Materials, ASTM Internationa*l*, West Conshohocken, PA 19428-2959, United States.

[106] ASTM E407-07, Standard Practice for Microetching Metals and Alloys, ASTM International, West Conshohocken, PA 19428-2959, United States.

[107] ASTM E92-17, Standard Test Methods for Vickers Hardness and Knoop Hardness of Metallic Materials, ASTM International, West Conshohocken, PA 19428-2959, United States.

[108] R. L. Smith and G. E. Sandly, “An Accurate Method of Determining the Hardness of Metals, with Particular Reference to Those of a High Degree of Hardness,” *Proc. Inst. Mech. Eng.*, 1922, doi: 10.1243/pime_proc_1922_102_033_02.

[109] ASTM G59 - 97, Standard Test Methods for Conducting Potentiodynamic Polarization Resistance Measurements, ASTM International, West Conshohocken, PA 19428-2959, United States.

[110] ASTM G 102 - 89, Standard Practice for Calculation of Corrosion Rates and Related Information from Electrochemical Measurements, ASTM International, West Conshohocken, PA 19428-2959, United States.

[111] Y. J. Chao, “Failure mode of spot welds: Interfacial versus pullout,” *Sci. Technol. Weld. Join.*, 2003, doi: 10.1179/174329313X13789830157267.

[112] M. Pouranvari and S. P. H. Marashi, “Failure mode transition in AHSS resistance spot welds. Part I. Controlling factors,” *Mater. Sci. Eng. A*, 2011, doi: 10.1016/j.msea.2011.08.017.

[113] M. Pouranvari and S. P. H. Marashi, “Critical review of automotive steels spot welding: Process, structure and properties,” *Science and Technology of Welding and Joining*, 2013, doi: 10.1179/1362171813Y.0000000120.

[114] M. Pouranvari, S. P. H. Marashi, and D. S. Safanama, “Failure mode transition in AHSS resistance spot welds. Part II: Experimental investigation and model

validation," *Mater. Sci. Eng. A*, 2011, doi: 10.1016/j.msea.2011.08.016.

[115] P. Marashi, M. Pouranvari, S. Amirabdollahian, A. Abedi, and M. Goodarzi, "Microstructure and failure behavior of dissimilar resistance spot welds between low carbon galvanized and austenitic stainless steels," *Mater. Sci. Eng. A*, 2008, doi: 10.1016/j.msea.2007.07.007.

[116] M. S. M. Mansor, F. Yusof, T. Ariga, and Y. Miyashita, "Microstructure and mechanical properties of micro-resistance spot welding between stainless steel 316L and Ti-6Al-4V," *Int. J. Adv. Manuf. Technol.*, 2018, doi: 10.1007/s00170-018-1688-4.

[117] I. S. Hwang, M. J. Kang, and D. C. Kim, "Expulsion reduction in resistance spot welding by controlling of welding current waveform," 2011, doi: 10.1016/j.proeng.2011.04.461.

[118] H. Ghazanfari and M. Naderi, "Expulsion characterization in resistance spot welding by means of a hardness mapping technique," *Int. J. Miner. Metall. Mater.*, 2014, doi: 10.1007/s12613-014-0986-6.

[119] M. Motyka, K. Kubiak, J. Sieniawski, and W. Ziaja, "Phase Transformations and Characterization of α + β Titanium Alloys," in Comprehensive Materials Processing, 2014.

[120] J. Irwin, "Modeling Microstructure of AM Processes Using the FE Method," in Thermo-Mechanical Modeling of Additive Manufacturing, 2017.

[121] J. Dias Corpa Tardelli, C. Bolfarini, and A. Cândido dos Reis, "Comparative analysis of corrosion resistance between beta titanium and Ti-6Al-4V alloys: A systematic review," *Journal of Trace Elements in Medicine and Biology*. 2020, doi: 10.1016/j.jtemb.2020.126618.

[122] J. A. Petit, B. Kondro, and F. Dabosi, "Ion beam analysis investigation of pit nucleation on titanium in bromide media.," *Corrosion*, 1980, doi: 10.5006/0010-9312-36.3.145.

[123] F. E. T. Heakal and K. A. Awad, "Electrochemical corrosion and passivation behavior of titanium and its Ti-6AL-4V alloy in low and highly concentrated HBr solutions," *Int. J. Electrochem. Sci.*, 2011.

[124] S. Huo and X. Meng, "The states of bromide on titanium surface prior to pit initiation," *Corros. Sci.*, 1990, doi: 10.1016/0010-938X(90)90120-T.

[125] D. Song, A. B. Ma, J. H. Jiang, P. H. Lin, and D. H. Yang, "Corrosion behavior

of ultra-fine grained industrial pure Al fabricated by ECAP," *Trans. Nonferrous Met. Soc. China (English Ed.)*, 2009, doi: 10.1016/S1003-6326(08)60407-0.

[126] S. B. Basame and H. S. White, "Pitting Corrosion of Titanium The Relationship Between Pitting Potential and Competitive Anion Adsorption at the Oxide Film/Electrolyte Interface," *J. Electrochem. Soc.*, 2000, doi: 10.1149/1.1393364.

[127] J. Riskin and A. Khentov, "Electrocorrosion and protection of metals," 2019.

LIST OF PUBLICATIONS

[1] I. Fatmahardi, M. Mustapha, A. Ahmad, T. L. Ginta, I. Taufiqurrahman, and M. Danish, “Effect of welding parameters on the properties of the Ti-6Al-4V plate resistance spot weld joint,” *IOP Conf. Ser. Mater. Sci. Eng.*, 2021, doi: 10.1088/1757-899x/1101/1/012036.

[2] I. Fatmahardi, M. Mustapha, A. Ahmad, M. N. Derman, T. Lenggo Ginta, and I. Taufiqurrahman, “An exploratory study on resistance spot welding of titanium alloy Ti-6Al-4V,” *Materials (Basel).*, 2021, doi: 10.3390/ma14092336.

APPENDIX A

STANDARD OPERATING PROCEDURE (SOP) OF THE RSW MACHINE

Here are the procedures of using the RSW machine according to its standard operating procedure (SOP):

1. Before conducting the welding, ensure the operator wearing a minimum proper welding PPE (Apron, Welding gloves, and safety eyeglasses)
2. Ensure that the pressure on the manometer above the machine is 0 psi, if it's not release it first by turning its knob
3. Open the pressurized air and water valves, check all of the connections ensure it is not leaked as well as on the electrode tip holder
4. Turn on the power switch
5. Turn on the power button on the machine panel
6. Reset all of the parameters on the panel
7. Push the program button to set up the parameters
8. Set the parameters according to the desired parameters of current, weld cycles, and holding time (only for 1st phase, there is no need to set the parameters for 2nd phase and 3rd phase)
9. Push the program button once more to settle all the settings had been applied to the machine
10. To set up the pressure or force, turn the air pressure adjuster above the manometer until the desired pressure is achieved
11. For sample preparations, clean the sample's surface and clamp both of the samples with a quite small clamp but strong enough to ensure the sample welded correctly according to the standard drawing geometry.
12. To hold the samples, pliers can be used, but ensure the holder of the pliers is sleeved by an isolator material, so that the electric current that probably comes out from the electrode tips, may not directly flow through the hands.
13. After all parameters and samples are perfectly settled, check the electrode tip force to ensure the weld is held in the correct position by putting the sample to the middle of both electrode tips and place it between them, and then push the pressure button

on the panel so that the weld will not be conducted. Press the footswitch so that both of the electrode tips will clamp the sample, make sure that the predicted weld position is correct.

14. After the predicted weld position is correctly ensured, turn off the pressure button and turn on the weld button on the panel, and press the footswitch once more, and then the weld will be conducted to the sample by the electrode tips.
15. After welding had been conducted, check the weld on the sample, ensure that the weld is correct, the weld nugget shape is perfectly round with the HAZ circularly on its outer diameter.
16. If there is expulsion or cold weld happens, check all of the parameters and the electrode tips, if there is no problem, so that it is correctly the effect of the experiment parameters itself.
17. If there is something wrong with the electrode tips particularly regarding its possible damaged surface, the electrode tip dressing can be applied to put it into service and to maintain it into a pretty well condition. Electrode tips can also be replaced by the new ones, to maintain the weld conditions keep very well, but the cost element is still a critical thing to consider.

APPENDIX B

Standard Personal Protective Equipment (PPE)

Specific hazards such as drop objects, sparks, chemical substance or solution, noise, sharp chips, and imitating dust, or other potentially hazardous circumstances may all be found in the workplace. Personal protective equipment (PPE) must be prepared, given, and ensured to be used in any standard operating procedure (SOP), elimination, substitution, engineering, or administrative controls are not offering sufficient protection to the worker. PPE is clothing used to reduce exposure to a range of dangers or various hazards [104].   shows the minimum standard of PPE that must be worn during welding, those are leather apron, welding gloves, and safety glasses. A leather apron is one of the body protection types of PPE. It can protect the researcher from possible bodily injury of any kind such as dry heat, flames, dust, metal chip, and sparks. Leather, especially the thick one, gives the advantage to absorb heat and heavily withstand against any hot and sharp metal chip even sparks that can cause any burnt material. It is different from rubber or treated wool and cotton that provide more elasticity and comfortability.

As well as the special safety gloves for welding activity usage that is also made from leather can protect against skin absorption of hazardous chemicals, chemical or thermal burns, electrical risks, bruising, abrasions, cuts, punctures, fractures, and amputations which are all considered as possible hazards. It protects against sparks, moderate heat, blows, chips, and abrasive things well enough [104].

Some of examples potential eye injuries during welding include [104]:

1. Ingestion of dust, dirt, or metal shards.
2. Corrosive chemicals, heated liquids, solvents, or other dangerous solutions are splashed on the skin.
3. Swinging objects, such as tools or ropes, into the eye.

Welding rays, damaging rays from lasers, and other radiant light (as well as heat, glare, sparks, splash, and flying particles). Eyes are very important for human purposes in life to see anything. Short exposure of hazards into the eye can cause possible eye sicknesses such as irritation or soreness. Long time exposure of hazards into the eye particularly some of over brightening light or harmful rays can cause damage to the eye such as permanent irritation, lack of focus, and possibly blind.

Figure B. 1 : Standard welding PPE: (a) Leather apron, (b) Welding gloves, (c) Safety glasses.

Moreover working in the RSW in the workshop so many possibilities of sparks, metal chips, or dust that can expose to the eye directly. The safety eyeglasses that can be seen in c are made of light material, easy to clean, and scratch-resistant, which can ensure the comfortability to use during welding. For laboratory experiments such as tensile-shear testing, micro etching, micrographic analysis, and hardness test, safety glasses, a lab coat and chemical safety as seen in **Error! Reference source not found.** can be worn properly.

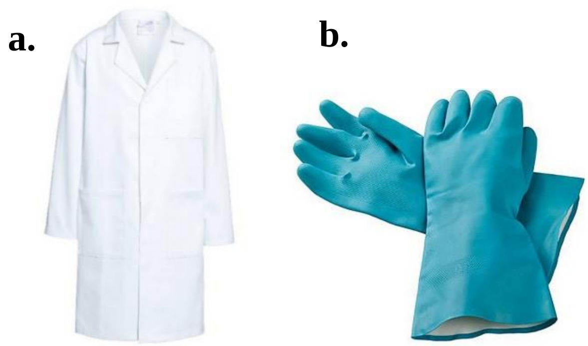

Figure B. 2 : Typical of PPE used for laboratory experiment : (a) Lab coat, (b) Chemical safety gloves.

Safety glasses, long-tailed lab coats, and chemical safety gloves can protect the body, eyes, and hands against any chemical splash and sharp metal chip or cut. The chemical safety gloves are usually made of nitrile that is puncture resistant and sometimes has a flocked lining to help keep the hands cool while working.

In addition, while working wears the PPE, the researcher must also wear proper clothes. A shirt or T-shirt with a trouser and a well-protected foot shoes can be worn during working. At last to endure the loss prevention during working or to reduce any potentially unsafe condition and unsafe act, all of it is depends on the researcher's behavior to follow the rule of HSSE policies.